2008-05-02

Luminescent Probes and Photochromic Switches Based on Semiconductor Quantum Dots

Ibrahim Yildiz
University of Miami, i.yildiz@umiami.edu

UNIVERSITY OF MIAMI

LUMINESCENT PROBES AND PHOTOCHROMIC SWITCHES BASED ON SEMICONDUCTOR QUANTUM DOTS

By

Ibrahim Yildiz

A DISSERTATION

Submitted to the Faculty
of the University of Miami
in partial fulfillment of the requirements for
the degree of Doctor of Philosophy

Coral Gables, Florida

May 2008

UNIVERSITY OF MIAMI

A dissertation submitted in partial fulfillment of
the requirements for the degree of
Doctor of Philosophy

LUMINESCENT PROBES AND PHOTOCHROMIC SWITCHES BASED ON SEMICONDUCTOR QUANTUM DOTS

Ibrahim Yildiz

Approved:

_____	_____
Dr. Françisco M. Raymo	Dr. Terri A. Scandura
Associate Professor of Chemistry	Dean of the Graduate School
_____	_____
Dr. Angel E. Kaifer	Dr. V. Ramamurthy
Professor of Chemistry	Professor of Chemistry

_____
Dr. Richard A. DeFazio
Research Assistant Professor of Neurology

IBRAHIM YILDIZ (Ph.D., Chemistry)

Luminescent Probes and Photochromic Switches Based on Semiconductor Quantum Dots (May 2008)

Abstract of a dissertation at the University of Miami.

Dissertation supervised by Professor Françisco M. Raymo.
No. of pages in text. (100)

A new strategy was developed to switch the luminescence of semiconductor quantum dots with chemical stimulations. It is based on the photoinduced transfer of either energy from CdSe–ZnS core–shell quantum dots to [1,3]oxazine ligands or electrons from the organic to the inorganic components. Upon addition of base or acid, energy or electron transfer pathways respectively become operative, leading to changes in the luminescence of the nanoparticles. These changes are fully reversible and can be exploited to probe the pH of aqueous solutions from 3 up to 11 and this design can lead to the development of pH-sensitive luminescent probes for biomedical applications based on the semiconductor quantum dots.

Secondly, an operating principle to transduce the supramolecular association of complementary receptor–substrate pairs into an enhancement in the luminescence of sensitive quantum dots was identified. This system is based on the electrostatic adsorption of cationic quenchers on the surface of anionic quantum dots. The adsorbed quenchers efficiently suppress the emission character of the associated nanoparticles on the basis of photoinduced electron transfer. In the presence of target receptors able to bind the quenchers and prevent electron transfer, however, the luminescence of the quantum dots is restored. Thus, complementary receptor–substrate pairs can be identified

with luminescence measurements relying on this system and this protocol can be adapted to signal protein–ligand interactions.

Thirdly, a photochromic spiropyran with dithiolane appendage to adsorb on the surface of cadmium sulfide system was designed. The properties of the resulting photochrome–nanoparticle assemblies vary significantly with the experimental conditions selected for the preparation of the inorganic component.

Finally, photochromic materials based on the photoinduced transfer of electrons from CdSe–ZnS core–shell quantum dots to bipyridinium dications were developed.

To my beloved wife and family.

Acknowledgements

First of all, I would like thank my research advisor, Professor Françisco M. Raymo, for his patience, advice and positive attitude for everything during these difficult but productive years.

Most importantly, I want to thank my wife, Banu Sizirici Yildiz, for her never ending presence and support in my life. We have shared everything in life and she gives me energy to tackle every difficulty.

I wish to thank Dr. Massimiliano Tomasulo for his collaboration during my graduate studies. He was a friend, good colleague and a good partner in the lab.

I have to mention my master study advisor, Professor Safiye Erdem in Turkey, for her encouragement to pursue an academic career in chemistry.

Also, I'd like to emphasize my family's contribution, support and positive energy during these years.

All the faculty and staff of the Chemistry Department deserve special thanks. Also I want to mention Dr. Sireesha L. Kaanumalle's help in some experiments during past years.

Finally, I apologize if I forgot to mention anyone else who has helped me in any way during my graduate studies.

List of Tables and Figures……viii

CHAPTER 1

LUMINESCENT CHEMOSENSORS BASED ON SEMICONDUCTOR QUANTUM DOTS

1.1. Introduction 1

1.2. Luminescent Chemosensors 2

1.3. Semiconductor Quantum Dots 3

1.3.1. History 3

1.3.2. Photophysical Properties of Quantum Dots 5

1.4. Semiconductor Quantum Dots Chemosensors 7

1.4.1. Chemosensors Based on Electron Transfer Mechanism 7

1.4.2. Chemosensors Based on Energy Transfer 13

1.5. Conclusions 19

CHAPTER 2

pH–SENSITIVE QUANTUM DOTS

2.1. Summary 22

2.2. Fluorescent pH Sensors 23

2.3. Results and Discussion 24

2.3.1. Design 24

2.3.2. Synthesis 25

2.3.3. ^{1}H NMR Spectroscopy 26

2.3.4. Absorption Spectroscopy 28

2.3.5. Electrochemistry 30

2.3.6. Synthesis and Physicochemical Properties of the Quantum Dots 31

2.4. Conclusions 38

CHAPTER 3

A MECHANISM TO SIGNAL RECEPTOR–SUBSTRATE INTERACTIONS WITH LUMINESCENT QUANTUM DOTS

3.1. Summary 39

3.2. Receptor-substrate Interactions 40

3.3. Results and Discussion 42

3.3.1. Synthesis of Hydrophilic Quantum Dots 42

3.3.2. Infrared Spectroscopy of Quantum Dots 43

3.3.3 Absorption and Emission Spectroscopy. 44

3.3.4. Signaling Protein-ligand Interactions with Quantum Dots. 47

3.3.5. Synthesis of Biotin Quencher 47

3.3.6. Absorption and Emission spectroscopy of Biotin/Streptavidin System 48

3.4. Conclusions 51

CHAPTER 4

LUMINESCENCE MODULATION WITH SEMICONDUCTOR QUANTUM DOTS AND PHOTOCHROMIC LIGANDS

4.1. Summary 52

4.2. Luminescence Modulation 53

4.3. Results and Discussion 54

4.3.1. Design and Synthesis 54

4.3.2. Photochromic Component. 55

4.3.3. Fluorescence Modulation. 56

4.4. Conclusions 59

CHAPTER 5

NANOPARTICLE-INDUCED TRANSITION FROM POSITIVE TO NEGATIVE PHOTOCHROMISM

5.1. Summary 60

5.2. Photochromic Systems 61

5.3. Results and Discussion 63

5.3.1. Design and Synthesis. 63

5.3.2. Photochromic Component 65

5.3.3 Synthesis of Nanoparticles and IR Spectroscopy 66

5.3.4. Photochrome–nanoparticle Assemblies. 68

5.4. Conclusions 71

CHAPTER 6

PHOTOCHROMIC NANOCOMPOSITES OF BIPYRIDINIUM DICATIONS AND SEMICONDUCTOR QUANTUM DOTS

6.1. Summary 73

6.2. Photochromism of Bipyridinium Dications 74

6.3. Results and Discussion 75

6.3.1. Design and Synthesis. 75

6.3.2. Photolysis in Solution 76

6.3.3 Photolysis on Quartz Substrate. 79

6.4. Conclusions 81

CHAPTER 7

EXPERIMENTAL PROCEDURES

7.1. General Methods 82

7.2. Experimental Procedures 82

References and notes 91

List of Tables and Figures

Figure 1.1. The association of the receptor with a complementary analyte can suppress either an electron or an energy transfer process and switch the fluorescence of the adjacent fluorophore on. 3

Figure 1.2. TOPO coated CdSe–ZnS core-shell quantum dots..... 4

Figure 1.3. Absorption and emission spectra of different sizes of CdSe–ZnS quantum dots. 5

Figure 1.4. Emission ranges of quantum dots with different elemental compositions and sizes. 6

Table 1.1. Geometrical and photophysical parameters of typical organic dyes and quantum dots. 7

Table 1.2. Redox potentials of CdSe quantum dots relative to the ferrocene/ferrocenium couple. 8

Figure 1.5. The association of MBP with maltose moves the ruthenium donor **2** away from the CdSe quantum dot, preventing the electron transfer process and switching the luminescence of the nanoparticle on. 9

Figure 1.6. The association of the analyte with receptor on the surface of CdSe–ZnS particles can quench luminescence of CdSe–ZnS particles by allowing electron transfer from excited particles to receptor-analyte compex. ..... ……..10

Figure 1.7. Enzymatic activity of tyrosinase oxidizes tyrosine to o-quinone on the surface of CdSe–ZnS and resulting o-quinone quenches luminescence by electron transfer…..… 11

Figure 1.8. Enzymatic transformation of tyrosine into o-quinone. 12

Figure 1.9. Enzymatic activity of tyrosinase oxidizes tyrosine to o-quinone on the surface of CdSe–ZnS and resulting o-quinone quenches luminescence by electron transfer. Luminescence of CdSe–ZnS can be recovered by removal of o-quinone after exposure to thrombin.. 13

Table 1.3. Förster radii of typical donor–acceptor pairs. 14

Figure 1.10. The hybridization of an oligonucleotide labeled with a CdSe–ZnS core–shell quantum dot and an oligonucleotide labeled with a complementary acceptor encourages the transfer of energy from the former to the latter with a concomitant luminescence quenching**.** 15

Figure 1.11. The association of TNT with the antibody moves the acceptor **8** away from the quantum dot, preventing the energy transfer process and switching the luminescence of the nanoparticle on..... 16

Figure 1.12. Collagenase cleaves the peptide bridging the CdSe–ZnS core–shell quantum dot to the rhodamine acceptor **9**, suppressing the energy transfer process and switching the luminescence of the nanoparticle on……. 17

Figure 1.13. Demonstration of improved energy transfer derived from arraying multiple acceptor dyes around a single QD donor acting as a protein scaffold…… 19

Figure 2.1. Design of pH–sensitive quantum dot based chemo sensor…….. 25

Figure 2.2. Synthesis of the model compound **13** and the target ligand **15**…… 26

Figure 2.3. Transformations of **13** and **15** upon addition of base or acid…….. 27

Figure 2.4. ^{1}H-NMR spectra (20 mM, CD_3CN, 20ºC, 500 MHz) of **13** before (***a***) and after the addition of either Bu_4NOH (3 eq., ***b***) or CF_3CO_2H (5 eq., ***c***)…….. ..... ……..27

Figure 2.5. Model compounds **16**, **17a**, 1**7b** and **18**. 28

Figure 2.6. Absorption spectra (0.1 mM, MeCN, 20ºC) of **13** before (***a***) and after the addition of either Bu_4NOH (100 eq., ***b***) or CF_3CO_2H (16 eq., ***c***). Absorption spectra (0.1 mM, MeCN, 20ºC) of **16** (***d***) and of **17a** before (***e***) and after the addition of Bu_4NOH (4 eq., ***f***). 29

Figure 2.7. Cyclic voltammograms (1.0 mM, MeCN, 0.1 M Bu_4NPF_6, 100 mV s^{-1}, V *vs.* Ag/AgCl) of **13** before (***a***) and after the addition of either Bu_4NOH (6 eq., ***b***) or CF_3CO_2H (25 eq., ***c***). Cyclic voltammograms (1.0 mM, MeCN, 0.1 M Bu_4NPF_6, 100 mV s^{-1}, V *vs.* Ag/AgCl) of **18** (***d***) and of **17a** before (***e***) and after the addition of Bu_4NOH (6 eq., ***f***).. 31

Table 2.1. Luminescence quantum yields and lifetimes of the quantum dots.. ..... ……32

Figure 2.8. Absorption spectra (1.8 µM, $CHCl_3$, 20ºC) of CdSe–ZnS core–shell quantum dots before (***a***) and after (***b***) the attachment of **15** to their surface and the subsequent addition of either Bu_4NOH (***c***, 4.8 mM) or CF_3CO_2H (***d***, 4.8 mM). Emission spectra (0.9 µM, $CHCl_3$, 20ºC, λ_{Ex} = 426 nm) of CdSe–ZnS core–shell quantum dots before (***e***) and

after (***f***) the attachment of **15** to their surface and the subsequent addition of either Bu_4NOH (***g***, 2.5 mM) or CF_3CO_2H (***h***, 2.5 mM)..... 34

Figure 2.9. Temporal evolution of the luminescence intensity (2.6 μM, $CHCl_3$, 20ºC, $\lambda_{Ex.}$ = 430 nm, $\lambda_{Em.}$ = 558 nm) of CdSe–ZnS core–shell quantum dots before (***a***) and after (***b***) the attachment of **15** to their surface and the subsequent addition of either Bu_4NOH (***c***, 5.0 mM) or CF_3CO_2H (***d***, 10.8 mM)..... 35

Figure 2.10. Emission intensity of CdSe–ZnS core–shell quantum dots (0.4 μM, 550 μL, $CHCl_3$, 0.1 M Bu_4NCl, 20ºC, $\lambda_{Ex.}$ = 430 nm, $\lambda_{Em.}$ = 552 nm) with (***a***) and without (***b***) **15** on their surface after the addition of sodium phosphate buffer (200 μL) with pH ranging from 3.2 to 10..... 36

Figure 2.11. Emission intensity of a solution of CdSe–ZnS core–shell quantum dots (0.8 μM, 300 μL, $CHCl_3$, 20ºC, λ_{Ex} = 430 nm, λ_{Em} = 555 nm) with (***a***) and without (***b***) **15** on their surface and Bu_4NCl (1 M, 50 μL, dichloroethane) after treatment with sodium phosphate buffer (500 μL) and dilution with $CHCl_3$ (4.3 mL). Photographs of solutions of CdSe–ZnS core–shell quantum dots (0.8 μM, 300 μL, $CHCl_3$) coated with **15** and Bu_4NCl (1 M, 50 μL, dichloroethane) under ultraviolet illumination after treatment with sodium phosphate buffer (500 μL) at the pH values (***I–III***) indicated in the plot. ..... ……..37

Figure 3.1. The supramolecular association of quencher and receptor prevents the electron transfer process and activates the luminescence of the quantum dot. ..... ……41

Figure 3.2. Ligand exchange process of hydrophobic TOPO molecules with hydrophilic mercaptoacetate groups..... 43

Figure 3.3. Infrared spectra of neat tri-*n*-octylphopshine oxide (***a***), hydrophobic CdSe–ZnS core–shell quantum dots before (***b***) and after (***c***) treatment with mercaptoacidic acid(**19** in Figure 3.2) and potassium hydroxide, (***d***) potassium mercaptoacetate. 44

Figure 3.4. Absorption spectrum (***a***) of hydrophilic CdSe–ZnS core–shell quantum dots (1.5 μM, sodium phosphate buffer, pH = 7.8, 20°C). Emission spectrum (λ_{Ex} = 350 nm) of the same solution recorded before (***b***) and after the consecutive addition of **20** (***c***, 4.1 μM) and **22** (***d***, 21 μM). Stern–Volmer plot (***e***) of hydrophilic CdSe–ZnS core–shell quantum dots (1.5 μM, sodium phosphate buffer, pH = 7.8, 20°C, λ_{Ex} = 350 nm) upon addition of increasing amounts of **20**..... 45

Figure 3.5. The bipyridinium-based quenchers **20** and **21** and the macrocyclic receptor **22**..... 46

Figure 3.6. Activation of the luminescence of the quantum dot by means of the supramolecular association of protein and ligand..... 47

Figure 3.7. Synthesis of the bipyridinium dication **21**.. 48

Figure 3.8. Emission spectra of hydrophilic CdSe–ZnS core–shell quantum dots (1.5 μM, sodium phosphate buffer, pH = 7.8, 20°C, λ_{Ex} = 350 nm) recorded before (***a***) and after the consecutive addition of **21** (***b***, 4.1 μM) and streptavidin (***c***, 21 μM). Stern–Volmer plot (***d***) of hydrophilic CdSe–ZnS core–shell quantum dots (1.5 μM, sodium phosphate buffer, pH = 7.8, 20°C, λ_{Ex} = 350 nm) upon addition of increasing amounts of **2**..... 49

Figure 3.9. Emission spectra of hydrophilic CdSe–ZnS core–shell quantum dots (1.5 μM, sodium phosphate buffer, pH = 7.8, 20°C, λ_{Ex} = 350 nm) recorded before (***a***) and after the consecutive addition of **21** (***b***, 4.1 μM) and bovine serum albumin (***c***, 7.4 μM).. 51

Figure 4.1. Modulation of the luminescence of the nanoparticle by interconversion of a photochromic spiropyran.. 53

Figure 4.2. The photoinduced and reversible interconversion of colorless spiropyrans (**26** and **27**) into colored merocyanines (**26a** and **27a**).. ……..55

Figure 4.3. The absorption spectra of a solution of **27** (0.1 mM, dichloroethane, 20°C) before (***a***) and after (***b***) continuous irradiation (365 nm, 0.4 mW cm^{-2}, 10 min) and the emission spectrum (***c***) of a solution of CdSe–ZnS core–shell quantum dots (0.7 μM, dichloroethane, 20°C, λ_{Ex} = 450 nm)..... 56

Figure 4.4. The absorption spectra of a solution of CdSe–ZnS core–shell quantum dots (0.7 μM, dichloroethane, 20°C) with **27** adsorbed on their surface before (***a***) and after (***b***) continuous irradiation (365 nm, 0.4 mW cm^{-2}, 10 min) and the corresponding emission spectra (***c***) and (***d***) respectively (λ_{Ex} = 380 nm). The emission spectrum (***e***) of a solution of **27** (0.1 mM, dichloroethane, 20°C, λ_{Ex} = 380 nm) after continuous irradiation (365 nm, 0.4 mW cm^{-2}, 10 min).. 57

Figure 5.1. Nanoparticle-induced transition from positive to negative photochromism…. 63

Figure 5.2. The ultraviolet (UV) irradiation of the spiropyrans **26** and **27** in organic solvents generates the corresponding merocyanines **26a** and **27a**, which revert to the original isomers under visible (VIS) irradiation or upon storage in the dark. ..... ……64

Figure 5.3. The ultraviolet–visible absorption spectra of a solution (0.1 mM, dichloroethane, 20°C) of **27** before (***a***) and after (***b***) continuous irradiation (365 nm, 0.4 mW cm^{-2}, 10 min). The evolution of the absorbance at 592 nm after irradiation (***c***) and the associated monoexponential curve-fitting (***d***)..... 66

Figure 5.4. The emission spectra of solutions (dichloroethane, 20°C, λ_{Ex} = 380 nm) of **CdS–I** (***a***, 0.1 μM) and **CdS–II** (***b***, 0.5 μM). 67

Figure 5.5. The infrared absorption spectra (20°C) of powders of **27** (***a***), **CdS–I–27** (***b***) and **CdS–II–27** (***c***). 68

Figure 5.6. The ultraviolet–visible absorption spectra of solutions (0.1 μM, dichloroethane, 20°C) of **CdS–I** (***a***) or **CdS–I–27** before (***b***) and after (***c***) continuous irradiation (365 nm, 0.4 mW cm^{-2}, 10 min). The evolution of the absorbance at 530 nm (***d***) after irradiation and the associated monoexponential curve-fitting (***e***). ..... ……69

Figure 5.7. The ultraviolet–visible absorption spectra of solutions (0.5 μM, dichloroethane, 20°C) of **CdS–II** (***a***) or **CdS–II–27a** before (***b***) and after (***c***) continuous irradiation (562 nm, 0.3 mW cm^{-2}, 15 min). The evolution of the absorbance at 531 nm (***d***) after irradiation and the associated monoexponential curve-fitting (***e***).. ..... ……71

Figure 6.1. The Absorption spectra of solution of **20** (1mM, 0.1 M KCl_{aq}, 20 ^{o}C) recorded before (a) and after (b) electrolysis at -1.5 V, relative to the platinum pseudo-reference electrode. 74

Figure 6.2. The absorption spectrum (***a***) of CdSe–ZnS core–shell quantum dots (2 μM, $CHCl_3$, 20°C) and the emission spectra ($\lambda_{ex.}$ = 350 nm) of the same solution recorded before (***b***) and after (***c***) the addition of the chloride salt of the bipyridinium dication **28** (85 μM). 76

Figure 6.3. The absorption spectra of a solution ($CHCl_3$, 20°C) of CdSe–ZnS core–shell quantum dots (2 μM), the chloride salt of **28** (85 μM) and triethanolamine (100 mM) recorded before (***a***) and after (***b***) continuous irradiation (562 nm, 0.2 mW cm^{-2}, 30 min) and the corresponding difference spectrum (***c***). The evolution of the absorbance at 397 nm during continuous irradiation (***d***) and the subsequent exposure to air (***e***)…… 77

Figure 6.4. The excitation of a CdSe–ZnS core–shell quantum dot causes the transfer of an electron to the bipyridinium dication **28**. A second electron transfer step from triethanolamine (TEA) to the nanoparticle fills the photogenerated hole. ..... ……..78

Figure 6.5. The excitation of a CdSe–ZnS core–shell quantum dot on quartz causes the transfer of an electron to the bipyridinium dication **29**. A second electron transfer step from triethanolamine (TEA) to the nanoparticle fills the photogenerated hole…….. 79

Figure 6.6. The absorption spectra of a film, prepared from CdSe–ZnS core–shell quantum dots and the chloride salt of **29**, deposited on quartz and in contact with a solution of triethanolamine (100 mM, MeCN, 20°C) recorded before (***a***) and after (***b***) continuous irradiation (562 nm, 0.2 mW cm^{-2}, 8 min) and the corresponding difference spectrum (***c***). The evolution of the absorbance at 397 nm during continuous irradiation (***d***) and the subsequent exposure to air (***e***). 80

CHAPTER 1

LUMINESCENT CHEMOSENSORS BASED ON SEMICONDUCTOR QUANTUM DOTS

1.1. Introduction

Semiconductor quantum dots are inorganic nanoparticles with unique photophysical properties. In particular, their huge one- and two-photon absorption cross sections, tunable emission bands and excellent photobleaching resistances are stimulating the development of luminescent probes for biomedical imaging and sensing applications. Indeed, electron and energy transfer processes can be designed to switch the luminescence of semiconductor quantum dots in response to molecular recognition events. On the basis of these operating principles, the presence of target analytes can be transduced into detectable luminescence signals. In fact, luminescent chemosensors based on semiconductor quantum dots are starting to be developed to detect small molecules, monitor DNA hybridization, assess protein–ligand complementarities and test enzymatic activity and probe pH distributions. With all these features, quantum dots have also rapidly emerged as potential new fluorescent probes for the imaging of biological samples. Indeed they offer many advantages over conventional flourophore for imaging techniques such as two-photon or time-gated microscopy, while allowing multicolor, long term and high sensitivity fluorescence imaging. A wide range of surface functionality can be fabricated to provide flexible routes to the creation of different sensing and imaging aims. Although fundamental research is still very much needed to

understand further the fundamental factors regulating the behavior of these systems and refine their performance, it is becoming apparent that sensitive probes based on semiconductor quantum dots will become invaluable analytical tools for a diversity of applications in biomedical research.

1.2. Luminescent Chemosensors

Fluorescence microscopy and spectroscopy have become invaluable analytical tools in biomedical research.[1] A wealth of imaging and sensing protocols for *in vitro* and *in vivo* applications has been devised on the basis of these convenient techniques. The amazing development of these methods over the past few decades has been, and continues to be, mainly a result of the tremendous progress in the basic understanding of the photophysical and recognition properties of organic molecules. Indeed, sensitive compounds with fluorescent responses tailored to specific analytes can now be designed and synthesized relying on established strategies.[2-8] Molecular recognition events, coupled to either electron or energy transfer, are generally the mechanisms of choice to operate these fluorescent chemosensors. In fact, these processes can be engineered to switch the fluorescence lifetimes and quantum yields of organic dyes. Under these conditions, the presence of target analytes is effectively transduced into detectable fluorescence signals. For example, electron transfer from a receptor to a fluorophore or energy transfer in the opposite direction (Figure 1.1) can be designed to quench the fluorescence of the emissive component.

The molecular or supramolecular association of the receptor with a complementary analyte, however, prevents the electron and energy transfer processes. As a result, the receptor–analyte binding is transduced into a significant enhancement in the fluorescence of the emissive component.

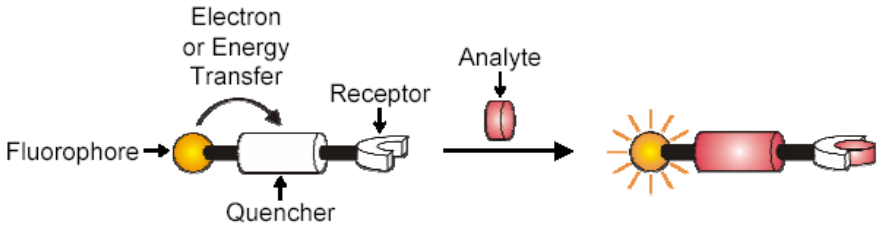

Figure 1.1. The association of the receptor with a complementary analyte can suppress either an electron or an energy transfer process and switch the fluorescence of the adjacent fluorophore on.

1.3. Semiconductor Quantum Dots

1.3.1. History

Decades of investigations on the photophysical properties of organic dyes in conjunction with the sophistication of modern chemical synthesis have delivered an impressive number of sensitive fluorophores.[2-8] However, the high radiation intensities required to excite organic chromophores, their poor photobleaching resistances and short fluorescence lifetimes are serious drawbacks in practical imaging and sensing applications. Recent investigations suggest that the photophysical properties of certain semiconductor nanoparticles, the so-called quantum dots (QDs), can offer valuable solutions to the problems associated with conventional organic dyes.[9-21] The breakthrough in synthesizing high-quality colloidal semiconductor quantum dots can be traced to the work of Bawendi et al.[22] They showed that narrowly dispersed (8–11%)

highly crystalline CdSe QDs could be synthesized at high temperatures using a mixture of organometallic precursors and trioctyl phosphine oxide (TOPO (**1** in Figure 1.2)) growth solvent ligand.[22] This same reaction can be used to further overcoat the CdSe core with a layer of wider bandgap semiconductor (Figure 1.2) such as ZnS and CdS.[14b,23,24] This secondary layer passivates surface traps and increases the photoluminescent yield [24-26]. Peng et al. made further refinements to this scheme by using less pyrophoric precursors such as CdO and $Cd(Ac)_2$.[27] To date, CdSe–ZnS core-shell QDs remain among the best available for almost all biological applications.[23,28-30] Other QDs including ZnS, CdS, CdTe and PbSe with emissions ranging from the UV to the IR have also been synthesized with similar experimental procedures, however these nanoparticles are not as common as CdSe nanoparticles in biological assays.[28-30]

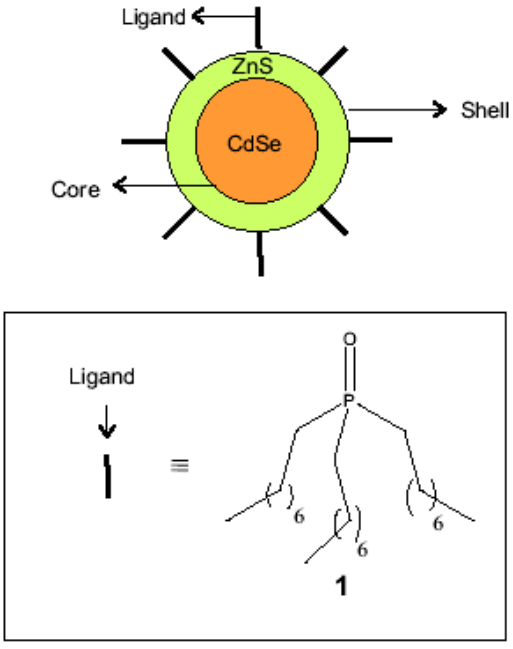

Figure 1.2. TOPO coated CdSe–ZnS core-shell quantum dots.

1.3.2. Photophysical Properties of Quantum Dots

Table 1 compares the photophysical parameters associated with a representative collection of organic fluorophores and CdSe–ZnS quantum dots with a core diameter (*d* in Table 1) of 2.9 nm. The molar extinction coefficient (ε in Table 1.1) for the band-gap absorption of these particular quantum dots[31] is comparable to those of the organic dyes at their excitation wavelengths (λ_{Ex} in Table 1.1).[32-33] The broad absorption of the quantum dots (Figure 1.3), however, extends continuously from the visible to the ultraviolet region with a significant enhancement in ε. As a result, they can efficiently be excited over a wider selection of wavelengths. In addition, the luminescence lifetime (τ in Table 1.1) of the quantum dots[34] is approximately one order of magnitude greater than those of the organic counterparts.[35-38] Thus, the auto-fluorescence of biological samples can effectively be filtered with time-gated measurements in the case of these inorganic luminophores.

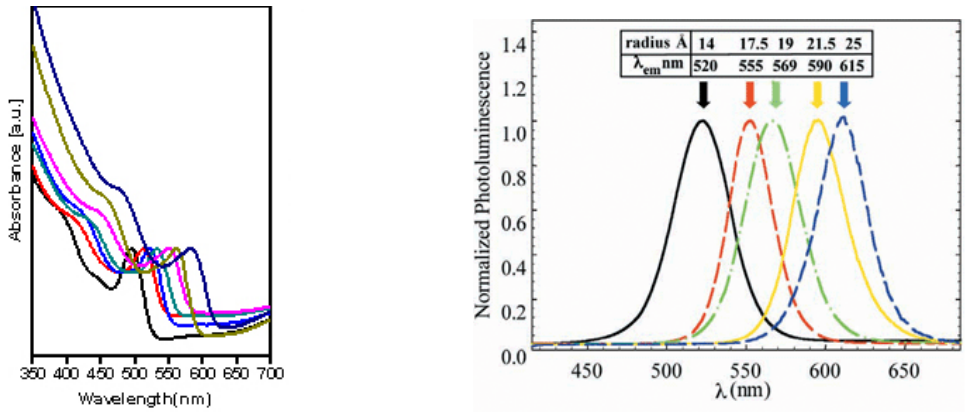

Figure 1.3. Absorption and emission spectra of different size of CdSe–ZnS quantum dots.

Furthermore, the width (Δλ in Table 1.1) at half maximum for the emission band of the quantum dots[34] is smaller than those of the organic dyes. In addition, the narrow

emission band of the inorganic nanoparticles can carefully be positioned across the visible and near-infrared regions by regulating their elemental compositions and physical dimensions (Figure 1.4). It follows that multiple signals can be probed in parallel with pools of slightly different quantum dots.

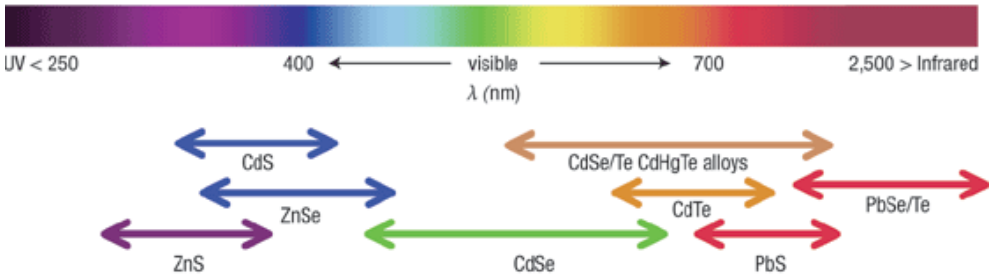

Figure 1.4. Emission ranges of quantum dots with different elemental compositions and sizes.

Finally, the two-photon absorption cross section (α) of the quantum dots[39] (α in Table 1.1) is several orders of magnitude greater than those of the organic fluorophores[40-42] and, therefore, permits unprecedented penetration depths. Moreover, quantum dots can be passivated with protective shells to ensure outstanding photobleaching resistances. It is important to stress, however, that most passivation strategies tend to make the physical dimensions of the overall nanostructures significantly greater than those of the organic dyes. In any case, it is becoming apparent that the development of luminescent probes based on quantum dots can eventually overcome the inherent limitations of organic fluorophores, especially in the context of biomedical imaging applications.[30,43-58] As a result, sensing schemes to signal specific analytes with quantum dots are starting to be developed on the basis of electron[34,59-63] and energy[35,64-83] transfer process. These

mechanisms resemble the operating principles of conventional fluorescent chemosensors[2-8] (Figure 1.1) and are based on the conjugation of the luminescent inorganic nanoparticles with sensitive organic ligands. The communication between the inorganic and organic components, in the form of an exchange of either electrons or energy upon excitation, then dictates the emissive behavior of the resulting assemblies.

Table 1.1. Geometrical and photophysical parameters of typical organic dyes and quantum dots.

	ε [a] (mM^{-1} cm^{-1})	α [b] (GM)	λ_{Ex} [c] (nm)	λ_{Em} [d] (nm)	Δλ [e] (nm)	τ [f] (ns)	*d* [g] (nm)
Fluorescein	83	54	492	515	44	4.0	1.2
Oregon Green 488	81	—	491	515	58	4.1	1.3
Cy3	150	—	548	562	50	0.2	1.8
Rhodamine 6G	95	6	550	576	45	4.1	1.6
Texas Red	116	—	583	603	37	4.2	1.6
Cy5	250	400	646	664	40	2.1	2.1
CdSe–ZnS	98	47,000	430	552	31	17.1	2.9

[a] Molar extinction coefficients of the organic dyes (ref. 32 and 33) and of the quantum dots (ref. 31) at λ_{Ex}. [b] Two-photon absorption cross section of fluorescein at 800 nm (ref. 41), of rhodamine 6G at 798 nm (ref. 42), of Cy5 at 820 nm (ref. 43) and of the quantum dots at 900 nm (ref. 39). [c] Excitation wavelengths of the organic dyes (ref. 32 and 33) and wavelength for the band-gap absorption of the quantum dots (ref. 34). [d] Emission wavelengths of the organic dyes (ref. 32 and 33) and quantum dots (ref. 34). [e] Width at half maximum of the emission bands for the organic dyes (ref. 32) and quantum dots (ref. 34). [f] Luminescence lifetimes of the organic dyes (ref. 32, 35–38) and average luminescence lifetime of the quantum dots (ref. 35). [g] Length of the organic dyes estimated on their AM1-optimized geometries using GaussView 2.1 (Gaussian, Inc., Pittsburgh PA, 1998) and core diameter of the quantum dots (ref. 35).

1.4. Semiconductor Quantum Dots Chemosensors

1.4.1. Chemosensors Based on Electron Transfer Mechanism

Semiconductor quantum dots can be reduced or oxidized at relatively moderate potentials, which tend to vary slightly with the physical dimensions of the

nanoparticles.[84-86] For example, Table 1.2 shows the dependence of the reduction (E_{Red} in Table 1.2) and oxidation (E_{Ox} in Table 1.2) potentials of CdSe quantum dots on their diameter.[86] Furthermore, quantum dots can exchange electrons with complementary acceptors or donors upon excitation.[20b]

Table 1.2. Redox potentials of CdSe quantum dots relative to the ferrocene/ferrocenium couple.

d [a] (nm)	E_{Red} [b] (V)	E_{Ox} [c] (V)
3.0	–1.29	+0.94
4.3	–1.27	+0.80
6.5	–1.16	+0.79

[a] Diameter. [b] Reduction potential (ref. 86). [c] Oxidation potential (ref. 86).

These processes quench effectively the nanoparticle luminescence and, thus, can be exploited to regulate the emissive behavior of a quantum dot.[20b,84,87] In particular, molecular recognition events can be designed to activate or suppress a photoinduced electron transfer process switching the luminescence off or on respectively. Under these conditions, the supramolecular association of a target analyte is transduced into a significant change in luminescence intensity.[34,59–63] For example, the recognition properties of a maltose-binding protein (MBP) can be engineered to switch the luminescence of a conjugated quantum dot on the basis of photoinduced electron transfer.[59] Specifically, a chimeric MBP-metallothionein protein with surface cysteine residues can be conjugated to ruthenium donor (**2** in Figure 1.5), after the nucleophilic attack of a thiol group of the former to the maleido residue of the latter. The modified protein can be attached to CdSe nanoparticles capped with 6-mercaptohexadecanoate,

after the adsorption of the thiol groups of the protein on the surface of the quantum dot. In the resulting assembly, the ruthenium donor **2** is sufficiently close to the surface of the quantum dot to effectively transfer an electron to the nanoparticle upon excitation (Figure 1.5).

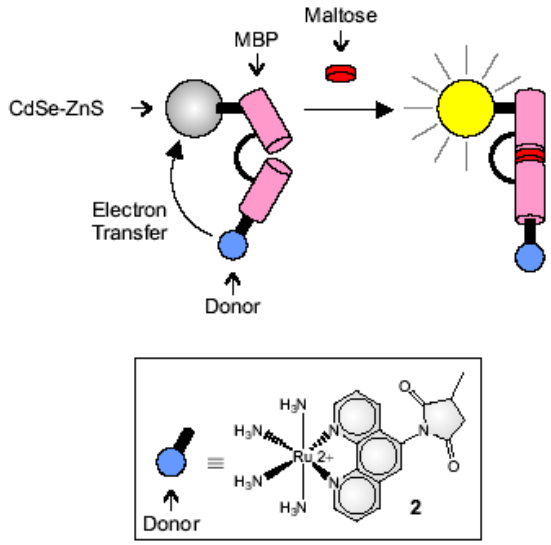

Figure 1.5. The association of MBP with maltose moves the ruthenium donor **2** away from the CdSe quantum dot, preventing the electron transfer process and switching the luminescence of the nanoparticle on.

This process leads to a 5.0-fold decrease in the luminescence quantum yield of the nanoparticle. Upon binding of maltose, the protein changes its conformation significantly, moving the ruthenium donor **2** away from the quantum dot surface. As a result, the electron transfer efficiency decreases with a concomitant 1.4-fold increase in the luminescence quantum yield. Thus, the presence of maltose is transduced into a significant luminescence enhancement on the basis of these operating principles, even although the original emission intensity is not fully restored.

In the system illustrated in Figure 1.5, a molecular recognition event induces a conformational change and increases the separation between an electron donor and a luminescent quantum dot.[59] An alternative approach to signal recognition events is shown schematically in Figure 1.6.[88] In this instance, CdSe–ZnS core–shell quantum dots were functionalized with 1-(2-mercapto-ethyl)-3-phenyl-thiourea receptor in the fluorophore–spacer–receptor format typical of Photoinduced Electron Transfer (PET) based organic dye sensors.

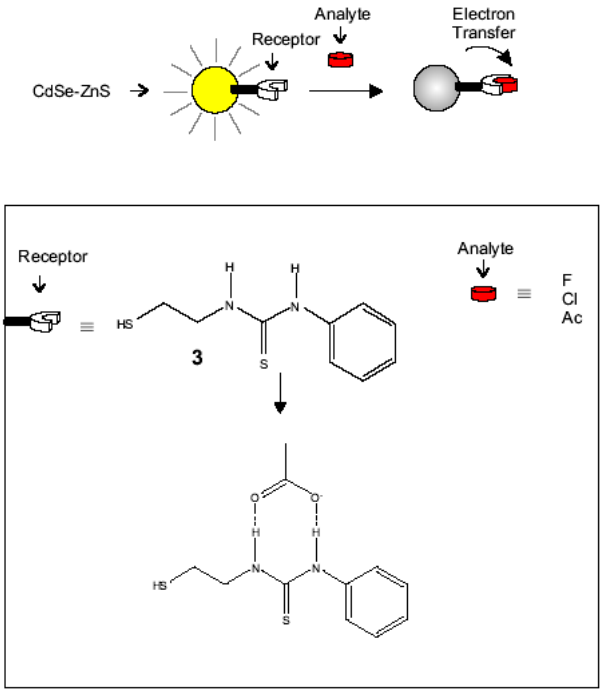

Figure 1.6. The association of the analyte with receptor on the surface of CdSe–ZnS particles can quench luminescence of CdSe–ZnS particles by allowing electron transfer from excited particles to receptor-analyte compex.

The resulting system was tested for selectivity toward the tetrabutylammonium salts of fluoride, chloride, bromide, hydrogen sulfate and acetate. Addition of fluoride, chloride and acetate ions resulted in an approximate 90% quenching of the original

fluorescence intensity, while bromide and hydrogen sulfate had almost no effect. The observed quench was attributed to an increase in the reduction potential of the receptor **3** upon anion binding resulting in an increase in electron transfer process from the excited particles to the receptor and a concomitant reduction in fluorescence intensity. The selectivity and sensitivity were comparable to an analagous organic dye based sensor where a similar receptor was bound to an anthracene fluorophore.[89] Thus a modular approach is evident where a receptor used in an organic dye based sensor can be adapted and successfully used with quantum dots.

Electron transfer mechanism can be also employed in monitoring enzyme activities. A clever assay to monitor the enzymatic activity of tyrosinase illustrated in Figure 1.7 was developed by using tyrosine conjugated CdSe-ZnS quantum dots.[90]

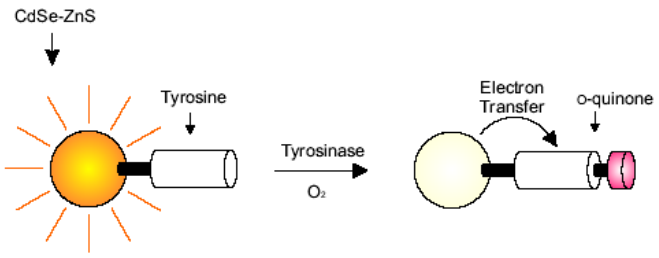

Figure 1.7. Enzymatic activity of tyrosinase oxidizes tyrosine to o-quinone on the surface of CdSe–ZnS and resulting o-quinone quenches luminescence by electron transfer.

Tyrosinase catalyzes the oxidation of tyrosine (**4** in Figure 1.8) to L-DOPA (**5** in Figure 1.8) that is subsequently oxidized to respective o-quinone (**6** in Figure 1.8). o-quinone is expected to quench fluorescence of QDs and provides a path for optical detection of tyrosinase. The emission of QDs is quenched in the presence of tyrosinase and as the exposure to enzymatic conditions is prolonged, 45% quenching occurred. As

the concentration of tyrosinase increased, the quenching efficiency increased. Tyrosinase could be assayed with a sensitivity limit corresponding to 0.2 U of tyrosinase.

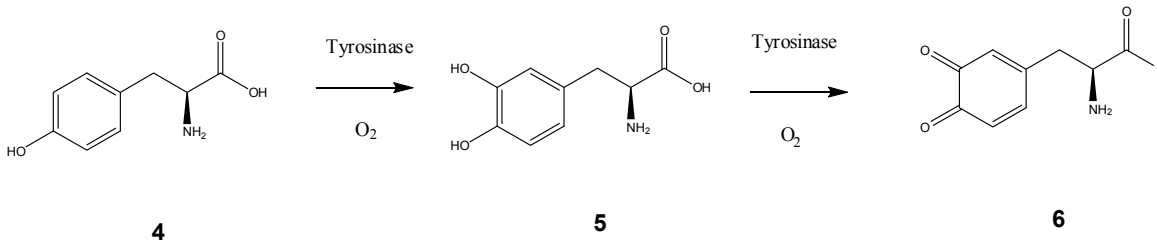

Figure 1.8. Enzymatic transformation of tyrosine into o-quinone.

In order to generalize the application of semiconductor QDs as optical reporters for biocatalytic transformations, a peptide was attached to QDs as illustrated in Figure 1.9.[124] The peptide includes a tyrosine residue that is oxidizable to the respective L-DOPA and *o*-quinone units and, thus, is anticipated to yield the quencher units upon reaction with tyrosinase. Indeed, effieciency of luminescence quenching was 33%. The peptide includes, however, the appropriate amino acid sequence that is cleavable by the proteolytic enzyme thrombin. Thus, the hydrolytic cleavage of the *o*-quinone units by thrombin is anticipated to restore the fluorescence properties of the QDs. The fluorescence intensity was quenched due to the biocatalyzed formation of the *o*-quinone derivative and later treatment with thrombin resulted in removal of quencher from particles and recovery of fluorescence has occurred. Electron transfer quenching mechanism could be employed in enzymatic studies as succesful as in the case of energy transfer.

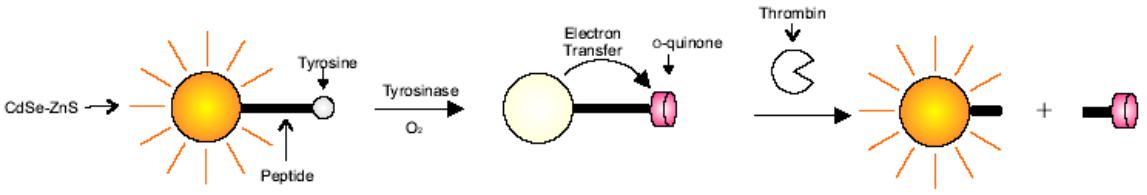

Figure 1.9. Enzymatic activity of tyrosinase oxidizes tyrosine to o-quinone on the surface of CdSe–ZnS and resulting o-quinone quenches luminescence by electron transfer. Luminescence of CdSe–ZnS can be recovered by removal of o-quinone after exposure to thrombin.

1.4.2. Chemosensors Based on Energy Transfer

Semiconductor quantum dots can transfer energy to one or multiple complementary acceptors upon excitation.[47c] The nanoparticle and the acceptor, however, need to be in close proximity and the emission bands of the former must overlap the absorption bands of the latter for energy transfer to occur. Förster showed that FRET efficiency depended on the inverse sixth power of the distance (R) between the two fluorophores (Eq. (1)) and this is the basis of the use of the technique to provide structural information [91]:

$$\boldsymbol{E = (1 + R^6/R_0^6)^{-1}} \quad (1)$$

R_0 is the characteristic Förster radius for a given donor–acceptor pair, which is given by:

$$\boldsymbol{E = 8.8 \times 10^{-28}\, \Phi_D K^2 n^{-4} J(v)} \quad (2)$$

where Φ_D is the fluorescent quantum yield of the donor in the absence of the acceptor, κ^2 is parameter that depends on the relative orientation of the donor and acceptor transition moments, n is the refractive index of the medium, and $J(v)$ is the spectral overlap between donor emission and acceptor absorption. From the Eq. (1) it is clear that for $R = R_0$, the efficiency of FRET is 50%.

Table 1.3 compares the typical Förster radii (R_0 in Table 3) of representative donor–acceptor pairs based on organic dyes[32] and quantum dots.[92-94] In principle, molecular recognition events can be designed to alter the physical separation between a quantum dot and an energy acceptor as well as their spectral overlap. Thus, the efficiency of energy transfer and the luminescence quantum yield of the nanoparticle can be engineered to vary with the supramolecular association of a specific substrate. Under these conditions, the presence of target analytes can be transduced into detectable luminescence signals.[34,65a,66–84]

Table 1.3. Förster radii of typical donor–acceptor pairs.

Donor	*Acceptor*	R_0 [a] (nm)
Fluorescein	Tetramethylrhodamine	5.5
IAEDANS	Fluorescein	4.6
EDANS	Dabcyl	3.3
Fluorescein	Fluorescein	4.4
BODIPY FL	BODIPY FL	5.7
Fluorescein	QSY 7	6.1
Fluorescein	QSY 9	6.1
CdSe–ZnS	Cy3	4.7
CdSe–ZnS	AF 488	6.6
CdSe–ZnS	AF 594	6.1
CdSe–ZnS	AF 680	8.4

[a] Förster radii of the dye–dye pairs (ref. 32) and of the quantum dot–dye pairs (ref. 92-94).

For example, the hybridization of oligonucleotide strands can be monitored on the basis of these operating principles.[67b] In particular, an oligonucleotide strand with a

terminal thiol group at the 5' end can be attached to the surface of CdSe–ZnS core–shell quantum dots (Figure 1.10). In the presence of a complementary strand labeled with Texas Red (**7** in Figure 1.10) at the 3' end, hybridization occurs to generate the corresponding double-stranded DNA. In the resulting assembly, the quantum dot and organic dye are in close proximity. Furthermore, the organic chromophore **7** absorbs in the same region of wavelengths where the inorganic nanoparticle emits. Consistently, energy transfer from the quantum dot to **7** occurs upon excitation of the former with a 2.5-fold decrease in the luminescence intensity of the quantum dot at 580 nm. Furthermore, a new band corresponding to the sensitized fluorescence of the **7** appears in the emission spectrum at 615 nm. Upon exposure of the duplex structure to DNase I, the oligonucleotide strands are cleaved and the **7** moves away from the quantum dot. As a result, the efficiency of energy transfer decreases and a 2.0-fold increase in the luminescence intensity of the quantum dot is observed.

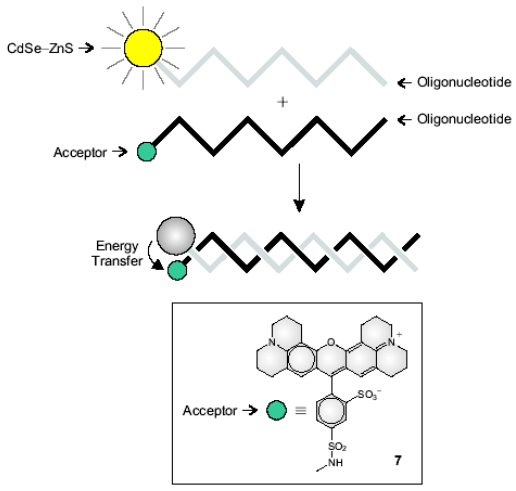

Figure 1.10. The hybridization of an oligonucleotide labeled with a CdSe–ZnS core–shell quantum dot and an oligonucleotide labeled with a complementary acceptor encourages the transfer of energy from the former to the latter with a concomitant luminescence quenching.

Transduction mechanisms based on energy transfer can also be adapted to signal the presence of small molecules. The system illustrated in Figure 1.5 is a representative example of these operating principles in action.[66d] A CdSe–ZnS core–shell quantum dot, coated by dihydrolipoic acid, is conjugated to an antibody able to recognize and bind 2,4,6-trinitrotoluene (TNT) (Figure 1.11). This particular antibody carries an oligohistidine residue, which binds the zinc cations on the surface of the nanoparticle.

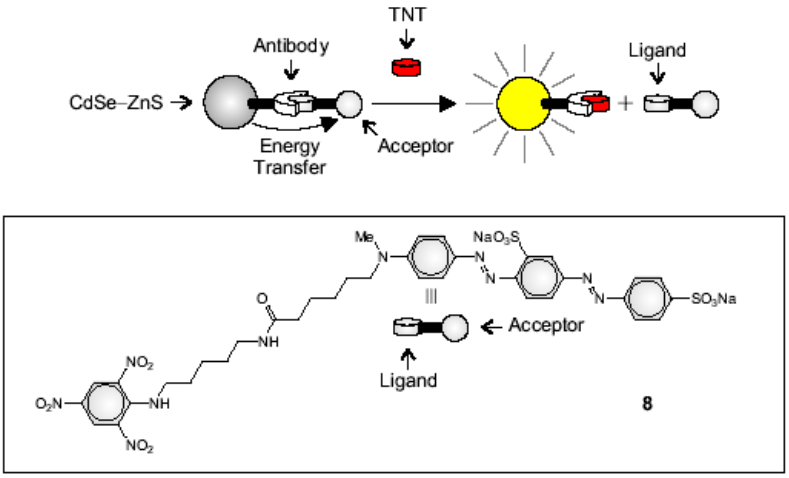

Figure 1.11. The association of TNT with the antibody moves the acceptor **8** away from the quantum dot, preventing the energy transfer process and switching the luminescence of the nanoparticle on.

The addition of compound **8** results in the association of its 2,4,6-trinitrophenyl appendage with the antibody–nanoparticle assembly. The extended π-system at the other end of compound **8** absorbs in the same range of wavelengths where the quantum dot emits. As a result, the excited quantum dot transfers energy to this particular chromophore, which is not emissive and dissipates the transferred energy nonradiatively.

Consistently, a 2.5-fold decrease in the luminescence intensity of the quantum dots is observed upon addition of **8**. In the presence of TNT, however, the 2,4,6-trinitrophenyl appendage of **8** is displaced from the recognition site of the antibody and the conjugated energy acceptor moves away from the quantum dot. As a consequence, the energy transfer process is suppressed and, in fact, the luminescence of the nanoparticle increases significantly with the concentration of TNT. Thus, this mechanism offers the opportunity to signal the presence of TNT with a noticeable enhancement in luminescence, relying on the combination of energy transfer and competitive binding events.

Similar processes can also be exploited to probe enzymatic activity. For example, a CdSe–ZnS core–shell quantum dot can be connected to a peptide with a terminal rhodamine dye (**9** in Figure 1.12).[82]

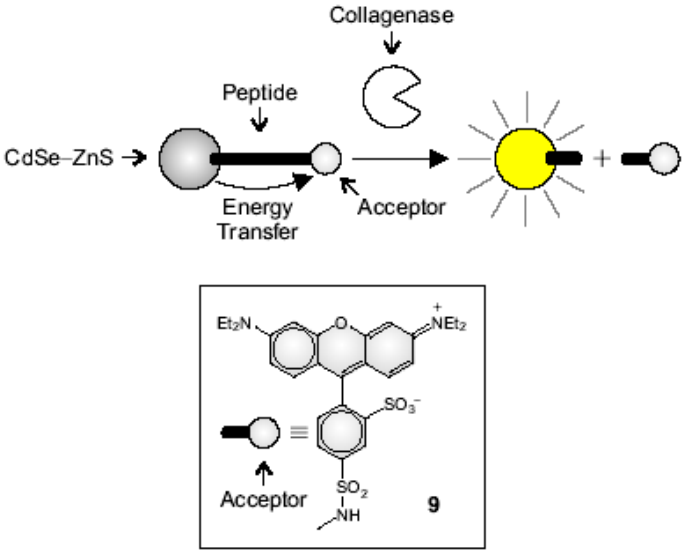

Figure 1.12. Collagenase cleaves the peptide bridging the CdSe–ZnS core–shell quantum dot to the rhodamine acceptor **9**, suppressing the energy transfer process and switching the luminescence of the nanoparticle on.

In the resulting assembly, the local excitation of the inorganic nanoparticle is followed by efficient energy transfer to the adjacent organic dye **9**. As a result, the corresponding emission spectrum shows a band at 545 nm for the quantum dot and one at 590 nm for the rhodamine acceptor. The addition of collagenase, however, results in the enzymatic cleavage of the peptide bridge with the separation of the energy donor and acceptor. Consistently, the energy transfer process is effectively suppressed, the luminescence intensity at 545 nm increases and that at 590 nm decreases. Thus, the enzymatic cleavage of the peptide linker is transduced into detectable luminescence signals on the basis of these operating principles.

Quantum dots can also serve as an effective protein nanoscaffolds and donors for targeting analytes such as maltose by using Maltose Binding Protein (MBP).[66b] CdSe-ZnS nanoparticles could be used as biosensors through a two-step energy transfer mechanism thus avoiding inherent donor–acceptor distance limitations (Figure 1.13). In the system illustrated in Figure 1.10, Cyanine-3 dye (Cy3 in Figure 1.13) labeled MPB was adsorbed on the surface quantum dots (QD 530 in Figure 1.13) via histidine groups. An energy transfer between Cy3 and quantum dots occured. β-cyclodextrin (β-CD in Figure 1.13) is known to bind to the MBP central binding pocket. Binding of cyanine-3.5(Cy3.5) dye labeled β-CD to MBP central binding pocket yielded another energy transfer from Cy3 to Cy3.5. Excitation of the QD results in energy transfer from QD to MBP-Cy3, through β -CD-Cy3.5, overcoming the low direct QD-Cy3.5 energy transfer. When QD is exicited, Cy3.5 emission could be observed. Maltose competitively binds to MBP central binding pocket thus removes β-CD from MBP. Addition of maltose cause termination of Cy3-Cy3.5 energy transfer since cy3.5 is not in the vicinity of Cy3. After

addition of maltose, Cy3 emission was enhanced whereas the emission of Cy3.5 decreased.

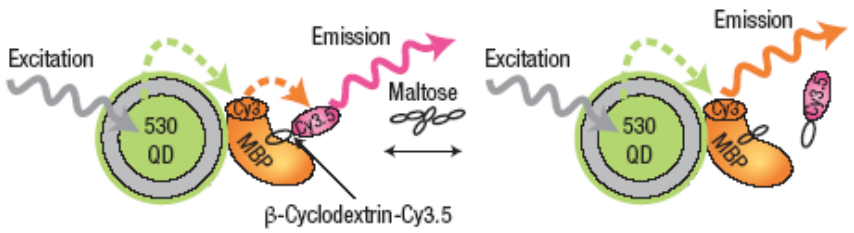

Figure 1.13. Demonstration of improved energy transfer derived from arraying multiple acceptor dyes around a single QD donor acting as a protein scaffold.

1.5. Conclusions

Electron and energy transfer processes can be designed to switch the luminescence of semiconductor quantum dots. In particular, either electron acceptors or electron donors can be attached to the surface of these inorganic nanoparticles, relying on a diversity of experimental protocols. The excitation of the quantum dots in the resulting assemblies then results in the effective exchange of electrons with a concomitant luminescence quenching. The supramolecular association of target analytes can be engineered to alter the physical separation between the luminescent nanoparticle and the quencher. Under these conditions, the recognition of the analyte is transduced into a significant luminescent enhancement. Similarly, chromophores able to absorb radiations in the same range of wavelengths where quantum dots emit can also be attached to the surface of these inorganic nanoparticles. The local excitation of the inorganic component is then followed by efficient energy transfer with a concomitant quenching of the nanoparticle

fluorescence. Once again, molecular recognition events can be designed to alter either the physical separation between the emissive nanoparticle and the energy acceptor or the degree of spectral overlap between the emission bands of the former and the absorption bands of the latter. As a result, the supramolecular association of a target analyte is transduced into a significant luminescent enhancement. Finally, electron and energy transfer mechanisms can be designed to operate within the same nanostructured assembly and signal the recognition of a specific substrate with a detectable luminescence signal. Indeed, a number of systems based on semiconductor quantum dots and these operating principles have already been designed to detect small molecules, monitor DNA hybridization, assess protein–ligand complementarities, test enzymatic activity and probe pH distributions. These fascinating systems might well evolve into valuable analytical tools for biomedical imaging and sensing applications. It is important to note, however, that fundamental research aimed at elucidating the properties of these systems is still very much needed to improve the performance of these family of luminescent chemosensors. Indeed, the development of valuable strategies to impose aqueous solubility on semiconductor quantum dots, while preserving their photophysical properties and ensuring their long term stability, is somewhat challenging given the stringent distance requirements associated with electron and energy transfer process. Furthermore, the long-term effect of these inorganic nanoparticles and their ligands on living organisms are still rather unclear. Nonetheless, the unique photophysical properties of semiconductor quantum dots are extremely promising in the context of the development of luminescent probes and it is becoming apparent that these inorganic luminophores can

complement, if not replace, conventional organic fluorophores in a diversity of practical applications.

CHAPTER 2

pH–SENSITIVE QUANTUM DOTS

2.1. Summary

We have identified a strategy to switch the luminescence of CdSe–ZnS core–shell quantum dots with chemical stimulations. In particular, we have designed a pH-sensitive organic ligand for these inorganic nanoparticles. This heterocyclic compound can be adsorbed on the surface of inorganic nanoparticles and it can switch from a neutral to an anionic state in the presence of base and from a neutral to a cationic form after the addition of acid on the surface of quantum dots. These transformations are fully reversible and are accompanied by significant changes in oxidation potential and absorbance. As a result, the efficiency of electron transfer from the ligand to the excited nanoparticle and of energy transfer in the opposite direction varies with the state of the organic component. Indeed, the luminescence quantum yield of these nanostructured assemblies decreases monotonically with an increase in pH as a result of electron transfer from ligand to quantum dots and energy transfer from quantum dots to ligand and furthermore increases with the decrease in the pH as a result of hindrance of electron transfer from ligand to quantum dots. In fact, this mechanism can be exploited to probe the pH of aqueous solutions with luminescent measurements. In principle, the structural design of the organic ligand can be engineered to respond to environmental stimulations or target analytes with similar transformations. Thus, a new generation of luminescent

chemosensors based on the unique photophysical properties of semiconductor quantum dots can eventually emerge from these results.

2.2. Fluorescent pH Sensors

Recent years have seen growing interest in the research and development of fluorescence pH sensors for acidity monitoring especially in biological fluids and cells, medicine analyses, environmental monitoring and other fields, in which the fluorescence pH chemical sensors play a significant role for the pH value can provide important information of the object characters. Many fluorescence pH sensors have been reported in the literature. These sensors are based on the measurement of fluorescence intensity [95-104] fluorescence intensity ratio at two emission wavelengths [105-107] or fluorescence lifetime [108,109]. The most widely used techniques are the measurements of fluorescence intensity. Lifetime-based measurements are superior because lifetime is not affected by intensity. However, the complexity and demands on instrumentation have restricted their wide application. The measurement of the ratio of fluorescence intensities at two different wavelengths, namely the ratiometric detection, provides an alternative approach to circumvent the problems associated with intensity-based measurements. One of the conceivable means for this purpose is to use a polymeric linker between donor and acceptor fluorophore in such a way that a pH-induced coil-globule transition of selected polymer linker gives rise to a drastic change in the donor-acceptor distance. As a result, the FRET shows on-and-off characteristics around a transition pH, where the coil-globule transition of polymer linker occurs. Another possible way of sensing pH by FRET technique utilizes the pH dependence of absorption properties of acceptor dye.[110] With

the change pH, the change in the overlap integral of donor-acceptor pair translates into different FRET efficiency thus allowing quantification of pH.

The extension of these clever mechanisms can be expanded to quantum dots to develop a new generation of luminescence chemosensors with superior luminescent properties. Indeed, viable sensing protocols based on the exchange of either electrons or energy between quantum dots and appropriate organic ligands are now starting to be developed. [110-112] In this context, we have developed a sensor system, which includes semi-conductor quantum dots and a chromogenic unit which can modulate the emission of particles by a pH stimulus.

2.3. Results and Discussion

2.3.1. Design

Some chromogenic molecules are able to change their ability to absorb electromagnetic radiation in response to chemical stimulations.[112-115] These heterocyclic compounds incorporate a [1,3]oxazine ring at their core. Upon addition of base, the [1,3]oxazine ring opens to generate a phenolate chromophore. This process is accompanied by the appearance of an intense band in the visible region of the absorption spectrum. In principle, this chromogenic transformation can be exploited to regulate the luminescence of complementary quantum dots on the basis of energy transfer. Indeed, the elemental composition and diameter of these inorganic nanoparticles can be adjusted to ensure an optimal overlap between their emission band and the developing absorption of our chromogenic [1,3]oxazines. If the inorganic and organic components are then

constrained in close proximity, the chromogenic transformation of the latter can be exploited to switch off the luminescence of the former (Figure 2.1). Thus, the resulting system should be able to sense the presence of base with significant changes in luminescence intensity.

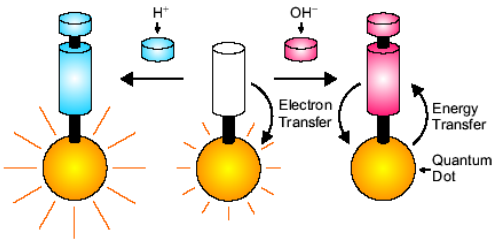

Figure 2.1. Design of pH–sensitive quantum dot based chemo sensor.

In order to explore these operating principles, I have envisaged the possibility to modify the structural design of our [1,3]oxazines and encourage their adsorption on the surface of the inorganic nanoparticles. In this chapter, I summarize the design, synthesis and properties of these chromogenic organic ligands, as well as their attachment to CdSe–ZnS core–shell quantum dots and the photophysical properties of the resulting nanostructured assemblies.

2.3.2. Synthesis

The affinity of the dithiolane ring for CdSe–ZnS core–shell quantum dots can be exploited to encourage the adsorption of organic compounds on the surface of these particular nanoparticles.[113a] As a result, we have envisaged the possibility of appending an aliphatic tail terminated by a dithiolane ring to one of chromogenic [1,3]oxazines relying on an ester linkage. In particular, we have designed the target ligand **15**, its model **13** and prepared these compounds starting from the 4-nitrophenylazophenol (**10**)

and the indoles **12** and **13** (Figure 2.2). Specifically, the bromination of **10** with PBr_3 in the presence of Et_3N and the reaction of the resulting bromide with either **11** or **12** *in situ* gives the [1,3]oxazine **13** or **14** respectively. The esterification of **14** with (±)-α-lipoic acid in the presence of *N*,*N*'-dicyclohexylcarbodiimide (DCC) and 4-dimethylaminopyridine (DMAP) then yields the target molecule **15**.

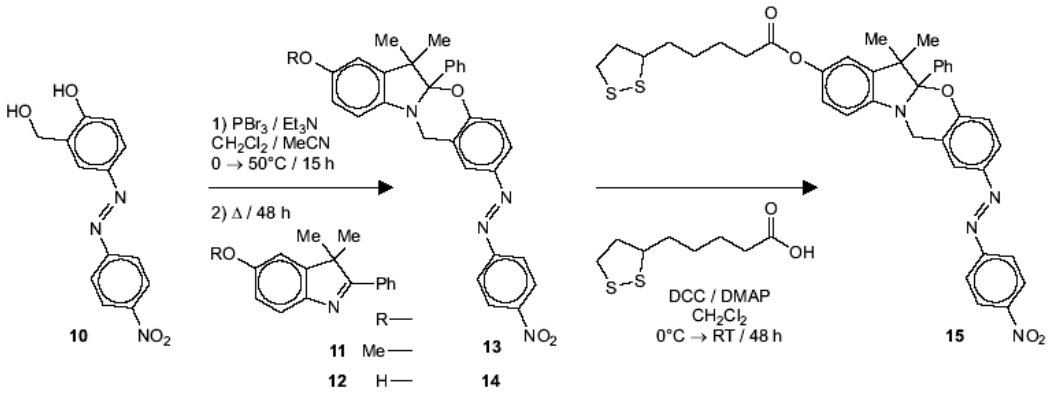

Figure 2.2. Synthesis of the model compound **13** and the target ligand **15**.

2.3.3. ^{1}H NMR Spectroscopy

The addition of Bu_4NOH to a solution of **13** encourages the opening of its [1,3]oxazine ring with the formation of the hemiaminal (**13-HA** in Figure 2.3). Both compounds incorporate a chiral center in position 2 of their indole fragments. As a result, the two protons of the adjacent methylene group are diastereotopic and give rise to an AB system in the corresponding ^{1}H NMR spectra (***a*** and ***b*** in Figure 2.4). However, this set of resonances shifts from 4.64 to 4.00 ppm with the transformation of **13** into **13-HA**. The addition of CF_3CO_2H to a solution of **13** also opens the [1,3]oxazine ring, but generates the indolium **13-IN** instead (Figure 2.4). This process converts the chiral sp^3 center of **13** into the achiral sp^2 atom of **13-IN**. Thus, the two diastereotopic methylene

protons of **13** become homotopic in **13-IN**. Consistently, the AB system observed in the spectrum of **4-OX** is replaced by a singlet in that of **13-IN** (***a*** and ***c*** in Figure 2.4).

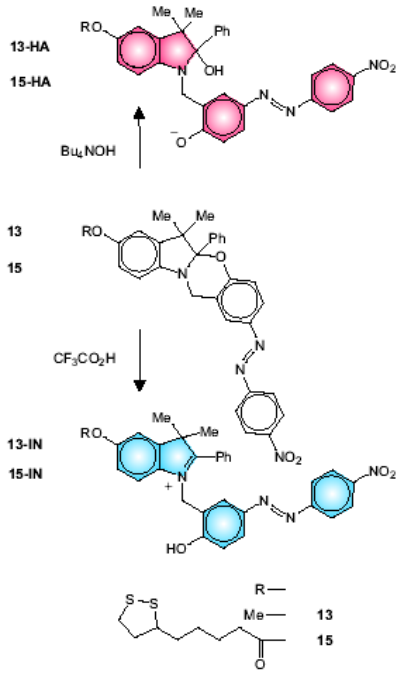

Figure 2.3. Transformations of **13** and **15** upon addition of base or acid.

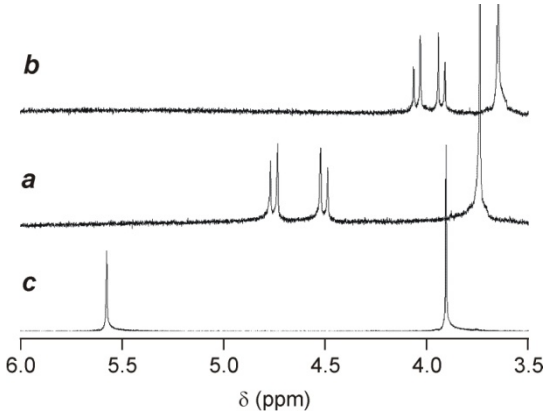

Figure 2.4. ^{1}H-NMR spectra (20 mM, CD_3CN, 20ºC, 500 MHz) of **13** before (***a***) and after the addition of either Bu_4NOH (3 eq., ***b***) or CF_3CO_2H (5 eq., ***c***).

Furthermore, the chemical shift for the methylene protons increases from 4.64 to 5.57 ppm with the transformation of **13** into **13-IN**, in agreement with a decrease in electron density on the adjacent nitrogen atom.

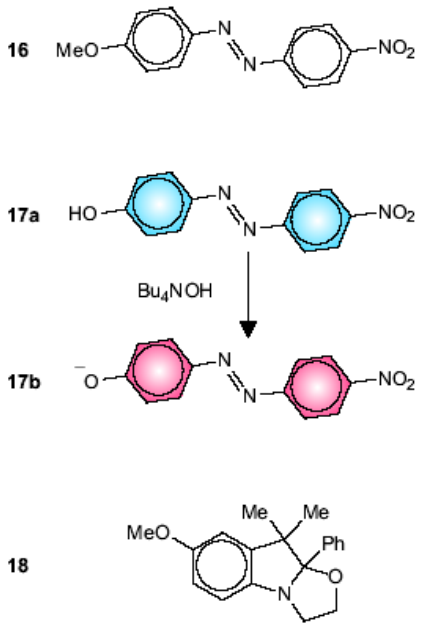

Figure 2.5. Model compounds **16**, **17a**, **17b** and **18**.

2.3.4. Absorption Spectroscopy

The opening of the [1,3]oxazine ring of **13** under basic conditions converts its phenoxy group into the phenolate chromophore of **13-HA**. In fact, this transformation causes significant changes in the ultraviolet and visible regions of the absorption spectrum. In particular, the spectrum of **13** shows a band at 376 nm (***a*** in Figure 2.6), which is essentially coincident with the absorption of **16** (Figure 2.4, ***d*** in Figure 2.6). This band shifts to 567 nm (***b*** in Figure 2.6) with the formation of **13-IN** to resemble the absorption of **17b** (Figure 2.4, ***e*** in Figure 2.6). Instead, the transformation of **13** into **13-**

IN converts the phenoxy group into a phenol chromophore similar to **17a** (Figure 2.5), which absorbs in the ultraviolet region (***f*** in Figure 2.6). In fact, the spectrum of **13-IN** shows a band at 360 nm (***c*** in Figure 2.6). Thus, only one of the three interconvertible states **13**, **13-HA** and **13-IN** absorbs significantly in the visible region.

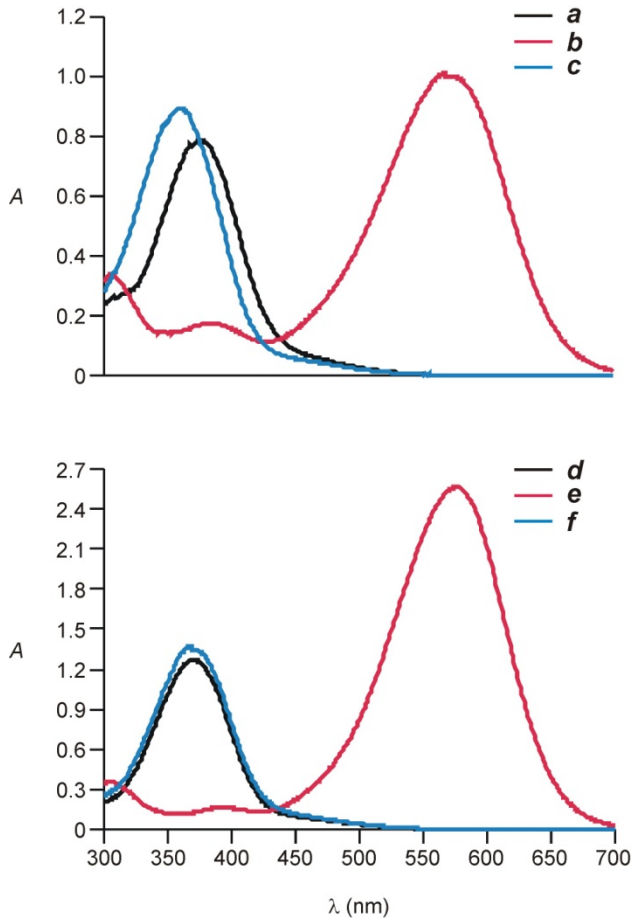

Figure 2.6. Absorption spectra (0.1 mM, MeCN, 20ºC) of **13** before (***a***) and after the addition of either Bu_4NOH (100 eq., ***b***) or CF_3CO_2H (16 eq., ***c***). Absorption spectra (0.1 mM, MeCN, 20ºC) of **16** (***d***) and of **17a** before (***e***) and after the addition of Bu_4NOH (4 eq., ***f***).

Specifically, the 4-nitrophenylazophenolate chromophore of **13-IN** absorbs in the range of wavelengths where CdSe–ZnS core–shell quantum dots with a core diameter of ca. 2.9

nm emit. Therefore, this compound can in principle accept energy from the excited quantum dots, if the two components are constrained in close proximity.

2.3.5. Electrochemistry

Diverse electron acceptors and donors have been observed to exchange electrons with the CdSe core of core–shell quantum dots upon excitation despite the presence of an insulating shell around it.[62,63b,64] In particular, tertiary amines can transfer electrons to the emissive core or CdSe–ZnS nanoparticles upon excitation with a concomitant luminescence quenching.[116] Thus, the relatively electron rich nitrogen atom of the indole fragment of **15** can in principle donate electrons to these particular inorganic nanoparticles. Consistently, the cyclic voltammogram of the model **13** shows an oxidation wave at +0.88 V vs. Ag/AgCl (***a*** in Figure 2.7). This wave is similar to that of the model **18** (Figure 2.4, ***d*** in Figure 2.7) and, therefore, can be assigned to the oxidation of the indole fragment of **13**. Upon addition of Bu_4NOH, **13** is converted into **13-HA** and the oxidation wave moves to +0.48 V (***b*** in Figure 2.7) and becomes similar to that of **17b** (***e*** in Figure 2.7). Instead, the transformation of **13** into **13-IN** shifts the oxidation potential in the opposite direction. Indeed, the oxidation wave moves to +1.35 V (***c*** in Figure 2.6) after the addition of CF_3CO_2H and resembles that of **8a** (***d*** in Figure 2.7). Thus, these changes in oxidation potential suggest that the ability of the organic ligand **15** to transfer electrons to CdSe–ZnS core–shell quantum dots upon excitation should increase after the addition of base and decrease after the addition of acid.

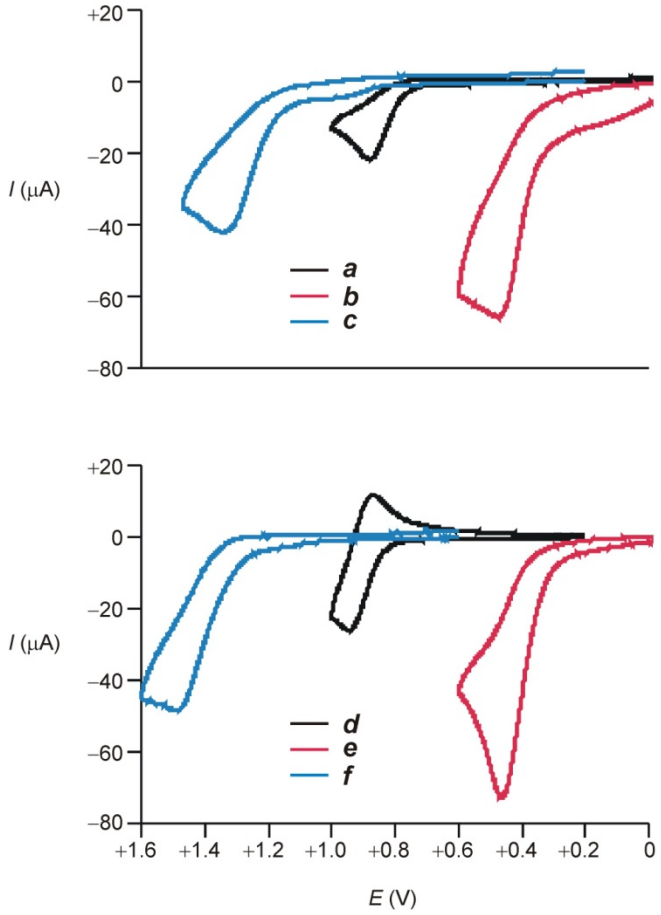

Figure 2.7. Cyclic voltammograms (1.0 mM, MeCN, 0.1 M Bu_4NPF_6, 100 mV s^{-1}, V *vs.* Ag/AgCl) of **13** before (***a***) and after the addition of either Bu_4NOH (6 eq., ***b***) or CF_3CO_2H (25 eq., ***c***). Cyclic voltammograms (1.0 mM, MeCN, 0.1 M Bu_4NPF_6, 100 mV s^{-1}, V *vs.* Ag/AgCl) of **18** (***d***) and of **17a** before (***e***) and after the addition of Bu_4NOH (6 eq., ***f***).

2.3.6. *Synthesis and Physicochemical Properties of the Quantum Dots.*

The CdSe core of the quantum dots was prepared from CdO and Se in the presence of tri-*n*-octylphosphine oxide adapting a literature procedure.[27] A ZnS shell was then assembled around the CdSe core from $ZnEt_2$ and hexamethyldisilathiane following an established experimental protocol.[23] The absorption spectrum (***a*** in Figure 2.8) of the

resulting CdSe–ZnS core–shell quantum dots shows the band-gap absorption to be centered at 540 nm. This value corresponds to a diameter of *ca.* 2.9 nm for the CdSe core.[31] The emission spectrum (***e*** in Figure 2.8) reveals a narrow and symmetric band centered at 552 nm with a quantum yield (Φ) of 0.28 (Table 2.1). The luminescence intensity decays biexponentially on a nanosecond time scale (***a*** in Figure 2.9).[117] The lifetimes (τ_1 and τ_2) are 23.1 and 9.9 ns (Table 2.1) with fractional contributions (f_1 and f_2) of 0.54 and 0.46 respectively. These values correspond to an average lifetime ($\bar{\tau}$) of 17.1 ns (Table 2.1).

Table 2.1. Luminescence quantum yields and lifetimes of the quantum dots.

	Φ [a]	τ_1 (ns) [b]	f_1 [b]	τ_2 (ns) [b]	f_2 [b]	$\bar{\tau}$ (ns) [b]
CdSe–ZnS	0.28	23.1	0.54	9.9	0.46	17.1
CdSe–ZnS–**15**	0.12	14.5	0.58	4.7	0.42	10.4
CdSe–ZnS–**15-HA**	0.02	11.7	0.72	3.0	0.28	9.3
CdSe–ZnS–**15-IN**	0.18	14.8	0.76	4.1	0.24	12.2

[a] The quantum yields (Φ) were determined from the emission spectra in Figure 7 using fluorescein as standard. [b] The lifetimes (τ_1 and τ_2), fractional contributions (f_1 and f_2) and average lifetimes ($\bar{\tau}$) were determined from the plots in Figure 2.9. The corresponding biexponential fittings had a coefficient of determination (C.O.D.) greater than 0.998.

The dithiolane anchoring group of **15** encourages the adsorption of this compound on the surface of CdSe–ZnS core–shell quantum dots, when the organic ligand and the inorganic nanoparticles are heated under reflux for 24 h in $CHCl_3$. The absorption spectra of the quantum dots, recorded before and after this treatment, show an increase in absorbance at 398 nm (***a*** and ***b*** in Figure 2.8), where the 4-nitrophenylazophenoxy chromophore of **15** absorbs (***a*** in Figure 2.5). On the basis of the absorbance increase at

this wavelength relative to the band-gap absorbance of the quantum dots, the average number of ligands per nanoparticle can be estimated to be *ca.* 6. The emission spectra of the quantum dots, recorded before and after their treatment with **15**, reveal a significant decrease in luminescence intensity at 552 nm (***e*** and ***f*** in Figure 2.8). In fact, Φ drops from 0.28 to 0.12 (Table 2.1) and $\bar{\tau}$ decreases from 17.1 to 10.4 ns (Table 2.1, ***a*** and ***b*** in Figure 2.8) with the attachment of the ligand. This partial luminescence quenching is consistent with the expected photoinduced electron transfer from the indole fragment of the ligand to the excited nanoparticle.

The addition of Bu_4NOH to the coated CdSe–ZnS core–shell quantum dots induces the opening of the [1,3]oxazine ring of **15** with the formation of **15-HA** (Figure 2.3). The 4-nitrophenylazophenolate chromophore of **15-HA** absorbs in the visible region (***b*** in Figure 2.6). As a result, a new band appears at 553 nm (***b*** and ***c*** in Figure 2.8) in the absorption spectrum of the quantum dots.[118,119] This absorption overlaps the emission of the quantum dots and, therefore, the transformation of **15** into **15-HA** on the surface of the nanoparticles activates an energy transfer pathway from the inorganic to the organic components. Consistently, the emission intensity at 552 nm (***f*** and ***g*** in Figure 2.8) decreases significantly, Φ drops from 0.12 to 0.02 (Table 2.1) and $\bar{\tau}$ changes from 10.4 to 9.3 ns (Table 2.1, ***b*** and ***c*** in Figure 2.9).[118, 120] It is important to stress, however, that the transformation of **15** into **15-HA** shifts the oxidation potential in the negative direction by 0.40 V (***a*** and ***b*** in Figure 6). This change facilitates the photoinduced electron transfer from the ligand to the nanoparticle.

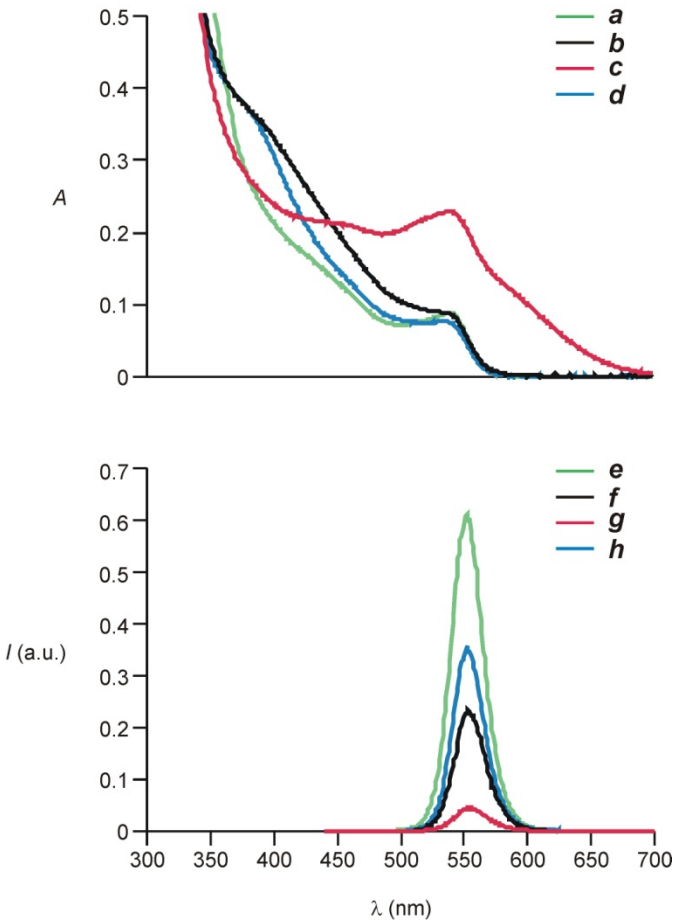

Figure 2.8. Absorption spectra (1.8 μM, $CHCl_3$, 20ºC) of CdSe–ZnS core–shell quantum dots before (***a***) and after (***b***) the attachment of **15** to their surface and the subsequent addition of either Bu_4NOH (***c***, 4.8 mM) or CF_3CO_2H (***d***, 4.8 mM). Emission spectra (0.9 μM, $CHCl_3$, 20ºC, λ_{Ex} = 426 nm) of CdSe–ZnS core–shell quantum dots before (***e***) and after (***f***) the attachment of **15** to their surface and the subsequent addition of either Bu_4NOH (***g***, 2.5 mM) or CF_3CO_2H (***h***, 2.5 mM).

Thus, the luminescence quenching increases with the conversion of **15** into **15-HA** because of the activation of an energy transfer pathway and also for the enhancement in the electron transfer efficiency. The addition of CF_3CO_2H to the coated CdSe–ZnS core–shell quantum dots induces the opening of the [1,3]oxazine ring of **15** with the formation of **15-HA** (Figure 2.3).

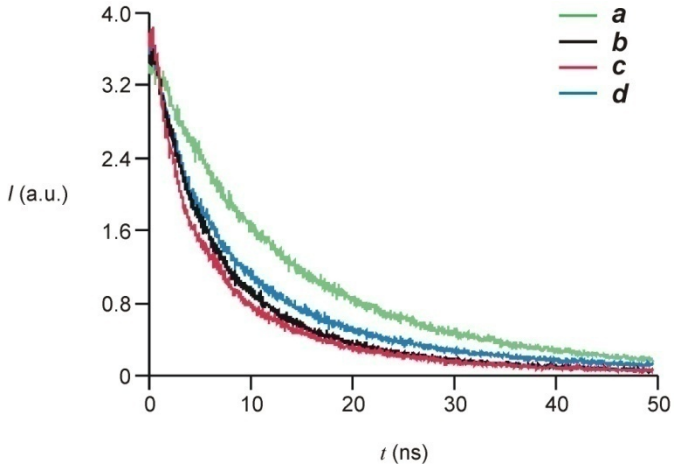

Figure 2.9. Temporal evolution of the luminescence intensity (2.6 μM, $CHCl_3$, 20ºC, $\lambda_{Ex.}$ = 430 nm, $\lambda_{Em.}$ = 558 nm) of CdSe–ZnS core–shell quantum dots before (***a***) and after (***b***) the attachment of **15** to their surface and the subsequent addition of either Bu_4NOH (***c***, 5.0 mM) or CF_3CO_2H (***d***, 10.8 mM).

The 4-nitrophenylazophenol chromophore of **15-IN** absorbs mainly at ultraviolet wavelengths (***c*** in Figure 2.5). As a result, the absorption spectra of the quantum dots do not show any significant change in the visible region (***b*** and ***d*** in Figure 2.7) with the transformation of **15** into **15-IN**.[121] Thus, the excitation energy of the nanoparticles cannot be transferred to the adsorbed ligands neither before nor after the conversion of **15** into **15-IN**. In addition, this process shifts the oxidation potential of the ligand in the positive direction by 0.47 V (***a*** and ***c*** in Figure 2.7), inhibiting the photoinduced electron transfer from the organic ligand to the inorganic nanoparticle. In fact, the emission intensity at 552 nm (***f*** and ***h*** in Figure 2.8) increases after the formation of **15-IN** with an enhancement in Φ from 0.12 to 0.18 (Table 2.1) and in $\bar{\tau}$ from 10.4 to 12.2 ns (Table 2.1, ***b*** and ***d*** in Figure 2.9).[122,123]

The emission behavior of the CdSe–ZnS core–shell quantum dots conjugated to **15** demonstrates that the transformations of the organic ligand in the presence of either acid or base regulate the luminescence intensity of the inorganic nanoparticles. In fact, these sensitive nanostructures can be employed to probe the pH of aqueous solutions in biphasic systems with the assistance of a phase transfer catalyst. Specifically, the luminescence intensity of a $CHCl_3$ phase containing Bu_4NCl and the coated quantum dots varies with the pH of an overlaid aqueous phase (***a*** in Figure 2.10). Under these conditions, a pH increase from 3.2 to 10.7 in the aqueous phase translates into a luminescence decrease of *ca.* 29% in the organic phase. Indeed, the ligand **15-IN** is converted into **15** and then eventually into **15-HA** as the pH increases (Figure 2.3) with a concomitant decrease in Φ (Table 2.1).

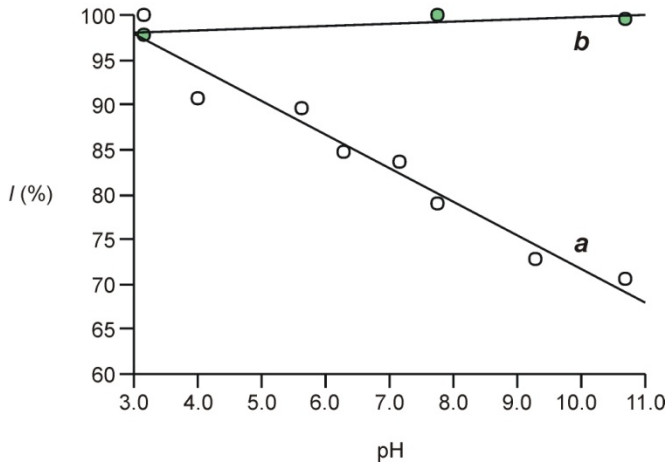

Figure 2.10. Emission intensity of CdSe–ZnS core–shell quantum dots (0.4 μM, 550 μL, $CHCl_3$, 0.1 M Bu_4NCl, 20ºC, $\lambda_{Ex.}$ = 430 nm, $\lambda_{Em.}$ = 552 nm) with (***a***) and without (***b***) **15** on their surface after the addition of sodium phosphate buffer (200 μL) with pH ranging from 3.2 to 10.

In fact, the intensity at 555 nm decreases by *ca.* 35% with an increase in pH from 7.1 to 8.5 (***a*** in Figure 2.10). The fading in luminescence with the gradual pH increase is also evident in the corresponding photographs (***I–III*** in Figure 2.10). By contrast, quantum dots lacking the chromogenic ligand **15** on their surface are insensitive to the pH of the aqueous phase (***b*** in Figure 2.10) under otherwise identical conditions. Thus, the chromogenic and pH-sensitive organic ligands are, indeed, responsible for the regulation of the emissive behavior of the inorganic nanoparticles.

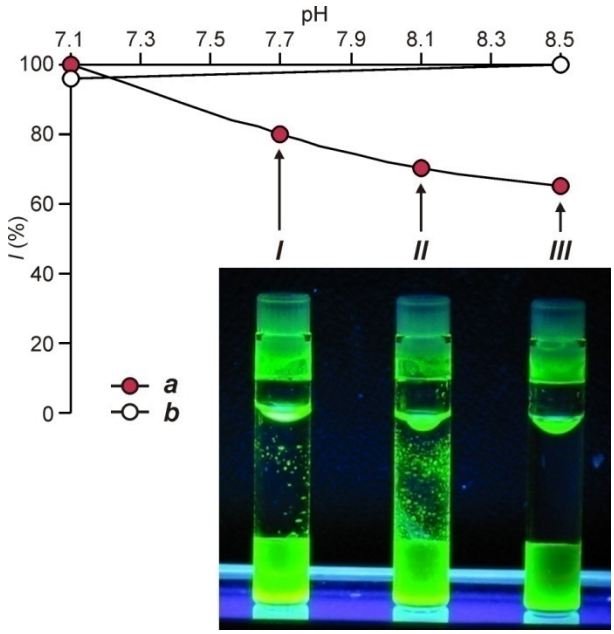

Figure 2.11. Emission intensity of a solution of CdSe–ZnS core–shell quantum dots (0.8 μM, 300 μL, $CHCl_3$, 20ºC, λ_{Ex} = 430 nm, λ_{Em} = 555 nm) with (***a***) and without (***b***) **15** on their surface and Bu_4NCl (1 M, 50 μL, dichloroethane) after treatment with sodium phosphate buffer (500 μL) and dilution with $CHCl_3$ (4.3 mL). Photographs of solutions of CdSe–ZnS core–shell quantum dots (0.8 μM, 300 μL, $CHCl_3$) coated with **15** and Bu_4NCl (1 M, 50 μL, dichloroethane) under ultraviolet illumination after treatment with sodium phosphate buffer (500 μL) at the pH values (***I–III***) indicated in the plot.

2.4. Conclusions

The adsorption of pH-sensitive [1,3]oxazines on the surface of CdSe–ZnS core–shell quantum dots offers the opportunity to switch the luminescence of these inorganic nanoparticles with chemical stimulations. Indeed, the [1,3]oxazine rings of the organic ligands open upon addition of base to generate 4-nitrophenylazophenolate chromophores. This transformation activates an energy transfer pathway from the excited quantum dots to the ligands and facilitates electron transfer in the opposite direction. As a result, the luminescence quantum yields decreases by 85%. The addition of acid also causes the opening of the [1,3]oxazine rings. However, the resulting 4-nitrophenylazophenol groups cannot accept the excitation energy of the nanoparticles and are poor electron donors. Consistently, the luminescence quantum yield increases by 33%. Thus, the organic ligands adsorbed on the inorganic nanoparticles impose pH sensitivity on their emissive behavior. In fact, these quantum dots can probe the pH of aqueous solutions by adjusting their luminescence intensity to pH changes in the 3–11 range. In principle, similar organic ligands can be designed to alter their absorption and redox properties in response to target analytes other than hydroxide anions and protons, regulating the luminescence of the associated quantum dots as a result. Therefore, a new generation of luminescent chemosensors based on the unique photophysical properties of quantum dots can ultimately emerge on the basis of these operating principles.

CHAPTER 3

A MECHANISM TO SIGNAL RECEPTOR–SUBSTRATE INTERACTIONS WITH LUMINESCENT QUANTUM DOTS

3.1. Summary

The unique photophysical properties of semiconductor quantum dots are encouraging the use of these inorganic nanoparticles as luminescent probes for biomedical applications in alternative to organic dyes. In fact, operating principles to signal target analytes relying on the luminescence of these fascinating nanostructures are starting to be developed. Most of these strategies, however, are based on energy transfer from quantum dots to organic acceptors upon excitation. Photoinduced electron transfer processes, instead, have hardly been explored in this context, notwithstanding the profound implications that these mechanisms continue to have in the design of fluorescent chemosensors based on organic dyes. We have identified a viable protocol to probe receptor–substrate interactions on the basis of photoinduced electron transfer from quantum dots to organic acceptors. This method can transduce the supramolecular association of a receptor with a complementary substrate into a significant luminescent enhancement. In the first part of design, luminescence of anionic hydrophilic quantum dots was quenched by a cationic electron acceptor. Furthermore, addition of receptor which is able to bind and remove the cationic electron acceptor from surface of quantum dots restored the luminescence. In fact, I have demonstrated with a representative

example that our design logic can be adapted to the identification of protein–ligand interactions. Biotin attached quencher was removed from surface of quantum dots by addition of streptavidin. Thus, the operating principles and choice of materials can lead to the development of innovative and sensitive probes based on the unparalleled properties of semiconductor quantum dots.

3.2. Receptor-substrate Interactions

Promising studies demonstrate that semiconductor quantum dots can donate energy to complementary partners.[47c] In fact, clever assays for the recognition of various analytes are starting to be designed on the basis of energy transfer processes.[64-77] Instead, mechanisms based on electron transfer yet remain to be explored.[59-60] Literature data demonstrates that CdSe quantum dots can efficiently transfer electrons to complementary organic acceptors upon excitation.[124] As a result of electron transfer, luminescence of quantum dots can be quenched. Bipyridinium dications have greater affinities for electrons[125,126] and they can accept electrons from quantum dots. In fact, fundamental investigations have demonstrated that these inorganic nanostructures can exchange electrons with complementary organic partners upon excitation with a concomitant luminescence quenching.[20b,84,87] In particular, the ability of CdSe–ZnS core–shell QDs to inject electrons into bipyridinium dications can facilitate development of photochromic materials[116] and probing protein–ligand interactions.[63b] These strategies are based on the adsorption of appropriate bipyridinium dications on the surface of the inorganic nanoparticles in the ground state and on the exchange of electrons between them in the excited state. In order to develop target analyte recognition with luminescent quantum

dots, host quest chemistry of methyl viologen and cucurbiturils can be utilized. Cucurbit[7]urils known as **CB7** (**22** in Figure 3.5) form very stable 1:1 inclusion complexes with methyl viologen and other simple viologens in aqueous solutions.[127,128]

In this context, we have designed a competitive binding assay based on the photoinduced transfer of electrons from quantum dots to methyl viologen. This method relies on the electrostatic association of a quencher on the surface of a quantum dot (Fig. 3.1). Under these conditions, the photoinduced transfer of electrons from the excited nanoparticles to the adsorbed acceptors is expected to translate into an efficient luminescence quenching. The luminescence of the quantum dots, however, can be restored by adding a **CB7** receptor able to sequester and remove the quencher from the surface of the nanoparticles. Thus, the presence of the receptor can be transduced into a luminescent enhancement on the basis of this mechanism.

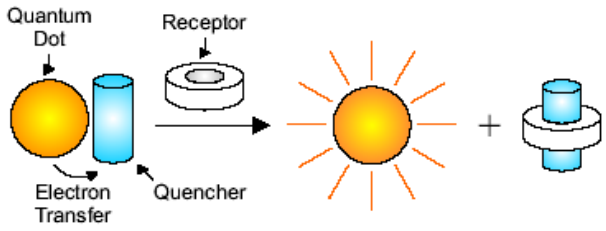

Figure 3.1. The supramolecular association of quencher and receptor prevents the electron transfer process and activates the luminescence of the quantum dot.

The biological function of many proteins is triggered and modulated by the binding of ligands. For this reason, an understanding of the mechanism of protein-ligand interactions is essential for a detailed knowledge of protein function at the molecular level. Ligand binding, in most cases, involves the formation of noncovalent bonds at specific

interacting surfaces between the protein and the ligand. The binding of a ligand can be accompanied by conformational changes at the protein site that sometimes are propagated throughout the entire protein. It is desirable to have a way to monitor these structural changes to understand any new properties acquired by the complex. The high affinity of the biotin-streptavidin binding not only offers useful bio-analytical advantages, but it also makes this system an attractive model for studying protein-ligand interactions.[129-132] The biotin-streptavidin association constant of about 10^{15} is the highest known in biochemistry. The very same luminescent sensing principle for methyl viologen-CB7 system can also be applied to biotin-streptavidin interaction. An organic acceptor covalently attached to biotin can quench the luminescence of quantum dots and furthermore addition of streptavidin molecule will be able to remove biotin ligand from the surface of quantum dots thereby preventing electron transfer (Figure 3.1). Here, we demonstrate that these operating principles can indeed be implemented experimentally and that they can even be extended to signal protein–ligand interactions.

3.3. Results and Discussion

3.3.1. Synthesis of Hydrophilic Quantum Dots

In order to demonstrate the viability of this design, I have prepared CdSe–ZnS core–shell quantum dots coated with tri-*n*-octylphosphine oxide (TOPO) ligands adapting literature procedures.[23,27] Then, I have exchanged the hydrophobic ligands with hydrophilic mercaptoacetate groups (**19** in Figure 3.2).[133]

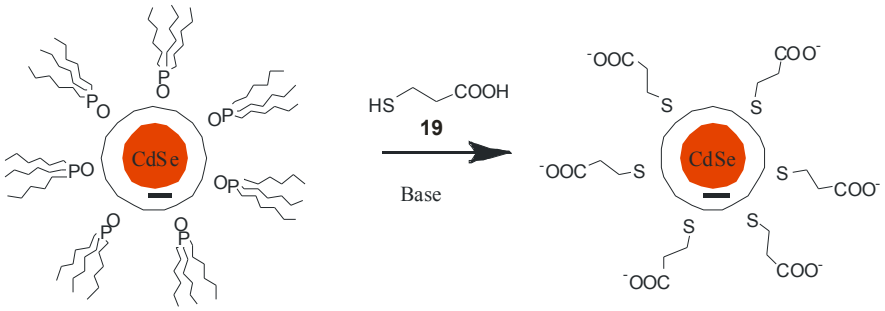

Figure 3.2. Ligand exchange process of hydrophobic TOPO molecules with hydrophilic mercaptoacetate groups.

3.3.2. Infrared Spectroscopy of Quantum Dots

In order to verify the ligand exchange process, infrared spectra of neat tri-*n*-octylphopshine oxide (**1** in Figure 1.2), hydrophobic CdSe–ZnS core–shell quantum dots before and after treatment with mercaptoacetic acid and potassium hydroxide, and potassium mercaptoacetate were performed. IR spectra of hydrophobic particles (**a** Figure 3.3) and TOPO molecule (**b** Figure 3.3) clearly indicate that before ligand exchange process, the surface of particles consists mainly of TOPO molecules. After ligands exchange with hydrophilic mercaptoacetate, IR spectra of the resulting particles (**c** Figure 3.3) and potassium mercaptoacetate (**d** Figure 3.3) shows that the surface are covered mainly with mercaptoacetate groups. The infrared spectra recorded before (***b*** in Fig. 3.3) and after (***c***) treatment of the CdSe–ZnS core–shell quantum dots with mercaptoacetic acid and potassium hydroxide show the disappearance of the [C–H] stretching vibrations at 2800–3000 cm^{-1} (***a***) for the hydrophobic ligands and the appearance of the [C=O] stretching vibrations at 1300–1700 cm^{-1} (***d***) for the hydrophilic ones.

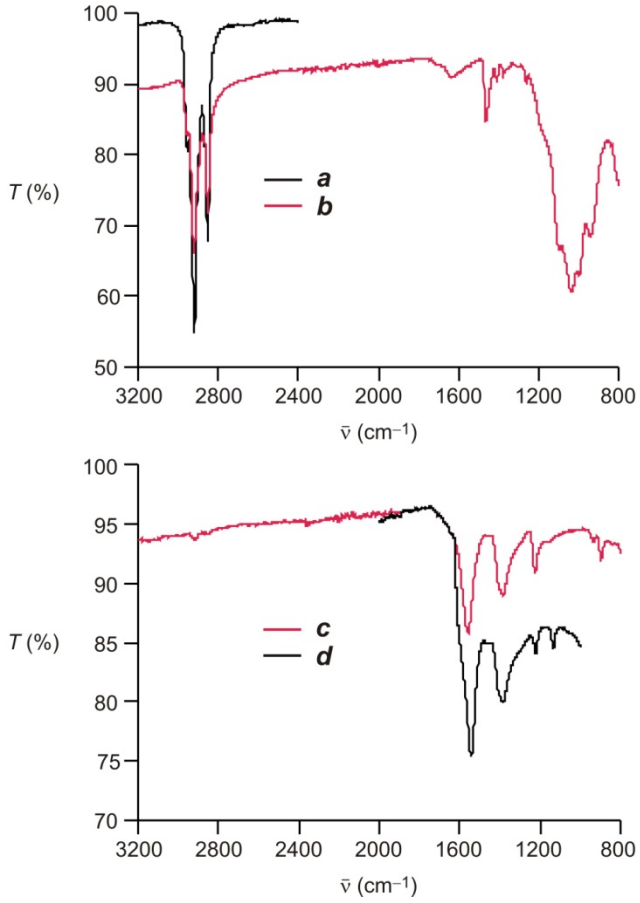

Figure 3.3. Infrared spectra of neat tri-*n*-octylphopshine oxide (***a***), hydrophobic CdSe–ZnS core–shell quantum dots before (***b***) and after (***c***) treatment with mercaptoacidic acid (**19** in Figure 3.2) and potassium hydroxide, (***d***) potassium mercaptoacetate.

3.3.3. Absorption and Emission Spectroscopy

The resulting nanoparticles are soluble in water, absorb at 548 nm (***a*** in Fig. 3.4) and emit at 563 nm (***b*** in Fig. 3.4). The addition of increasing amounts of methyl viologen (**20** in Fig. 5), however, results in a significant decrease in luminescence intensity (***c*** in Fig. 3.4). Indeed, bipyridinium dications are known to accept electrons from excited CdSe and CdSe–ZnS core–shell quantum dots, quenching their luminescence. [116,124]

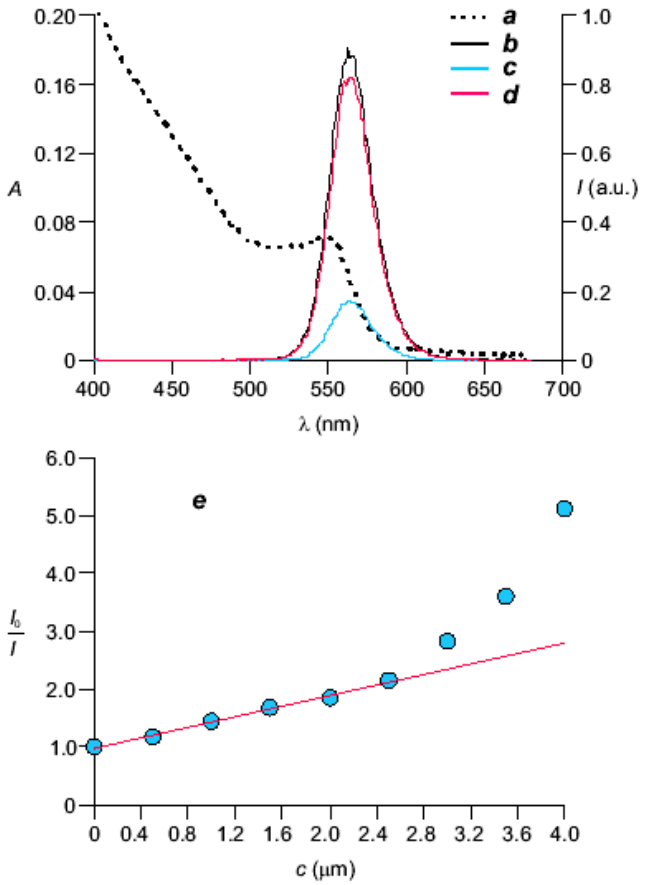

Figure 3.4. Absorption spectrum (***a***) of hydrophilic CdSe–ZnS core–shell quantum dots (1.5 μM, sodium phosphate buffer, pH = 7.8, 20°C). Emission spectrum (λ_{Ex} = 350 nm) of the same solution recorded before (***b***) and after the consecutive addition of **20** (***c***, 4.1 μM) and **22** (***d***, 21 μM). Stern–Volmer plot (***e***) of hydrophilic CdSe–ZnS core–shell quantum dots (1.5 μM, sodium phosphate buffer, pH = 7.8, 20°C, λ_{Ex} = 350 nm) upon addition of increasing amounts of **20**.

The corresponding Stern–Volmer plot (***e*** in Fig. 3.4) deviates from linearity at quencher concentrations greater than *ca.* 2.5 μM. This behavior indicates that the quenching mechanism is predominantly static below this particular concentration with a Stern–Volmer constant of *ca.* 0.45 μM^{-1}, while dynamic terms contribute significantly to quenching only at higher concentrations. These observations suggest that the dicationic

quencher is presumably adsorbed on the surface of the hydrophilic quantum dots as a result of electrostatic interactions with their anionic carboxylate groups.

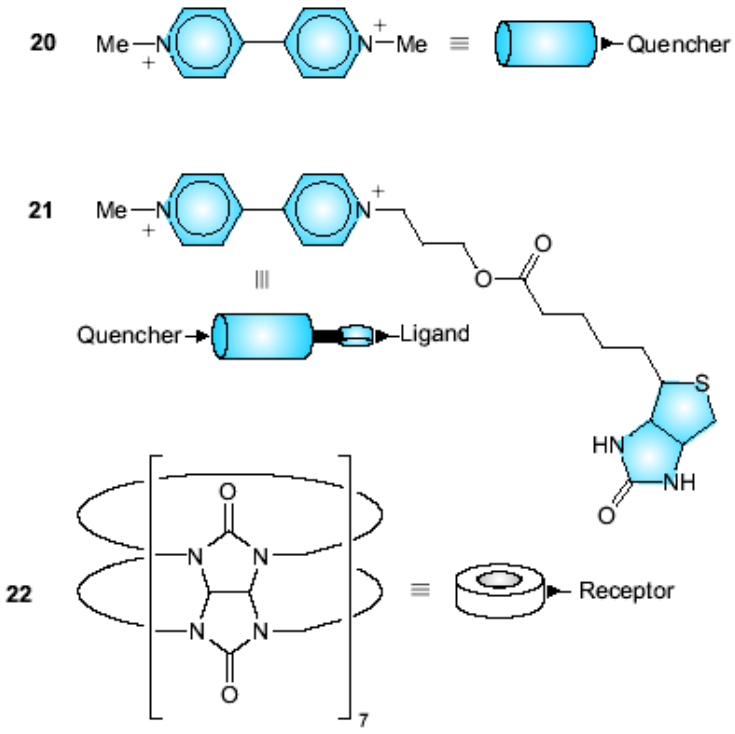

Figure 3.5. The bipyridinium-based quenchers **20** and **21** and the macrocyclic receptor **22**.

The change imposed on the luminescence of the hydrophilic quantum dots by the quencher **20** can be reversed with the addition of an excess of cucurbituril (**22** in Fig. 3.5). Indeed, this particular macrocyclic receptor is known to bind bipyridinium dications with high association constants in aqueous solutions. [127,128] Consistently, the emission spectrum (***d*** in Fig. 3.4) recorded in the presence of an excess of **22** relative to **20** closely resembles the one recorded before the addition of **20** (***b***). Thus, the receptor **22** binds the quencher, prevents the electron transfer process and restores the ability of the hydrophilic quantum dots to emit light.

3.3.4. Signaling Protein-ligand Interactions with Quantum Dots

In principle, the very same mechanism can be adapted to signal protein–ligand interactions with luminescence changes. For example, a ligand able to recognize a complementary protein can be covalently attached to the quencher (Fig. 3.6).

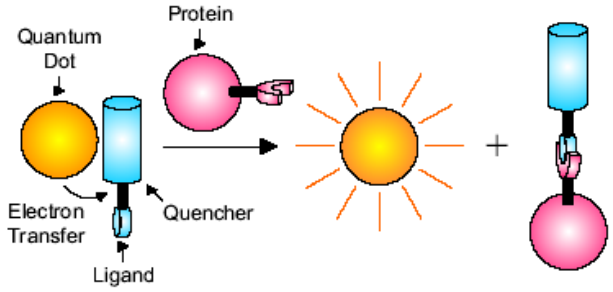

Figure 3.6. Activation of the luminescence of the quantum dot by means of the supramolecular association of protein and ligand.

In the absence of the protein, the quencher can adsorb on the surface of a hydrophilic quantum dot and suppress its ability to emit light as a result of photoinduced electron transfer. However, the supramolecular association of the ligand with the protein can remove the quencher from the nanoparticle surface and switch on its luminescence.

3.3.5. Synthesis of Biotin Quencher

In order to test the potential of our operating principles to signal protein–ligand interactions, we have designed a compound (**21** in Fig. 3.7) integrating a bipyridinium

quencher and a biotin ligand within the same molecular skeleton and prepared this molecule in two synthetic steps.

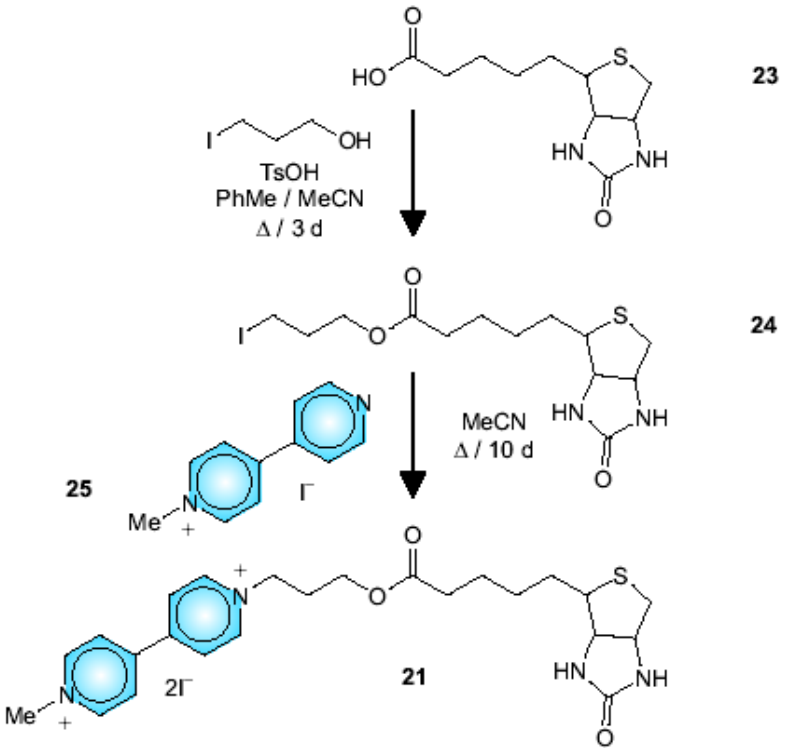

Figure 3.7. Synthesis of the bipyridinium dication **21**.

3.3.6. Absorption and Emission spectroscopy of Biotin/Streptavidin System

Once again, the luminescence of the hydrophilic quantum dots decreases upon exposure to **21** (***a*** and ***b*** in Fig. 3.8). As observed for **20**, the corresponding Stern–Volmer plot (***d*** in Fig. 3.8) is linear at relatively low quencher concentrations. It deviates from linearity only above *ca.* 2.5 μM, indicating that dynamic terms contribute significantly to quenching above this quencher concentration.

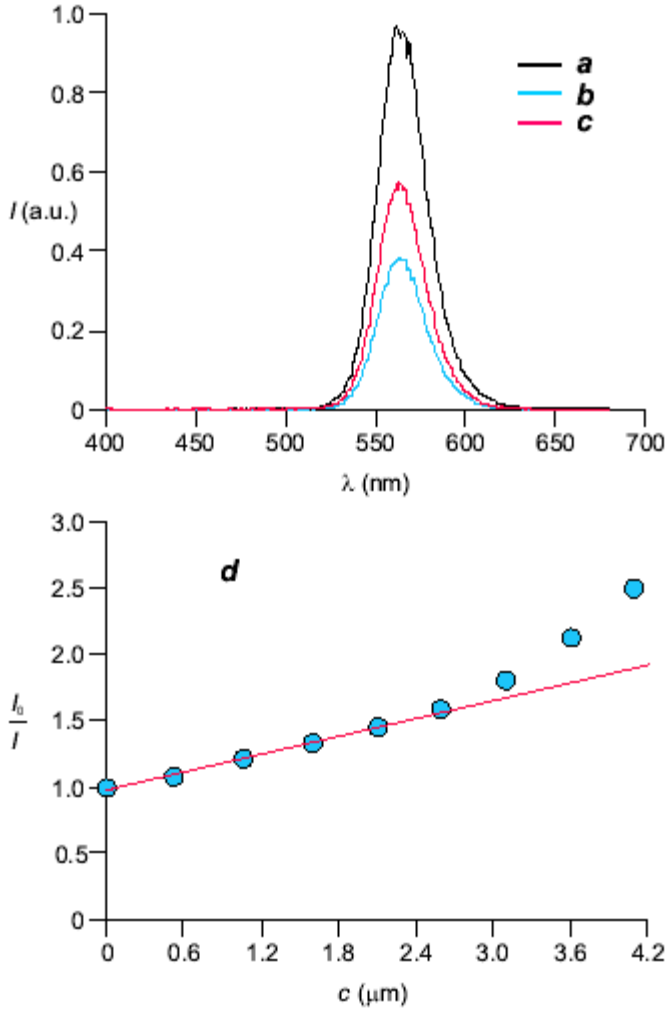

Figure 3.8. Emission spectra of hydrophilic CdSe–ZnS core–shell quantum dots (1.5 μM, sodium phosphate buffer, pH = 7.8, 20°C, λ_{Ex} = 350 nm) recorded before (***a***) and after the consecutive addition of **21** (***b***, 4.1 μM) and streptavidin (***c***, 21 μM). Stern–Volmer plot (***d***) of hydrophilic CdSe–ZnS core–shell quantum dots (1.5 μM, sodium phosphate buffer, pH = 7.8, 20°C, λ_{Ex} = 350 nm) upon addition of increasing amounts of **21**.

The Stern–Volmer constant derived from the linear region of the plot, however, is only *ca.* 0.22 μM^{-1}. Presumably, the biotin tail of **21** disturbs the interaction between the

appended quencher and the hydrophilic quantum dots, leading to a decrease in the Stern–Volmer constant of *ca.* 0.23 μM^{-1} relative to **20**.

The addition of increasing amounts of streptavidin to a mixture of the hydrophilic quantum dots and **21** leads to a luminescence enhancement (***c*** in Fig. 3.8). Instead, the addition of bovine serum albumin has no influence of the emission spectrum under otherwise identical conditions (Fig. 3.9). Indeed, only streptavidin can bind the biotin ligand **21** and, therefore, alter the quenching efficiency of the bipyridinium appendage.[131,132] Nonetheless, the original emission intensity is not fully restored even in the presence of a large excess of streptavidin. The luminescence increases only by 30% after the association of **21** and streptavidin, while it grows by 80% after the interaction of **20** and **22**. The different behavior is presumably a result of the different binding modes of the two receptors. While streptavidin can only bind the biotin appendage of **21**, the macrocycle **22** encapsulates the bipyridinium dication of **20** in its cavity, suppressing very effectively its quenching ability. Presumably, an adjustment in the length of the aliphatic spacer connecting the quencher to the ligand in **21** can be invoked to improve the luminescence enhancement upon streptavidin binding.

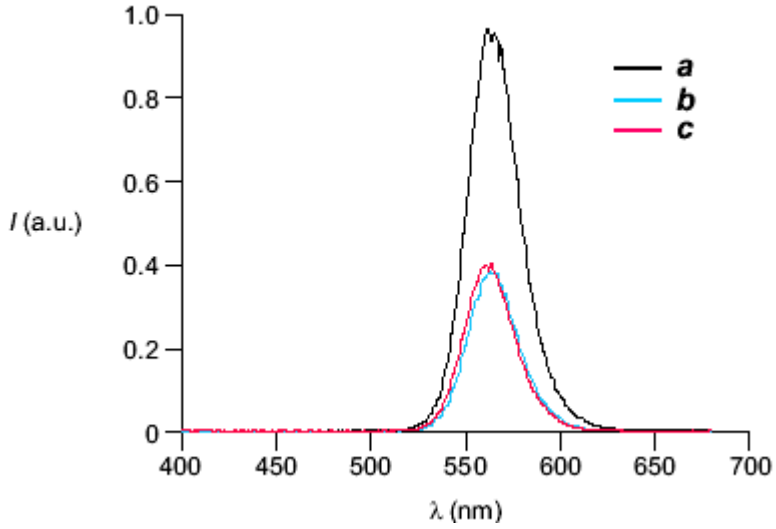

Fig. 3.9. Emission spectra of hydrophilic CdSe–ZnS core–shell quantum dots (1.5 μM, sodium phosphate buffer, pH = 7.8, 20°C, λ_{Ex} = 350 nm) recorded before (***a***) and after the consecutive addition of **21** (***b***, 4.1 μM) and bovine serum albumin (***c***, 7.4 μM).

3.4. Conclusions

In summary, we have identified a mechanism to signal receptor–substrate interactions based on photoinduced electron transfer. Our method relies on the electrostatic adsorption of cationic quenchers on the surface of anionic quantum dots. The supramolecular association of the quenchers with target receptors prevents the electron transfer process and turns on the luminescence of the inorganic nanoparticles. In fact, this protocol can be adapted to probe protein–ligand interactions with luminescent measurements. Thus, our operating principles and choice of materials can eventually lead to the development of valuable binding assays for biorelevant targets relying on the unique photophysical properties of semiconductor quantum dots.

CHAPTER 4

LUMINESCENCE MODULATION WITH SEMICONDUCTOR QUANTUM DOTS AND PHOTOCHROMIC LIGANDS

4.1. Summary

We have identified viable operating principles for the modulation of optical signals under the influence of optical stimulations. They are based on the overlap between the emission bands of a fluorescent CdSe–ZnS core–shell quantum dots and the absorption bands of one of the two forms of a photo chromic spiropyran. The photoinduced interconversion of the two states of the spiropyran modulates the emission intensity of the quantum dots. In this system, a photochromic spiropyran was attached to the surface of CdSe–ZnS core–shell quantum dots relying on a dithiolane anchoring group. In the resulting assembly, the reversible interconversion of the photochromic component activates and suppresses an energy transfer pathway from the excited quantum dots to the colored state of the ligand in solution. As a result, the luminescence intensity decreases by 45% with the photoinduced coloration of the spiropyran due to energy transfer from quantum dots to open form of spiropyran and returns to the original value after the thermal reisomerization of the ligand to its close form. The process is fully reversible and the original spiropyran is restored on the time scale of seconds. As a result, the luminescence of the nanoparticle–photochrome assembly can be switched between high and low values simply by turning an ultraviolet source on and off. This design can lead to

development of new photochromic switches based on semiconductor quantum dots with different photochromic molecules.

4.2. Luminescence Modulation

Photochromic compounds switch reversibly between distinct states under the influence of optical simulations.[134-137] Their interconvertible states differ in the ability to absorb visible light. As a result, a photochromic transformation is always accompanied by significant and reversible changes in the visible region of the absorption spectrum. In fact, a diversity of promising applications in the realm of photonics have been designed around the unique properties of these photoresponsive molecules.[138,139]

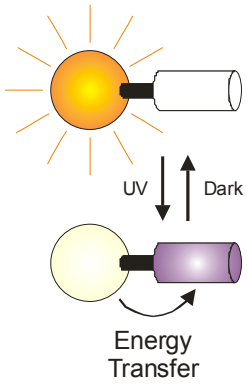

Figure 4.1. Modulation of the luminescence of the nanoparticle by interconversion of a photochromic spiropyran.

For example, the photoinduced interconversion of a photochromic compound can be exploited to modulate the emission of a fluorescent partner.[140] In these systems, the fluorescent and photochromic building blocks are generally integrated within a single molecular or supramolecular assembly. The emission of one component is then switched by operating the other with optical stimulations and relying on intercomponent electron

or energy transfer (Figure 4.1). The photophysical properties of semiconductor quantum dots offer numerous advantages over those of conventional organic fluorophores.[10c,12b,13b,16,20b] Indeed, the photoinduced interconversion of diarylethenes and spiropyrans has successfully been exploited to modulate the luminescence of nanoparticle–photochrome assemblies on the basis of energy transfer mechanisms similar to those originally developed to switch the emission of fluorophore–photochrome pairs.[140] These nanostructured assemblies can be prepared in multiple synthetic steps relying on protein bridges to connect the photochromic component to the luminescent nanoparticle.[141-143] Alternatively, photochromic ligands with thiol appendages can directly be adsorbed on the surface of semiconductor quantum dots.[141] The chemistry of thiols, however, is often complicated by their tendency to oxidize in air and, often, also by the need to resort to sequences of protection/deprotection steps.

4.3. Results and Discussion

4.3.1. Design and Synthesis

We have identified an alternative anchoring group for the convenient and direct attachment of photochromic compounds to the ZnS shell of CdSe–ZnS quantum dots, which does not suffer the limitations of thiols. Specifically, we have reacted the spiropyran **26** (Figure 4.2) with (±)-α-lipoic acid in the presence of *N*,*N*'-dicyclohexylcarbodiimide and 4-dimethylaminopyridine and isolated the resulting ester **27** in a yield of 64%. The dithiolane ring at the end of the aliphatic tail of **27** is, indeed,

expected to encourage the adsorption of this photochromic compound on CdSe–ZnS core–shell quantum dots.

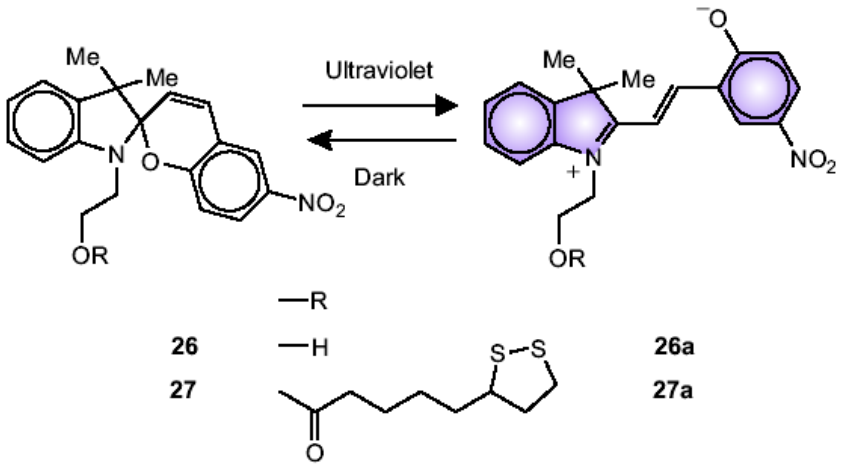

Figure 4.2. The photoinduced and reversible interconversion of colorless spiropyrans (**26** and **27**) into colored merocyanines (**26a** and **27a**).

4.3.2. Photochromic Component

The absorption spectrum (***a*** in Figure 4.3) of **27** does not show bands at wavelengths longer than 400 nm. Upon ultraviolet irradiation, however, an absorption centered at 592 nm appears in the spectrum (***b*** in Figure 4.3). This absorbance change in the visible region is as a result of the photoinduced transformation of **27** into the corresponding merocyanine **27a** (Figure 4.2). The photogenerated and colored isomer **27a** is thermally unstable and reverts to the original and colorless state **27** with first-order kinetics. The analysis of the absorbance decay at 592 nm in the dark indicates the lifetime of **27a** to be *ca.* 25 s in dichloroethane at 20°C. Thus, the visible band of **27a** can be modulated simply by turning on and off an ultraviolet source.

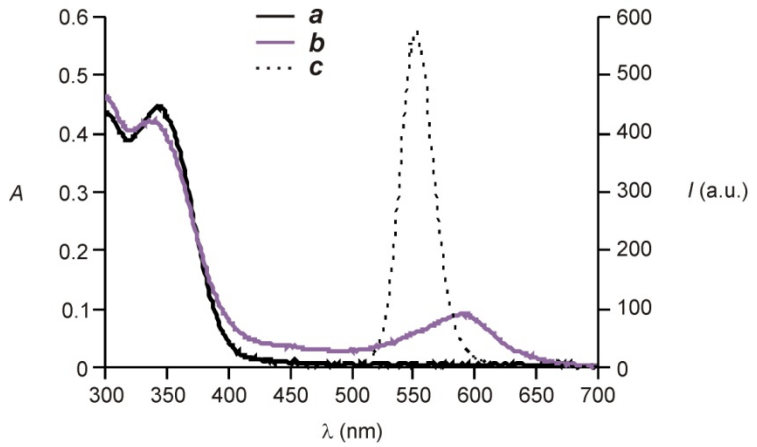

Figure 4.3. The absorption spectra of a solution of **27** (0.1 mM, dichloroethane, 20°C) before (***a***) and after (***b***) continuous irradiation (365 nm, 0.4 mW cm^{-2}, 10 min) and the emission spectrum (***c***) of a solution of CdSe–ZnS core–shell quantum dots (0.7 μM, dichloroethane, 20°C, λ_{Ex} = 450 nm).

4.3.3. Fluorescence Modulation

The absorption band of **27a** overlaps the emission band (***c*** in Figure 4.3) of CdSe–ZnS core–shell quantum dots with a diameter of *ca.* 2.8 nm. It follows that the photoinduced and reversible interconversion of **27** and **27a** can be exploited to activate and suppress the transfer of excitation energy from the quantum dots to the colored isomer of the photochromic component. First, however, the energy donor and acceptor have to be constrained in close proximity. In fact, the dithiolane appendage of **27** ensures the adsorption of the photochromic ligand on the surface of the quantum dots, when the two components are heated in chloroform over the course of one day. Consistently, the absorption spectrum of the modified quantum dots shows the appearance of the characteristic absorption of **27a** in the visible region after ultraviolet irradiation (***a*** and ***b*** in Figure 4.4).

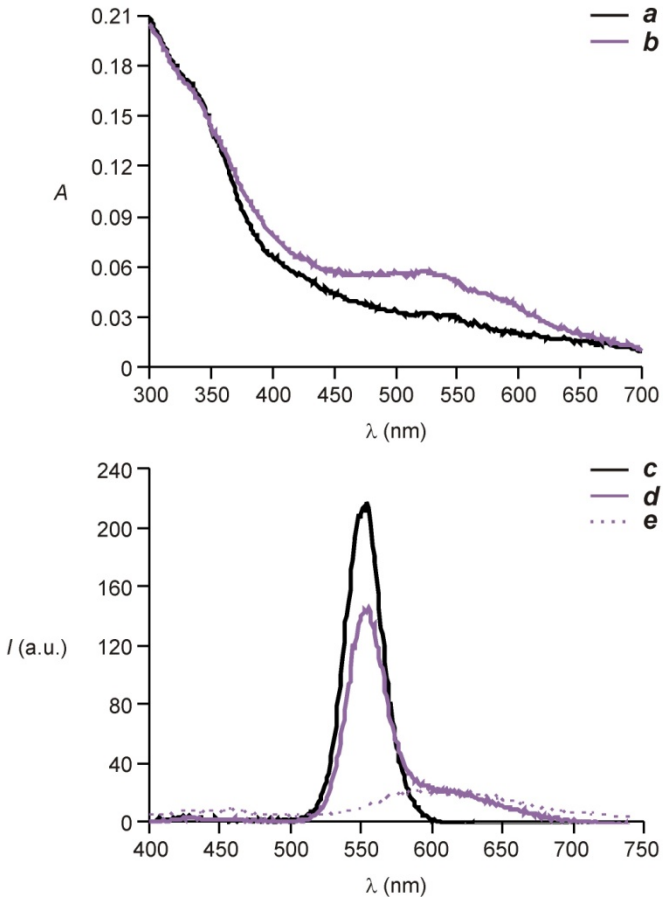

Figure 4.4. The absorption spectra of a solution of CdSe–ZnS core–shell quantum dots (0.7 μM, dichloroethane, 20°C) with **27** adsorbed on their surface before (***a***) and after (***b***) continuous irradiation (365 nm, 0.4 mW cm^{-2}, 10 min) and the corresponding emission spectra (***c***) and (***d***) respectively (λ_{Ex} = 380 nm). The emission spectrum (***e***) of a solution of **27** (0.1 mM, dichloroethane, 20°C, λ_{Ex} = 380 nm) after continuous irradiation (365 nm, 0.4 mW cm^{-2}, 10 min).

Once again, the photoinduced transformation is fully reversible. The photochromic ligand returns to the original and colorless state with first-order kinetics in the dark. The corresponding absorbance evolution, however, indicates that the thermal re-isomerization of **27a** to **27** on the surface of the quantum dot is significantly slower than in homogenous

solution. Indeed, the lifetime of **27a** increases from *ca.* 25 to 250 s after its attachment to the quantum dots, under otherwise identical experimental conditions.

The emission spectrum (***c*** in Figure 4.4) of the modified quantum dots shows the characteristic band of the emissive CdSe core at 554 nm. The attachment of the photochromic ligand, however, results in a decrease in the luminescence quantum yield from *ca.* 0.38 to 0.14. Upon ultraviolet irradiation, **27** switches to **27a** on the surface of the quantum dots, activating an energy transfer pathway from the inorganic nanoparticles to the colored state of the photochromic ligand. As a result, the luminescence intensity decreases by *ca.* 45% (***d*** in Figure 4.4), but is restored in full after the thermal reisomerization of **27a** back to **27.** The magnitude of the luminescence change is comparable to those observed with similar systems.[141,143] Presumably, this value can be enhanced by increasing (1) the number of photochromic ligands attached to each quantum dot and (2) the diameter of the nanoparticles in order to optimize the overlap between their emission band and the absorption band of **4** (***b*** and ***c*** in Figure 4.3). Interestingly, the spectrum of the modified quantum dots, recorded after ultraviolet irradiation, shows also a broad band centered at 615 nm (***d*** in Figure 4.4), in addition to the sharp emission of the inorganic component. This relatively weak band resembles the emission of **4** in homogenous solution (***e*** in Figure 4.4) and, therefore, can be assigned to the colored state of the photochromic component adsorbed on the quantum dots.

4.4. Conclusions

In summary, our results demonstrate that photochromic spiropyrans can be attached to the surface of CdSe–ZnS core–shell quantum dots relying on dithiolane anchoring groups. The photoinduced and reversible interconversion of the photochromic ligand occurs on the surface of the quantum dots. However, the inorganic nanoparticle affects significantly the reisomerization kinetics. Specifically, the lifetime of the colored isomer of the photochromic ligand increase by one order of magnitude after surface confinement. Furthermore, the reversible changes in absorbance accompanying the photochromic transformation activate and suppress an energy transfer pathway from the excited quantum dots to the colored state of the photochromic ligand. In fact, the luminescence of the quantum dots switches from a high to a low value with the photogeneration of the colored state and reverts to the original value after thermal isomerization. Thus, our operating principles and choice of components can lead to the development of a new family of luminescent materials based on semiconductor quantum dots and photochromic ligands.

CHAPTER 5

NANOPARTICLE-INDUCED TRANSITION FROM POSITIVE TO NEGATIVE PHOTOCHROMISM

5.1. Summary

We have designed and synthesized a photochromic spiropyran ligand with a dithiolane appendage. The two sulfur atoms of the dithiolane ring encourage the adsorption of this compound on the surface of cadmium sulfide nanoparticles. The properties of the resulting photochrome–nanoparticle assemblies vary significantly with the experimental conditions selected for the preparation of the inorganic component. Nanoparticles prepared in the presence of tri-*n*-octylphopshine impose positive photochromism on the ligands. After adsorption of spiropyran ligand on the surface of this particular nanoparticle, spiropyran prefers its closed form. Upon ultraviolet irradiation, spiropyran switches to its colored open form. Instead, nanoparticles prepared in the presence of sodium dioctylsulfosuccinate impose negative photochromism on the ligand. In this case, after adsorption ligand on the surface of nanoparticles, it prefers its open colored form. This behavior is a consequence of the difference in the surface morphology of the two sets of nanoparticles. Indeed, emission spectra confirm the presence of surface defects on the nanoparticles exhibiting negative photochromism. Presumably, electrostatic interactions between these surface defects and the colored and zwitterionic isomer of the ligand are responsible for the transition from positive to negative photochromism. Thus, these studies demonstrate that the microscopic environment around a photochromic

switch can regulate the relative stabilities of its colorless and colored states as well as their isomerization kinetics.

5.2. Photochromic Systems

Photochromic compounds respond to optical stimulations with significant absorbance changes in the visible region of the electromagnetic spectrum.[125,134-137] These photoinduced processes are reversible by definition. Indeed, the photogenerated state reverts back to the original one either thermally or after irradiation at a different wavelength. Thermally-reversible photochromic compounds can undergo coloration under irradiation and decoloration when stored in the dark or *vice versa*. In fact, the terms positive and negative photochromism are generally used to distinguish photoinduced coloration and decoloration processes.

The reversible transformations of photochromic compounds are generally based on ring opening/closing steps, *cis/trans* isomerizations, proton transfer, electron transfer or cycloadditions. [125,134-137] These processes impose significant structural changes on the interconverting compounds, which translate into profound alterations of molecular properties (electronic structure, geometry, dipole moment, polarizability). In turn, these modifications at the molecular level can control the macroscopic properties (absorption coefficient, refractive index) of the material hosting the photochromic system. Indeed, a number of applications in the realm of photonics have been envisaged and demonstrated experimentally on the basis of the absorptive and dispersive effects associated with photochromic compounds.[126,138,139,144] In particular, the reversible interconversion of these molecules has been exploited to modulate the emission properties of

complementary fluorophores.[140] In most of these systems, photochromic and fluorescent components are integrated within the same molecular skeleton. The photoinduced transformations of the photochrome are then designed to switch on and off the emission of the fluorophore mainly on the basis of intramolecular electron or energy transfer processes.

Similarly, the operating principles developed for the emission modulation of photochrome–fluorophore conjugates are starting to be extended to photochrome–quantum dot assemblies.[113a,141-143] In these systems, energy transfer from the excited inorganic component to one of the interconvertible states of the organic ligand regulates the emissive behavior.

The investigations of photochrome–quantum dot assemblies have mainly focused their interests on the influence of the organic ligand on the luminescence of the inorganic nanoparticle.[113a,141-143] The environment surrounding a photochromic compound, however, can have a profound influence on the coloration and decoloration processes.[125,134-137] Thus, the adsorption of these compounds on the surface of inorganic nanoparticles can affect, in principle at least, the reversible interconversion between their colorless and colorless states. Intrigued by these observations, we have designed, synthesized and characterized photochrome–nanoparticle assemblies combining spiropyran ligands[145-149] with cadmium sulfide quantum dots.[10c,12b,13b,16,20b] In this chapter, I report the preparation and properties of two different CdS-photochrome constructs illustrated in Figure 5.1 with particular emphasis on the nanoparticle influence on the switching processes associated with the photochromic ligand.

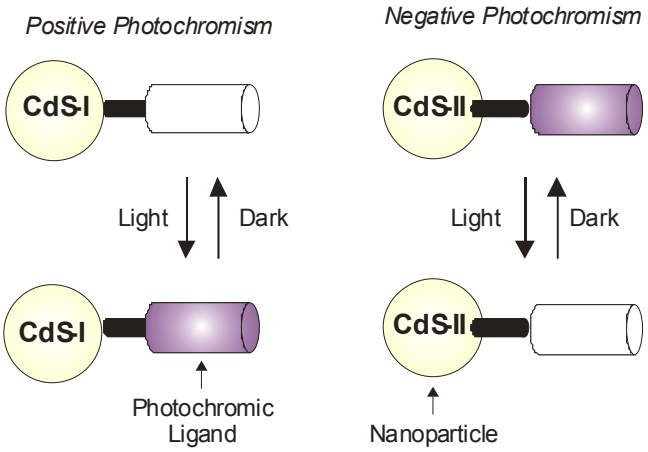

Figure 5.1. Nanoparticle-induced transition from positive to negative photochromism.

5.3. Results and Discussion

5.3.1. Design and Synthesis

The colorless spiropyran **26** (Fig. 5.2) switches to the colored merocyanine **26a** upon ultraviolet irradiation.[150] In organic solvents, the photogenerated isomer **26a** is not thermally stable and, eventually, reverts to the original state if the irradiated solution is stored in the dark. In dilute solutions, the thermal re-isomerization tends to follow first-order kinetics.[150] The corresponding decoloration constants range from 10^{-4} to 10^{-2} s^{-1} and decrease significantly with the polarity of the solvent.[151] In fact, the dipole moment of the zwitterionic isomer **26a** is significantly greater than that of **26**[140b] and, therefore, polar solvents stabilize **26a** relative to **26**. This effect is particularly evident when **26** is trapped inside silica monoliths prepared from a mixture of dimethylsulfoxide, ethanol and water.[152] Under these highly-polar conditions, the colorless form **26** switch gradually to the colored state **26a**, if the rigid material is stored in the dark. However, complete

decoloration occurs after visible irradiation of the doped silica monolith. Thus, this particular spiropyran displays positive photochromism in nonpolar environments, but negative photochromism in polar media.

The behavior of **26** and **26a** shows that the nature of the solvent has a pronounced influence on the kinetic and thermodynamic parameters regulating their thermal interconversion.[151,152] An alternative choice of *macroscopic* media in which the colorless and colored isomers are dissolved, the manipulation of the *microscopic* environment around them should also affect their interconversion. On the basis of these considerations, we have envisaged the possibility to anchor photochromic spiropyrans on the surface of semiconductor nanoparticles and regulate the properties of the inorganic component to control the isomerization of the organic ligands.

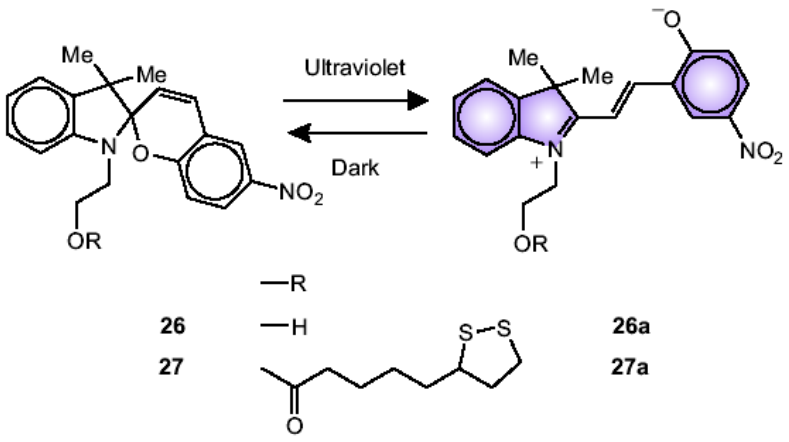

Figure 5.2. The ultraviolet (UV) irradiation of the spiropyrans **26** and **27** in organic solvents generates the corresponding merocyanines **26a** and **27a**, which revert to the original isomers under visible (VIS) irradiation or upon storage in the dark.

Specifically, we have designed the spiropyran **27** (Fig. 5.2), which has a dithiolane appendage able to encourage the adsorption of this compound on the surface of cadmium sulfide nanoparticles. We have prepared this molecule in a single synthetic step starting from **26**.[113a] In particular, the reaction of **26** with (±)-α-lipoic acid in the presence of *N*,*N*'-dicyclohexylcarbodiimide and 4-dimethylaminopyridine gives the target spiropyran **27** in a yield of 64%.

5.3.2. Photochromic Component

The ultraviolet–visible absorption spectrum (***a*** in Fig. 5.3) of a dichloroethane solution of **27** does not show any significant absorption at wavelengths longer than 400 nm. After ultraviolet irradiation, the colorless spiropyran **27** switches to the colored merocyanine **27a** with the concomitant appearance of a band centered at 592 nm in the absorption spectrum (***b*** in Fig. 5.3). This absorption decays with first-order kinetics upon storage of the irradiated solution in the dark (***c*** in Fig. 5.3). Non-linear curve fitting of the temporal evolution of the absorbance at 592 nm (***d*** in Fig. 5.3) indicates that the rate constant for the isomerization of **27a** back to **27** is *ca.* 4×10^{-2} s^{-1} in dichloroethane at 20°C. Thus, this photochromic switch undergoes thermal decoloration under these particular experimental conditions, displaying positive photochromism.

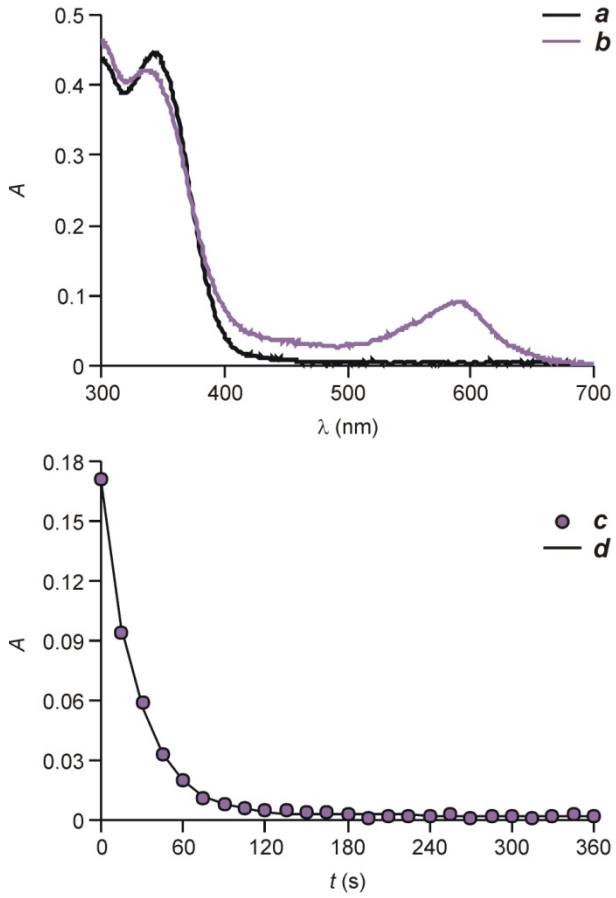

Figure 5.3. The ultraviolet–visible absorption spectra of a solution (0.1 mM, dichloroethane, 20°C) of **27** before (***a***) and after (***b***) continuous irradiation (365 nm, 0.4 mW cm^{-2}, 10 min). The evolution of the absorbance at 592 nm after irradiation (***c***) and the associated monoexponential curve-fitting (***d***).

5.3.3. Synthesis of Nanoparticles and IR Spectroscopy

We have prepared two sets of cadmium sulfide nanoparticles adapting literature protocols.[153,154] In one instance (**CdS–I**), we have reacted cadmium acetate and elemental sulfur in the presence of tri-*n*-octylposphine. In the other (**CdS–II**), we have treated cadmium perchlorate with sodium sulfite in the presence of sodium dioctylsulfosuccinate. In both instances, we have coated the resulting nanoparticles with 1-decanethiol. The

luminescence spectra of the final assemblies show a narrow band-gap emission for **CdS–I** (***a*** in Fig. 5.4) and a broad trap emission for **CdS–II** (***b***). The broad band of **CdS–II** is indicative of surface defects[10c,12b,13b,16,20b], which quench the band-gap emission of this particular set of particles and dominate their emission behavior. The distinct emissive behavior of **CdS–I** and **CdS–II** demonstrates that the two sets of particles have different surface morphologies. [10c,12b,13b,16,20b]

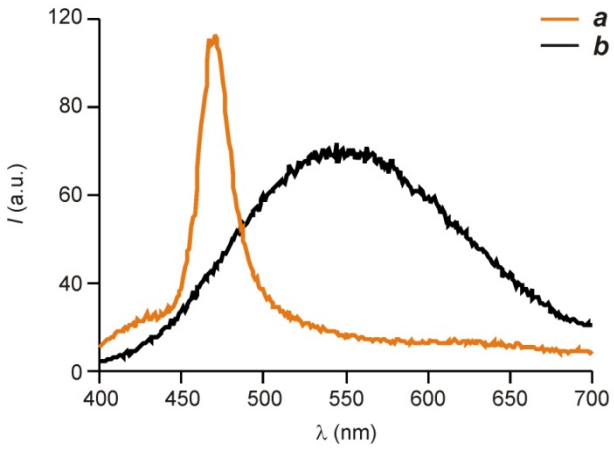

Figure 5.4. The emission spectra of solutions (dichloroethane, 20°C, λ_{Ex} = 380 nm) of **CdS–I** (***a***, 0.1 μM) and **CdS–II** (***b***, 0.5 μM).

Nonetheless, the treatment of either **CdS–I** or **CdS–II** with **27** in chloroform results in the adsorption of the photochromic component on both nanoparticles to generate **CdS–I–27** and **CdS–II–27**. Consistently, the characteristic peaks of **27** (***a*** in Fig. 5.5) can also be observed in the infrared absorption spectra of **CdS–I–27** (***b*** in Fig. 5.5) and **CdS–II–27** (**c** in Fig. 5.5). Furthermore, the ultraviolet regions of the absorption spectra of **CdS–I** (***a*** in Fig. 5.6) and **CdS–II** (***a*** in Fig. 5.7) show a significant absorbance increase after their conversion to **CdS–I–27** (***b*** in Fig. 5.6) and **CdS–II–27** (***b*** in Fig. 5.7), confirming the presence of the organic ligands on the surface of the inorganic nanoparticles.

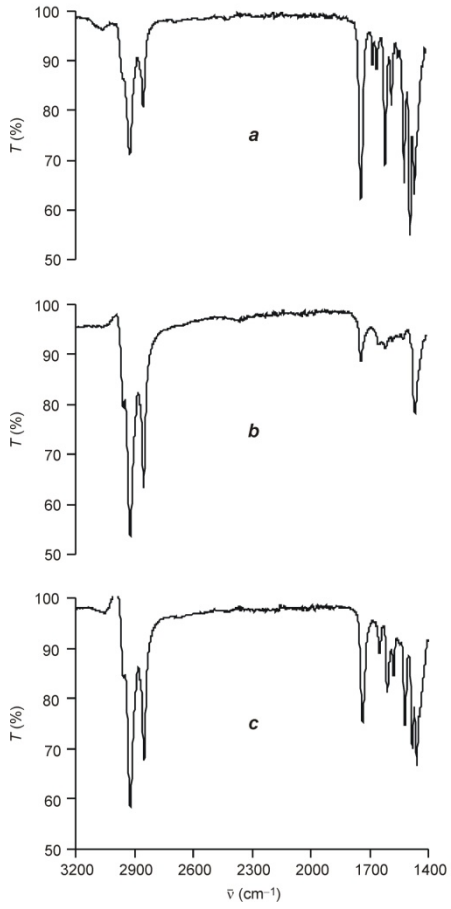

Figure 5.5. The infrared absorption spectra (20°C) of powders of **27** (***a***), **CdS–I–27** (***b***) and **CdS–II–27** (***c***).

5.3.4. Photochrome–nanoparticle Assemblies

After ultraviolet irradiation, the photochromic ligand of **CdS–I–27** switches to its merocyanine isomer forming **CdS–I–27a**. As a result, the characteristic band for the photogenerated isomer appears at 530 nm (***b*** and ***c*** in Fig. 5.6).

As observed for the thermal re-isomerization of **27a** back to **27**, the visible absorption band decays with first-order kinetics (***d*** in Fig. 5.6), when the photogenerated sample of **CdS–I–27a** is maintained in the dark. The non-linear curve fitting (***e*** in Fig. 5.6) of the

temporal evolution of the absorbance reveals the rate constant for the re-isomerization process to be *ca.* 2×10^{-2} s^{-1} in dichloroethane at 20°C. This value is smaller than the one determined in the absence of the nanoparticle. Thus, the photochromic switch still displays positive photochromism, albeit with slower thermal decoloration kinetics, despite its adsorption on these particular inorganic nanoparticles.

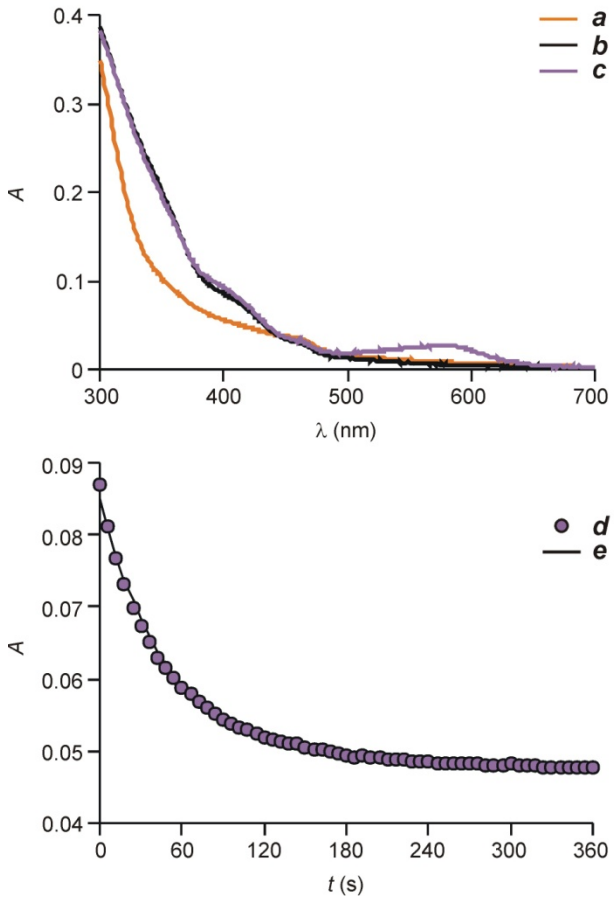

Figure 5.6. The ultraviolet–visible absorption spectra of solutions (0.1 µM, dichloroethane, 20°C) of **CdS–I** (***a***) or **CdS–I–27** before (***b***) and after (***c***) continuous irradiation (365 nm, 0.4 mW cm^{-2}, 10 min). The evolution of the absorbance at 530 nm (***d***) after irradiation and the associated monoexponential curve-fitting (***e***).

The behavior of **CdS–II–27** is significantly different than that of **CdS–I–27**. Indeed, the absorption spectrum (***b*** in Fig. 5.7), recorded after the adsorption of the photochromic ligand and storage in the dark, shows the characteristic band of the merocyanine isomer at 531 nm. This absorption disappears after visible irradiation of the sample (***c*** in Fig. 5.7), in agreement with the interconversion of **CdS–II–27a** into **CdS–II–27**. However, it grows again with first-order kinetics (***d*** in Fig. 5.7) if **CdS–II–27** is maintained in the dark. The non-linear curve fitting (***e*** in Fig. 5.7) of the temporal evolution of the absorbance indicates the rate constant for the isomerization of **CdS–II–27** into **CdS–II–27a** to be *ca.* 6×10^{-5} s^{-1} in dichloroethane at 20°C. Thus, the colored state **27b** of the photochromic ligand is stabilized relative to the colorless one **27**, when this species is adsorbed on the surface of **CdS–II**. As a result, these particular nanoparticles encourage the thermal coloration of the photochromic component.

The transition from the positive photochromism of **CdS–I–27** to the negative photochromism of **CdS–II–27** must be a result of the characteristic surface defects of **CdS–II**[10c,12b,13b,16,20b] whose presence is obvious from the emission spectrum (***b*** in Fig. 3). Indeed, these particular cadmium sulfide nanoparticles are known to encourage the adsorption of charged organic compounds on their surface as a consequence of electrostatic interactions.[155] Presumably, the very same interactions tend to stabilize the zwitterionic isomer **27a** relative **27**. In fact, the greater dipole moment of the colored state **27a** relative to the colorless form **27**[140b] is known to induce the thermal coloration of this photochromic system in polar environments.[152]

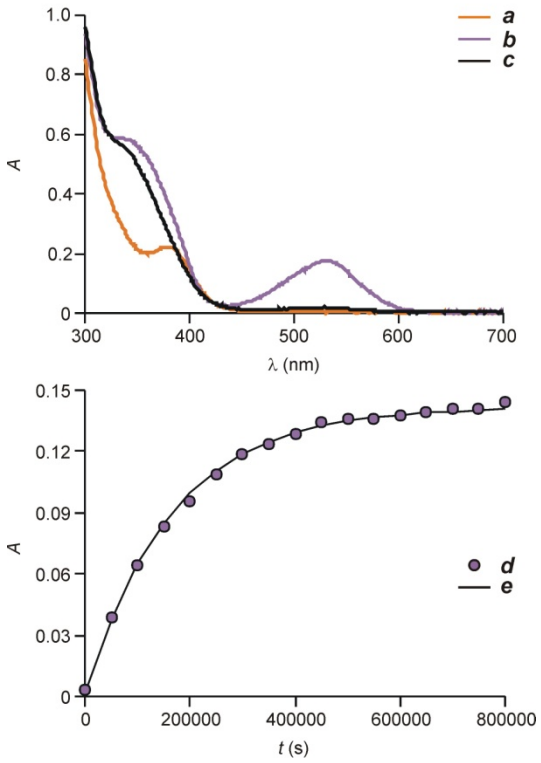

Figure 5.7. The ultraviolet–visible absorption spectra of solutions (0.5 μM, dichloroethane, 20°C) of **CdS–II** (***a***) or **CdS–II–27a** before (***b***) and after (***c***) continuous irradiation (562 nm, 0.3 mW cm^{-2}, 15 min). The evolution of the absorbance at 531 nm (***d***) after irradiation and the associated monoexponential curve-fitting (***e***).

5.4. Conclusions

A dithiolane anchoring group can be attached to a photochromic spiropyran relying on ester-bond formation. The resulting compound adsorbs spontaneously on the surface of cadmium sulfide quantum dots, when the organic ligands and the inorganic nanoparticles are combined in organic solvents. The significant changes in the ultraviolet and infrared regions of the absorption spectra confirm the formation of photochrome–nanoparticle assemblies. When cadmium sulfide nanoparticles prepared in the presence of tri-*n*-octylposphine are employed, the photochromic ligand displays positive photochromism.

However, the adsorption of the ligands on the surface of the nanoparticles delays the thermal decoloration kinetics. When cadmium sulfide nanoparticles prepared in the presence of sodium dioctylsulfosuccinate are employed instead, the photochromic ligand displays negative photochromism. The transition from positive to negative photochromism is a result of the surface defects introduced in the nanoparticles during their preparation. Presumably, electrostatic interactions between the nanoparticle defects and the colored state of the photochromic ligand are responsible for this behavior. Also, one should keep in mind that the size of nanoparticles prepared with different ways are not exactly the same. These factors also can affetct relative stabilities of color or colored states of photochromic unit. Thus, our studies demonstrate that the thermal isomerization associated with the reversible interconversion between spiropyrans and their merocyanine isomers are extremely sensitive to their microscopic environments. Therefore, the coloration and decoloration kinetics of a photochromic spiropyran can be regulated, in principle at least, with careful manipulations of the surface properties of a nanostructured partner in photochrome–nanoparticle assemblies.

CHAPTER 6

PHOTOCHROMIC NANOCOMPOSITES OF BIPYRIDINIUM DICATIONS AND SEMICONDUCTOR QUANTUM DOTS

6.1. Summary

The photoinduced transfer of electrons from appropriate donors to bipyridinium dications is a viable operating mechanism for the implementation of photochromic materials. The absorption bands of bipyridinium dications, however, are confined within the ultraviolet region. Therefore, these photochromic systems cannot be operated with visible photons. In order to overcome this limitation, we have exploited the photophysical properties of CdSe–ZnS core–shell quantum dots to mediate the transfer of electrons from sacrificial electron donors to bipyridinium acceptors. Our studies demonstrate that the excitation of the quantum dots with visible light in the presence of a sacrificial electron donor, triethanolamine, results in the reduction of colorless bipyridinium dications to the corresponding colored radical cations with a quantum yield of *ca.* 1 %. The photogenerated and colored state switches back to the original and colorless one upon exposure to molecular oxygen, which encourages the re-oxidation of the radical cation back to the initial dication. The photochromic process occurs in homogeneous solution as well as in films of bipyridinium bisthiols and CdSe–ZnS nanoparticles. Thus, our operating principles can lead to the development of a new family of photochromic materials base on bipyridinium dications and semiconductor quantum dots.

6.2. Photochromism of Bipyridinium Dications

In the presence of complementary electron donors, the ultraviolet irradiation of a colorless bipyridinium dication can induce its monoelectronic reduction to the corresponding radical cation.[156,157] The photogenerated and colored state can be switched back to the colorless one simply by exposing the sample to molecular oxygen. Under these conditions, the re-oxidation of the radical cation restores to original dication. In fact, numerous photochromic systems operating in solution, within polymer matrices or in the crystalline state have already been developed on the basis of these reversible transformations. [156,157] A serious limitation of bipyridinium dications, however, is that they can only absorb radiation within the ultraviolet region with modest molar extinction coefficients. Therefore, these photochromic systems can only be operated with ultraviolet photons. In principle, this drawback can be overcome relying on the excitation of chromophoric groups that can mediate the transfer of one electron from an appropriate donor to a bipyridinium acceptor.

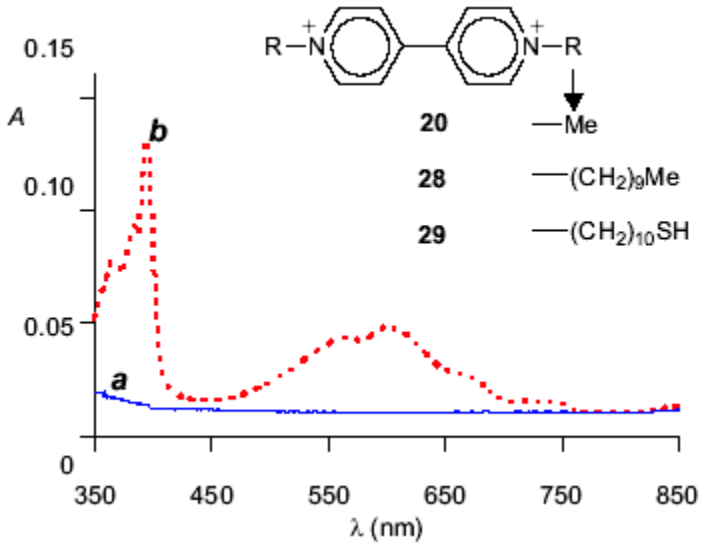

Figure 6.1. The Absorption spectra of solution of **20** (1mM, 0.1 M KCl_{aq}, 20 ^{o}C) recorded before (a) and after (b) electrolysis at -1.5 V, relative to the platinum pseudo-reference electrode.

These particular dicationic species are generally colorless, but turn violet/blue after monoelectronic reduction.[158] For example, the absorption spectrum of a solution of methyl viologen **20** shows intense bands in the visible region only after reductive electrolysis (***a*** and ***b*** in Fig. 6.1). Literature data demonstrate that CdSe quantum dots can efficiently transfer electrons to complementary organic acceptors upon excitation.[124] These inorganic nanoparticles absorb visible light with molar extinction coefficients greater than those of conventional organic chromophores.[10c,12b,13b,16,20b] For example, the molar extinction coefficient of CdSe quantum dots with a diameter of *ca.* 3 nm approaches the value of 100 mM^{-1} cm^{-1} at *ca.* 540 nm.[31] Thus, similar nanoparticles should be able to collect efficiently visible photons and inject electrons into bipyridinium partners, inducing their coloration.

6.3. Results and Discussion

6.3.1. Design and Synthesis

On the basis of these considerations, we have assessed the spectroscopic properties of CdSe–ZnS core–shell quantum dots in the presence of the chloride salt of the bipyridinium dication **28** and **29**(Fig. 6.1). The CdSe–ZnS core–shell quantum dots were synthesized following literature procedures.[23,27] Compounds **28** and **29** were synthesized following literature protocol.[160] The visible region of the absorption spectrum of the quantum dots (***a*** in Fig. 6.2) does not change after the addition of **28**. Instead, the pronounced emission band of the quantum dots (***b*** in Fig. 6.2) is completely suppressed in the presence of **28** (***c*** in Fig. 6.2). The effective luminescence quenching is consistent with the transfer of electrons from the excited quantum dots to the bipyridinium acceptors.

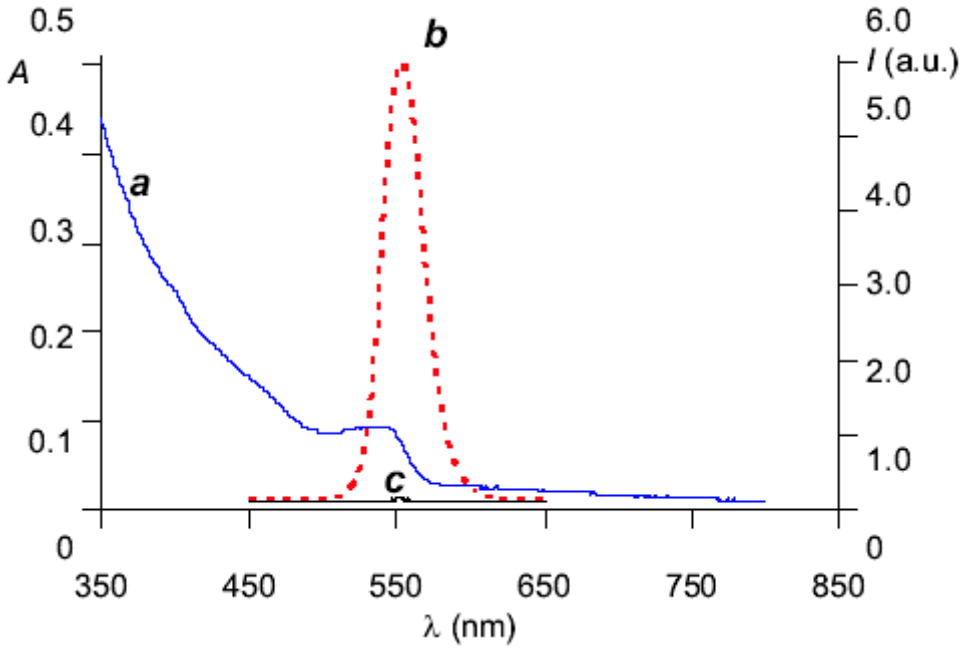

Figure 6.2. The absorption spectrum (***a***) of CdSe–ZnS core–shell quantum dots (2 μM, $CHCl_3$, 20°C) and the emission spectra ($\lambda_{ex.}$ = 350 nm) of the same solution recorded before (***b***) and after (***c***) the addition of the chloride salt of the bipyridinium dication **28** (85 μM).

6.3.2. Photolysis in Solution

In fact, the absorption spectrum (***a*** in Fig. 6.3), recorded in the presence of a sacrificial electron donor (triethanolamine), shows the appearance of additional bands (***b***) in the visible region, after continuous irradiation at 562 nm. The corresponding difference spectrum (***c*** in Fig. 6.4) confirms the formation of the radical cation of **28**. Indeed, this spectrum closely resembles that of **20** (***b*** in Fig. 6.1), recorded after electrochemical reduction.

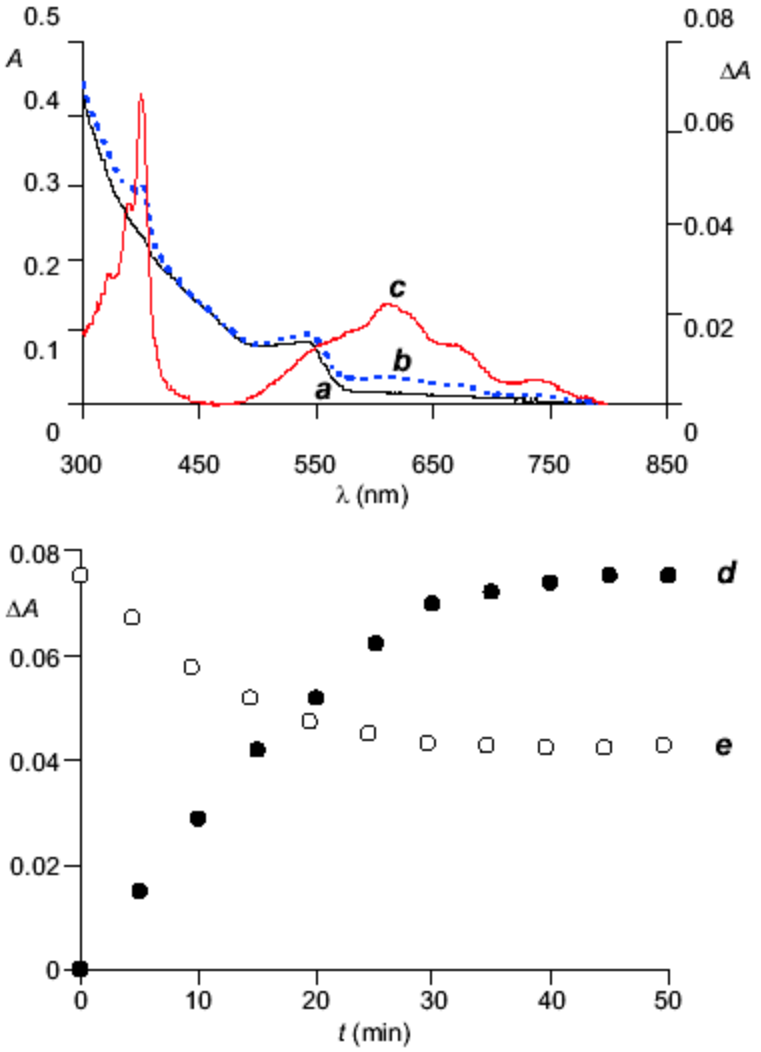

Figure 6.3. The absorption spectra of a solution ($CHCl_3$, 20°C) of CdSe–ZnS core–shell quantum dots (2 μM), the chloride salt of **28** (85 μM) and triethanolamine (100 mM) recorded before (***a***) and after (***b***) continuous irradiation (562 nm, 0.2 mW cm^{-2}, 30 min) and the corresponding difference spectrum (***c***). The evolution of the absorbance at 397 nm during continuous irradiation (***d***) and the subsequent exposure to air (***e***).

Thus, the excited quantum dots (Fig. 6.4) donate electrons to **28** and accept electrons from triethanolamine (TEA). The overall result is the photoinduced transfer of one electron from the sacrificial electron donor to the bipyridinium acceptor with the formation of the colored radical cation of **28**.

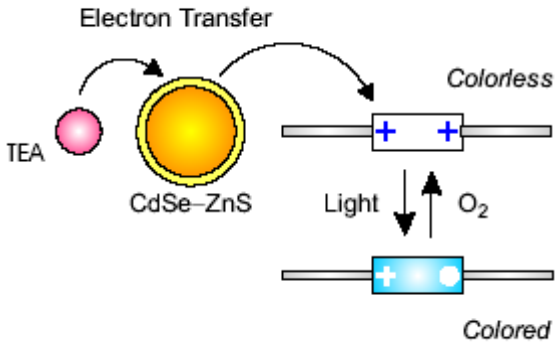

Figure 6.4. The excitation of a CdSe–ZnS core–shell quantum dot causes the transfer of an electron to the bipyridinium dication **28**. A second electron transfer step from triethanolamine (TEA) to the nanoparticle fills the photogenerated hole.

The photoinduced coloration of the mixture of **28** and the quantum dots is also evident from the absorbance increase at 397 nm with the irradiation time (***d*** in Fig. 6.3). The analysis of the linear portion of this plot suggests the quantum yield of photocoloration to be 0.015 ± 0.001. Interestingly the process can be reversed in full by exposing the colored solution to air for a prolonged time. After *ca.* 24 h, the absoprtion spectrum becomes virtually indistinguishable from the one of the initial state (***a*** in Fig. 6.3). Indeed, the gradual diffusion of molecular oxygen in the sample results in the re-oxidation of the radical cation of **28** with a concomitant decrease in absorbance at 397 nm (***e*** in Fig. 6.3).

6.3.2. Photolysis on Quartz Substrate

In order to extend these operating principles from solutions to films, we have synthesized the chloride salt of the bipyridinium dication **29** (Fig. 6.2). The terminal thiol groups of this compound are expected to adsorb on the surface of CdSe–ZnS core–shell quantum dots and, presumably, generate a cross-linked array of nanoparticles (Figure 6.5). Indeed, the combination of a solution of the quantum dots with a solution of **29** leads to the formation of a precipitate. The resulting material is virtually insoluble in any organic solvent as well as in water. The terminal thiol groups of **29** appear to be responsible for this behavior. In fact, no precipitate is instead formed when **28** is employed under otherwise identical conditions. Furthermore, mixtures of **28** and the quantum dots are readily soluble in many organic solvents.

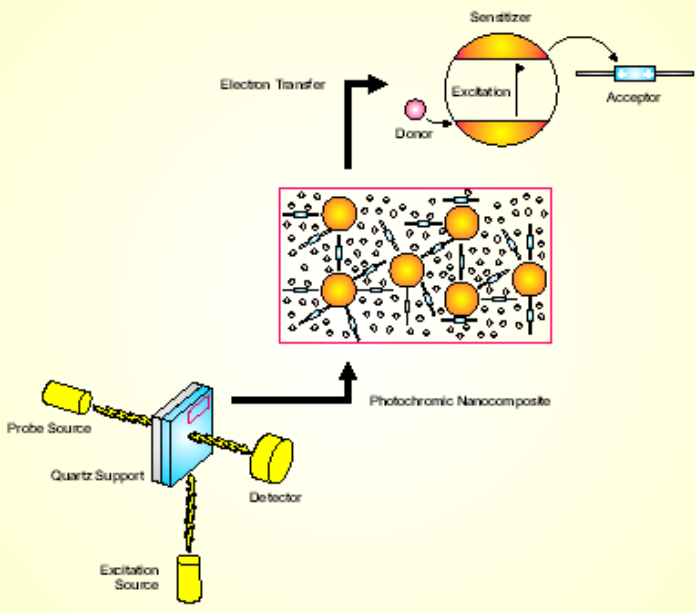

Figure 6.5. The excitation of a CdSe–ZnS core–shell quantum dot on quartz causes the transfer of an electron to the bipyridinium dication **29**. A second electron transfer step from triethanolamine (TEA) to the nanoparticle fills the photogenerated hole.

The absorption spectrum (***a*** in Fig. 6.6) of the precipitate obtained from **29** and the quantum dots, deposited on a quartz slide and in contact with a solution of TEA, shows the characteristic bands of the nanoparticles (Figure 6.5). After continuous irradiation at 562 nm, additional absorptions appear in the visible region (***b*** in Fig. 6.6). The corresponding difference spectrum (***c*** in Fig. 6.6) reveals the photogenerated bands to be the characteristic absorptions of a bipyridinium radical cation.

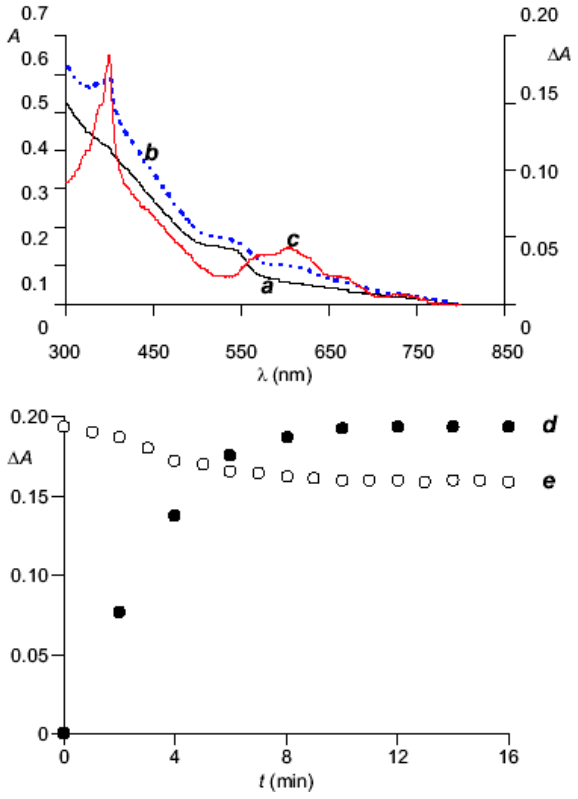

Figure 6.6. The absorption spectra of a film, prepared from CdSe–ZnS core–shell quantum dots and the chloride salt of **29**, deposited on quartz and in contact with a solution of triethanolamine (100 mM, MeCN, 20°C) recorded before (***a***) and after (***b***) continuous irradiation (562 nm, 0.2 mW cm^{-2}, 8 min) and the corresponding difference spectrum (***c***). The evolution of the absorbance at 397 nm during continuous irradiation (***d***) and the subsequent exposure to air (***e***).

Once again, the process can be followed by monitoring the increase in absorbance at 397 nm during irradiation (***d*** in Fig. 6.6). As observed for **28** in homogeneous solution, the exposure of the sample to air leads to a gradual absorbance decrease (***e*** in Fig. 6.6). The diffusion of molecular oxygen in the sample encourages the re-oxidation of the radical cations back to the dicationic form. In fact, the absorption spectrum recorded after exposing the sample to air for *ca.* 24 h is identical to the one measured before irradiation (***a*** in Fig. 6.6).

6.4. Conclusions

In summary, we have demonstrated that CdSe–ZnS core–shell quantum dots can efficiently mediate the transfer of electrons from sacrificial donors to bipyridinium acceptors upon visible irradiation. The process can be implemented in homogeneous solutions or in films with quantum yields of *ca.* 1%. The photocoloration of the bipyridinium dications can be reversed in both instances simply by exposing the samples to molecular oxygen. Thus, our operating mechanism and choice of building blocks can, in principle, lead to the development of a new family of photochromic materials that can be operated with visible photons relying on the unique photophysical properties of semiconductor quantum dots.

CHAPTER 7

EXPERIMENTAL PROCEDURES

7.1. General Methods

The chemicals were purchased from commercial sources and were used as received with the exception of MeCN and CH_2Cl_2, which were distilled over CaH_2. All reactions were monitored by thin-layer chromatography, using aluminum sheets coated with silica (60, F_{254}). The fast atom bombardment mass spectra (FABMS) were recorded with a VG Mass Lab Trio-2 in a 3-nitrobenzyl alcohol matrix. The nuclear magnetic resonance (NMR) spectra were recorded with Bruker Avance 300, 400 or 500 spectrometers. Infrared absorption spectra were recorded with a Perkin-Elmer Spectrum One Fourier transform spectrometer. The absorption spectra were recorded with a Varian Cary 100 Bio spectrometer, using quartz cells with a path length of 0.5 cm. The emission spectra were recorded with a Varian Cary Eclipse spectrometer in aerated solutions. The luminescence lifetimes were measured with a Edinburgh Instruments FL920 spectrometer in aerated solutions. The samples for Chapter 4 and 5 were irradiated with a Mineralight UVGL–25 lamp (365 nm, 0.4 mW cm^{-2}). The samples for Chapter 6 were irradiated with a Thermo Oriel liquid light guide coupled to a Spectral Energy LH 150/1 light source, a Spectral Energy 150 W xenon arc lamp and a Thermo Oriel 562 ± 10 nm interference filter.

7.2. Experimental Procedures

Materials

The compounds **10**, **16** and **17a**[114b]; **25**[159]; **26**[150] and **28**, **29**[160] were prepared according to literature procedures.

Experimental Section

2-Phenyl-3,3'-dimethyl-5-methoxy-3H-indole (**11**). A solution of *i*-propylphenylketone (2.2 mL, 14 mmol), 4-methoxyphenylhydrazine hydrochloride (2.5 g, 14 mmol) and 4-toluenesulfonic acid (27 mg, 0.1 mmol) in EtOH (30 mL) was heated under reflux for 6 h. After cooling down to ambient temperature, aqueous $NaHCO_3$ (5 w%, 10 mL) was added and the mixture was extracted with CH_2Cl_2 (4 × 10 mL). Then, the solvent was distilled off under reduced pressure and the residue was purified by column chromatography [SiO_2: hexane/$MeCO_2Et$ 1:1 (v/v)] to afford **11** (2.15 g, 60 %) as a brown-yellow oil. FABMS: *m/z* = 251 $[M + H]^+$; ^{1}H-NMR (300 MHz, $CDCl_3$): δ = 1.59 (6H, s), 3.82 (3H, s), 6.89–6.91 (2H, m), 7.47–7.49 (3H, m), 7.64 (1H, d, 9 Hz), 8.10–8.13 (2H, m); ^{13}C-NMR (75 MHz, $CDCl_3$): δ = 25.1, 53.3, 55.9, 107.7, 112.6, 121.5, 128.2, 128.5, 128.8, 130.4, 133.6, 149.5, 158.8, 181.5.

2-Phenyl-3,3'-dimethyl-5-hydroxy-3H-indole (**12**). A solution of BBr_3 (1 M) in CH_2Cl_2 (6 mL) was added dropwise to a solution of **11** (0.9 g, 4 mmol) in CH_2Cl_2 (30 mL) maintained at 0°C under Ar. After 1h, the mixture was allowed to warm up to ambient temperature and was maintained under these conditions for a further 12 h. Then, a saturated aqueous solution of $NaHCO_3$ (15 mL) was added and the resulting mixture was extracted with CH_2Cl_2 (3 × 20 mL). The solvent was distilled off under reduced pressure to afford **12** (0.75 g, 83%) as a green solid. FABMS: *m/z* = 238 $[M + H]^+$; ^{1}H-NMR (400 MHz, $CDCl_3$): δ = 1.64 (6H, s), 6.90 (1H, dd, 8 and 2 Hz), 6.97 (1H, d, 2 Hz), 7.55–7.58 (3H, m), 7.71 (1H, d, 8 Hz), 8.24 (2H, d, 8 Hz); ^{13}C-NMR (100 MHz, $CDCl_3$): δ = 25.9, 31.8, 53.8, 109.5, 115.7, 120.8, 128.4, 129.2, 129.5, 130.3, 132.8, 148.3, 156.9, 181.7.

2-(4'-Nitrophenylazo)-5a-phenyl-6,6-dimethyl-5a,6-dihydro-8-methoxy-12H-indolo[2,1-b][1,3]benzooxazine (**13**). A solution of PBr_3 (26 μL, 0.3 mmol) in CH_2Cl_2

(300 μL) was added dropwise to a solution of **10** (100 mg, 0.4 mmol) in MeCN (20 mL) maintained at 0°C under Ar. After the addition of Et_3N (77 μL, 0.6 mmol), the mixture was allowed to warm up to ambient temperature over 3 h and then it was heated at 50°C for 12 h. After the subsequent addition of **11** (112 mg, 0.5 mmol), the mixture was heated under reflux for 48 h. After cooling down to ambient temperature, the solvent was distilled off under reduced pressure and the residue was purified by column chromatography [SiO_2: CH_2Cl_2/hexane 3:1 (v/v)] to afford **13** (47 mg, 25%) as an orange solid. FABMS: *m/z* = 507 $[M + H]^+$; ^{1}H-NMR (500 MHz, $CDCl_3$): δ = 0.86 (3H, s), 1.59 (3H, s), 3.78 (3H, s), 4.55 (1H, d, 17 Hz), 4.60 (1H, d, 17 Hz), 6.64–6.70 (2H, m), 6.80 (1H, d, 2 Hz), 6.97 (1H, d, 9 Hz), 7.34–7.42 (3H, m), 7.64 (1H, d, 2 Hz), 7.38–7.73 (3H, m), 7.91 (2H, d, 9 Hz), 8.33 (2H, d, 9 Hz); ^{13}C-NMR (75 MHz, $CDCl_3$): δ = 18.8, 27.9, 41.5, 50.2, 56.2, 105.4, 109.6, 110.4, 111.8, 118.8, 120.7, 122.6, 123.4, 124.5, 125.1, 128.6, 128.8, 129.1, 136.8, 139.8, 141.4, 146.7, 148.6, 155.0, 156.4, 158.1.

2-(4'-Nitrophenylazo)-5a-phenyl-6,6-dimethyl-5a,6-dihydro-8-hydroxy-12H-indolo[2,1-b][1,3]benzooxazine (**14**). A solution of PBr_3 (18 μL, 0.2 mmol) in CH_2Cl_2 (160 μL) was added dropwise to a solution of **10** (60 mg, 0.2 mmol) in MeCN (15 mL) maintained at 0°C under Ar. After the addition of Et_3N (50 μL, 0.4 mmol), the mixture was allowed to warm up to ambient temperature over 3 h and then it was heated at 50°C for 12 h. After the subsequent addition of **12** (71 mg, 0.3 mmol), the mixture was heated under reflux for 48 h. After cooling down to ambient temperature, the solvent was distilled off under reduced pressure and the residue was purified by column chromatography [SiO_2: CH_2Cl_2/hexane 3:1 → 5:1 (v/v)] to afford **14** (27 mg, 25%) as an orange solid. FABMS: *m/z* = 493 $[M + H]^+$; ^{1}H-NMR (400 MHz, $CDCl_3$): δ = 0.85 (3H, s), 1.57 (3H, s), 4.43 (1H, s), 4.53 (1H, d, 16 Hz), 4.58 (1H, d, 16 Hz), 6.57–6.63 (2H, m), 6.72 (1H, d, 2 Hz), 6.95 (1H, d, 9 Hz), 7.32–7.43 (3H, m), 7.63 (1H, d, 2 Hz), 7.67–7.69 (2H, m), 7.73 (1H, dd, 2 and 9 Hz), 7.91 (2H, d, 9 Hz), 8.33 (2H, d, 9 Hz); ^{13}C-NMR

(100 MHz, $CDCl_3$): δ = 18.7, 27.8, 41.5, 50.2, 105.4, 109.8, 111.2, 113.9, 118.8, 120.7, 122.6, 123.4, 124.5, 125.1, 128.5, 128.8, 129.1, 136.7, 140.0, 141.4, 146.7, 148.6, 150.4, 156.4, 158.1.

2-(4'-Nitrophenylazo)-5a-phenyl-6,6-dimethyl-5a,6-dihydro-8-(1',2'-dithiolane-3')-pentacarboxy-12H-indolo[2,1-b][1,3]-benzooxazine (**15**). A solution of DCC (11 mg, 0.05 mmol) was added dropwise to a solution of **14** (23 mg, 0.05 mmol), (±)-α-lipoic acid (11 mg, 0.05 mmol) and DMAP (1 mg) in CH_2Cl_2 (25 mL) maintained at 0°C under Ar. After 1 h, the mixture was allowed to warm up to ambient temperature and maintained under these conditions for a further 48 h. Then, the solvent was distilled off under reduced pressure and the residue was purified by column chromatography [SiO_2: CH_2Cl_2/hexane 4:1 → 6:1 (v/v)] to afford **15** (32 mg, 94%) as an orange solid. FABMS: *m/z* = 681 $[M + H]^+$; ^{1}H-NMR (400 MHz, $CDCl_3$): δ = 0.86 (3H, s), 0.90–0.92 (2H, m), 1.58 (3H, s), 1.75–1.80 (4H, m), 1.93–1.95 (1H, m), 2.46–2.50 (1H, m), 2.56 (2H, t, 7 Hz), 3.12–3.20 (2H, m), 3.59–3.63 (1H, m), 4.57 (1H, d, 17 Hz), 4.63 (1H, d, 17 Hz), 6.69 (1H, d, 9 Hz), 6.85 (1H, dd, 2 and 8 Hz), 6.90 (1H, d, 2 Hz), 6.98 (1H, d, 9 Hz), 7.34–7.43 (3H, m), 7.63 (1H, d, 2 Hz), 7.65–7.67 (2H, m), 7.74 (1H, dd, 2 and 9 Hz), 7.92 (2H, d, 9 Hz), 8.34 (2H, d, 9 Hz); ^{13}C-NMR (100 MHz, $CDCl_3$): δ = 14.5, 18.8, 25.1, 27.9, 29.1, 34.5, 35.1, 38.9, 40.6, 50.1, 56.7, 105.2, 109.4, 116.6, 118.9, 120.4, 120.5, 122.5, 123.4, 124.6, 125.1, 128.5, 128.9, 129.2, 136.5, 139.4, 145.0, 145.3, 146.8, 148.6, 156.4, 157.9, 172.8.

7-Methoxy-9,9-dimethyl-9a-phenyl-2,3,9,9a-tetrahydro-oxazolo[3,2-a]indole (**18**). A solution of **10** (384 mg, 1.5 mmol) and 2-bromoethanol (300 μL, 4.2 mmol) in toluene (25 mL) was heated under reflux and Ar for 4 d. After cooling down to ambient temperature, the solvent was distilled off under reduced pressure. The solid residue was washed with CH_2Cl_2 / hexanes [1:20 (v/v), 40 mL] and dissolved in MeCN / H_2O [1:1 (v/v), 10 mL]. After the addition of aqueous KOH (2 M, 1 mL), the mixture was stirred

for 45 min and washed with CH_2Cl_2 (20 mL). The solvent of the organic phase was distilled off under reduced pressure and the residue was purified column chromatography [SiO_2: CH_2Cl_2 / $MeCO_2Et$, 1:1 (v/v)] to afford **18** (65 mg, 14%) as a pale yellow solid. FABMS: *m/z* = 295 $[M]^+$; ^{1}H-NMR (500 MHz, $CDCl_3$): δ = 0.79 (3H, s), 1.53 (3H, s), 3.28–3.32 (1H, m), 3.50–3.53 (1H, m), 3.60–3.67 (1H, m), 3.69–3.73 (1H, m), 3.82 (3H, s), 6.72 (1H, m), 6.77 (2H, m), 7.37–7.42 (3H, m), 7.67–7.72 (2H. m); ^{13}C-NMR (100 MHz, $CDCl_3$): δ = 20.4, 29.3, 48.1, 50.8, 56.1, 63.4, 109.5, 112.3, 112.5, 127.6, 128.1, 138.9, 141.0, 144.8, 155.6.

CdSe–ZnS. A mixture of CdO (51 mg, 0.4 mmol), tetra-*n*-decylphosphonic acid (223 mg, 0.8 mmol), tri-*n*-octylphosphine oxide (3.78 g, 9.8 mmol) was heated at 320°C under Ar until a clear solution was obtained. Then, the temperature was lowered to 220°C and a solution of Se (41 mg, 0.5 mmol) in tri-*n*-octylphosphine (2.4 mL) was added. After the addition, the mixture was maintained at 200°C for 40 min. Then, the temperature was lowered to 120°C and a solution of $ZnEt_2$ (1.6 mL, 0.16 mmol) and hexamethyldisilathiane (0.30 mL, 1.4 mmol) in tri-*n*-octylphosphine (5 mL) was added dropwise. After the addition, the mixture was maintained at 70°C for 5 h. After cooling down to ambient temperature, MeOH (200 mL) was added and the resulting precipitate was filtered and dissolved in $CHCl_3$ (50 mL). This procedure was repeated three more times and then the solvent was distilled off under reduced pressure to afford the CdSe–ZnS core–shell quantum dots (367 mg) as a reddish powder.

*CdSe–ZnS–**15***. A solution of CdSe–ZnS core–shell quantum dots (12 mg) and **15** (35 mg) in $CHCl_3$ (20 mL) was heated under reflux for 24 h. After cooling down to ambient temperature, the solvent was distilled off under reduced pressure. The residue was suspended in MeCN (8 mL) and the supernatant was removed after centrifugation. This procedure was repeated three more times to afford the modified CdSe–ZnS core–shell quantum dots (10 mg) as a reddish powder.

*Hydrophilic CdSe–ZnS Core–Shell Quantum Dots***.** A solution of hydrophobic CdSe–ZnS core–shell quantum dots (25 mg) and mercaptoacetic acid (**19**) (2 mL) in $CHCl_3$ (30 mL) was heated under reflux for 3 h. After cooling down to ambient temperature, the mixture was subjected to centrifugation. The residue was suspended in $CHCl_3$ (15 mL) and subjected to centrifugation. This treatment was repeated four additional times. The resulting solid was suspended in MeOH (15 mL) and subjected to centrifugation. This treatment was repeated two additional times. The residue was dried under reduced pressure and suspended in H_2O (5 mL). Aqueous KOH (0.1 M) was added dropwise until a clear solution was obtained. After the addition of Me_2CO (10 mL), the mixture was subjected to centrifugation to afford the modified CdSe–ZnS core–shell quantum dots (20 mg) as a reddish powder.

5-(2-Oxohexahydrothieno[3,4-d]imidazol-6-yl)-pentanoic Acid 3-Iodopropyl Ester **(24).** A solution of biotin (**23**) (125 mg, 0.5 mmol), 3-iodo-1-propanol (150 μL, 1.6 mmol) and TsOH (10 mg, 0.05 mmol) in PhMe (50 mL)) was heated under reflux and Ar for 3 d in a Dean–Stark apparatus. After cooling down to ambient temperature, the mixture was filtered and the solvent distilled off under reduced pressure. The residue was dissolved in CH_2Cl_2 (30 mL) and washed with H_2O (5 mL). The organic phase was dried ($MgSO_4$) and concentrated under reduced pressure to yield **24** (75 mg, 36%) as a white solid. FABMS: *m/z* = 413 $[M + H]^+$; ^{1}H-NMR (400 MHz, $CDCl_3$): δ = 1.40–1.45 (2H, m), 1.61–1.75 (4H, m), 2.10–2.16 (2H, m), 2.30 (2H, t, 7 Hz), 2.79 (1H, d, 13 Hz), 2.88 (1H, dd, 5 and 13 Hz), 3.15–3.18 (1H, m), 3.22 (2H, t, 7 Hz), 4.13 (2H, t, 6 Hz), 4.42–4.45 (1H, m), 4.61–4.65 (1H, m), 7.22 (1H, d, 8 Hz), 7.72 (1H, d, 8 Hz); ^{13}C-NMR (100 MHz, $CDCl_3$): δ = 25.0, 28.4, 28.8, 32.6, 34.2, 40.5, 55.8, 61.8, 63.6, 64.4, 164.5, 173.9.

1-*Methyl-1'-(3-(5-(2-Oxohexahydrothieno[3,4-d]imidazol-6-yl)-pentanoxy)-propyl)-4,4'-Bipyridinium Bisiodide* **(21).** A solution of **24** (37 mg, 0.09 mmol) and 1-methyl-

4,4′-pyridylpyridynium iodide (**25**) (9 mg, 0.03 mmol) in MeCN (15 mL) was heated under reflux and Ar for 10 d. After cooling down to ambient temperature, the solvent was distilled off and the residue was washed with MeCN (4 mL) to yield **21** (6 mg, 28%) as an orange solid. FABMS: *m/z* = 457 $[M - 2I]^+$; ^{1}H-NMR (500 MHz, CD_3OD): δ = 1.45–1.49 (2H, m), 1.53–1.71 (4H, m), 2.29–2.31 (2H, m), 2.49–2.51 (2H, m), 2.73 (1H, dd, 4 and 12 Hz), 2.93 (1H, dd, 5 and 12Hz), 3.20–3.23 (1H, m), 4.28–4.32 (3H, m), 4.48–4.52 (2H, m), 4.54 (3H, s), 4.77 (2H, d, 8 Hz), 8.69 (2H, d, 6 Hz), 8.73 (2H, d, 6 Hz), 9.21 (2H, d, 6 Hz), 9.34 (2H, d, 7 Hz).

2-(3',3'-Dimethyl-6-nitro-3'H-spiro[chromene-2,2'-indol]-1'-yl)ethyl-(1,2-dithiolane-3)-pentanoate (**27**). A solution of *N*,*N*'-dicyclohexylcarbodiimide (52 mg, 0.2 mmol) was added dropwise to a solution of **26** (81 mg, 0.2 mmol), (±)-α-lipoic acid (52 mg, 0.2 mmol) and 4-dimethylaminopyridine (3 mg) in dichloromethane (15 mL) maintained at 0°C under argon. After 1 h, the mixture was allowed to warm up to ambient temperature and maintained under these conditions for a further 48 h. Then, the solvent was distilled off under reduced pressure and the residue was purified by column chromatography [SiO_2: dichloromethane/hexane 4:1 → 6:1 (v/v)] to afford **27** (79 mg, 64%) as an orange solid. FABMS: *m/z* = 541 $[M + H]^+$; ^{1}H-NMR (chloroform-d_3): δ = 1.12 (3H, s), 1.30 (3H, s), 1.40–1.48 (2H, m), 1.59–1.67 (4H, m), 1.88–1.91 (1H, m), 2.27 (2H, t, 7 Hz), 2.41–2.48 (1H, m), 3.08–3.20 (2H, m), 3.40–3.54 (3H, m), 4.14–4.21 (1H, m), 4.21–4.30 (1H, m), 5.90 (1H, d, 10 Hz), 6.69 (1H, d, 8 Hz), 6.76 (1H, d, 8 Hz), 6.89–6.95 (2H, m), 7.10 (1H, dd, 1 and 7 Hz), 7.22 (1H, dt, 1 and 8 Hz), 8.01–8.06 (2H, m); ^{13}C-NMR (chloroform-d_3): δ = 20.3, 24.9, 26.3, 29.1, 34.3, 34.9, 38.9, 40.6, 42.8, 53.2, 56.7, 62.8, 106.9, 107.1, 116.0, 118.8, 120.3, 122.2, 123.2, 126.4, 128.2, 128.7, 136.1, 141.5, 147.1, 159.8, 173.6, 195.9.

CdSe–ZnS-27. A solution of CdSe–ZnS core–shell quantum dots (12 mg) and **SP-2** (35 mg) in chloroform (20 mL) was heated under reflux for 24 h. After cooling down to

ambient temperature, the solvent was distilled off under reduced pressure. The residue was suspended in MeCN (8 mL) and the supernatant was removed after centrifugation. This procedure was repeated three more times to afford the modified CdSe–ZnS-27 core–shell quantum dots (10 mg) as a reddish powder.

Preparation of ***CdS–I***. A solution of cadmium acetate hydrate (461 mg) in tri-*n*-octylphosphine (6 mL) and bis(2,4,4-trimethylpentyl)phosphinic acid (0.6 mL) was heated at 100°C under reduced pressure for 1 h. Similarly, a solution of elemental sulfur (64 mg) in oleylamine (3 mL) was maintained at ambient temperature under reduced pressure for 1 h. Then, the two solutions were combined under ambient conditions and added to a mixture of oleylamine (7 mL) and tri-*n*-octylphosphine (8 mL) maintained at 280°C. Prior to the addition, the mixture of oleylamine and tri-*n*-octylphosphine has also been heated at 100°C under reduced pressure for 1 h. After the addition, the temperature decreased to 250°C. The solution was maintained under these conditions for 30 min and then it was cooled down to ambient temperature. At this stage, a mixture of hexane (9 mL), *n*-butanol (18 mL) and methanol (72 mL) was added and the resulting suspension was centrifuged. After the removal of the supernatant, the solid residue was dissolved in the minimum amount of hexane (*ca.* 1 mL), re-precipitated by adding an excess of methanol (*ca.* 10 mL) and centrifuged again. This procedure was repeated three additional times. At this stage, 1-decanethiol (45 μL) was added to a solution of a portion (15 mg) of the resulting yellow powder in chloroform (15 mL). The mixture was stirred at ambient temperature under argon for 24 h and then the solvent was distilled off under reduced pressure. The solid residue was suspended in acetonitrile (8 mL), sonicated, centrifuged and separated from the supernatant. This procedure was repeated three additional times to afford **CdS–I** (9mg) as a yellow powder.

Preparation of ***CdS–II***. A mixture of an aqueous solution of cadmium perchlorate (0.4 M, 0.7 mL) and a heptane solution of sodium dioctylsulfosuccinate (0.2 M, 50 mL) was

stirred at ambient temperature under argon for 2 h. Similarly, a mixture of an aqueous solution of sodium sulfide (0.3 M, 0.7 mL) and a heptane solution of sodium dioctylsulfosuccinate (0.2 M, 50 mL) was also stirred at ambient temperature under argon for 2 h. Then, the two mixtures were combined and maintained under the same conditions for a further 1 h. At this stage, 1-decanethiol (1.5 mL) was added and the resulting solution was stirred at ambient temperature under argon for 24 h. The solvent was distilled off under reduced pressure and the solid residue was washed with methanol (100 mL) to afford **CdS–II** (47 mg) as a yellow powder.

Preparation of **CdS–I–27** *and* **CdS–II–27.** A solution of **27** (36 mg) and either **CdS–I** or **CdS–II** (10 mg) in chloroform (15 mL) was heated under reflux and argon for 24 h. After cooling down to ambient temperature, the solvent was distilled off under reduced pressure. The solid residue was suspended in acetonitrile (8 mL), sonicated, centrifuged and separated from the supernatant. This procedure was repeated three additional times to afford either **CdS–I–27** or **CdS–II–27** (9 mg) as a yellow powder.

Preparation of **CdSe–ZnS–29** A solution of CdSe–ZnS core–shell quantum dots (10 mg) in $CHCl_3$ (10 mL) was combined with a solution of the chloride salt of **29** (20 mg) in $CHCl_3$ (10 mL) and the mixture was stirred at ambient temperature for one hour. After centrifugation, the solid residue was suspended in $CHCl_3$ (5 mL) and sonicated. Then, the suspension was deposited dropwise on a quartz slide. After the evaporation of the solvent, the slide was washed with acetonitrile (10 mL) and dried under a stream of argon.

References and notes

1) Prasad, P. N. *Introduction to Biophotonics*, Wiley-Interscience: New York, **2003**.

2) Desvergne, J.-P. and Czarnik, A. W. (Eds.) *Chemosensors of Ion and Molecular Recognition*, Kluwer Academic Publishers: Dordrecht, **1997**.

3) Ricco, A. J. and Crooks, R. M. (Eds.) *Acc. Chem. Res.* **1998**, 31, 199.

4) Lakowicz, J. R. *Principles of Fluorescence Spectroscopy*, Kluwer Academic/Plenum Publishers: New York, 1999.

5) Ellis, A. B. and Walt, D. R. (Eds.) *Chem. Rev.* **2000**, 100, 2477.

6) Fabbrizzi, L. (Ed.) *Coord. Chem. Rev.* **2000**, 205, 1.

7) de Silva, A. P. and Tecilla, P. (Eds.) *J. Mater. Chem.* **2005**, 15, 2617.

8) Haugland, R. P. *The Handbook: A Guide to Fluorescent Probes and Labeling Technologies*, Molecular Probes: Eugene, 2005.

9) (a) Henglein, A. J. *Chim. Phys*. **1987**, 84, 1043. (b) Henglein, A. *Chem. Rev*. **1989**, 89, 1861.

10) (*a*) Steigerwald, M. L. and Brus, L. E. *Ann. Rev. Mater. Sci.* **1989**, 19, 471. (*b*) Steigerwald, M. L. and Brus, L. E. *Acc. Chem. Res.* **1990**, 23, 183. (*c*) Bawendi, M. G.; Steigerwald, M. L. and Brus, L. E. *Ann. Rev. Phys. Chem.* **1990**, 41, 477. (*d*) Nirmal M. and Brus, L. E. *Acc. Chem. Res.* **1999**, 32, 407.

11) (*a*) Weller, H. *Adv. Mater.* **1993**, 5, 88. (*b*) Weller, H. *Curr. Opin. Colloid Interf. Sci.* **1998**, 3, 194.

12) (*a*) Yoffe, A. D. *Adv. Physics*, **1993**, 42, 173. (*b*) Yoffe, A. D. *Adv. Physics*, **2001**, 50, 1.

13) (*a*) Alivisatos, A. P. *J. Phys. Chem.* **1996**, 100, 13266. (*b*) Alivisatos, A. P. *Science*, **1996**, 271, 933. (*c*) Alivisatos, A. P. *Endeavour*, **1997**, 21, 56. (*d*) Yin, Y. and Alivisatos, A. P. *Nature*, **2005**, 437, 664.

14) (*a*) Empedocles, S. and Bawendi, M. G. *Acc. Chem. Res*, **1999**, 32, 389. (*b*) Murray, C. B.; Kagan, C. R. and Bawendi, M. G. *Ann. Rev. Mater. Sci*, **2000**, 30, 545.

15) (*a*) Green, M. and O'Brien, P. *Chem. Commun.*, **1999**, 2235. (*b*) Trindade, T.; O'Brien, P. and Pickett, N. L. *Chem. Mater*, **2001**, 13, 3843.

16) Efros, A. L. and Rosen, M. *Ann. Rev. Mater. Sci.* **2000**, 30, 475.

17) Penner, R. M. *Acc. Chem. Res.* **2000**, 33, 78.

18) Wise, F. W. *Acc. Chem. Res.* **2000**, 33, 773.

19) (*a*) Eychmüller, A. and Rogach, A. L. *Pure Appl. Chem.* **2000**, 72, 179. (*b*) Rogach,A. L.; Talapin,D. V.; Shevchenko,E. V.; Kornowski,; Haase, A. M. and Weller, H. *Adv. Funct. Mater.* **2002**, 12, 653.

20) (*a*) El- Sayed, M. A. *Acc. Chem. Res.* **2004**, 37, 326. (*b*) Burda,C.; Chen,X. B.; Narayana,R. and El-Sayed, M. A. *Chem. Rev.* **2005**, 105, 1025.

21) Jun,Y.; Choi, J. and Cheon, J. *Angew. Chem. Int. Ed.* **2006**, 45, 3414.

22) Murray, C.B.; Norris, D.J. and Bawendi, M.G. *J. Am.Chem. Soc.* **1993**, *115*, 8706.

23) Dabbousi, B.O.; Rodriguez-Viejo, J.; Mikulec, F.V.; Heine, J.R.; Mattoussi, H.; Ober, R.; Jensen, K.F. and Bawendi, M.G. *J. Phys. Chem. B*. **1997**, 101, 9463.

24) Peng, X.; Schlamp, M.C.; Kadavanich, A.V. and Alivisatos, A.P. *J. Am. Chem. Soc*. **1997**, 119, 7019.

25) Hines, M.A. and Guyot-Sionnest, P. *J. Phys. Chem*. **1996**, 100, 468.

26) Derfus, A.M. and Chan, W.C.W.; Bhatia, S.N. *NanoLett*. **2004**, 4, 11.

27) Peng, Z.A. and Peng, X. *J. Am. Chem. Soc*. **2001**, 123, 183.

28) Michalet, X.; Pinaud, F.F.; Bentolila, L.A.; Tsay, J.M.; Doose, S.; Li, J.J.; Sundaresan, G.; Wu, A.M.; Gambhir, S.S. and Weiss, S. *Science* **2005**, 307, 538.

29) Ozkan, M. *Drug Discovery Today.* **2004**, 9, 1065.

30) Murphy, C. J. *Anal. Chem.* **2002**, 74, 526A.

31) Yu, W.; Qu, L.; Guo, W. and Peng, X. *Chem. Mater.* 2003, **15**, 2854.

32) Haugland, R. P. *The Handbook: A Guide to Fluorescent Probes and Labeling Technologies*; Molecular Probes: Eugene, 2005.

33) Mujumdar, R. B.; Ernst,L. A.; Mujumdar,S. R.; Lewis, C. J. and Waggoner, A. S. *Bioconj. Chem.* **1993**, 4, 105.

34) Tomasulo,M.; Yildiz,I.; Kaanumalle, S. L. and Raymo, F. M. *Langmuir*, **2006**, 24, 10284.

35) Sabanayagam, C. R.; Eid, J. S. and Meller, A. *J. Chem. Phys.*, **2005**, 122, 061103.

36) Hanley, Q. S.; Subramaniam, V. and Arndt-Jovin, D. J. *Cytometry*, **2001**, 43, 248.

37) Brismar, H.; Trepte, O. and Ulfhake, B. *Histochem. Cytochem.*, **1995**, 43, 699.

38) Tinnefeld, P.; Herten, D. P and Sauer, M. *J. Phys. Chem. A*. **2001**, 105, 7989.

39) Larson, D. R.; Zipfel, W. R.; Williams, R. M.; Clark, S. W.; Bruchez, M. P.; Wise, F. W. and Webb, W. W. *Science*, **2003**, 300, 1434.

40) Song, J. M.; Inoue, T.; Kawazumi, H. and Ogawa, T. *Anal. Sci*. **1999**, 15, 601.

41) Kauert,M.; Stoller, P. C.; Frenz, M. and Rička, J. *Opt. Express.*, **2006**, 14, 8434.

42) Lukomska, J.; Gryczynski, I.; Malicka, J.; Makowiec, S.; Lakowicz, J. R. and Gryczynski, Z. J. *Biochem. Biophys. Res. Commun.*, **2005**, 328, 78.

43) (*a*) Alivisatos, A. P. *Pure. Appl. Chem.* **2000**, 72, 3. (*b*) Michalet, X.; Pinaud, F.; Lacoste, T. D.; Dahan,M.; Bruchez, M. P.; Alivisatos, A. P. and Weiss,S. *Single Mol.*, **2001**, 2, 261. (*c*) Parak, W. J.; Gerion, D.; Pellegrino, T.; Zanchet,D.; Micheel, C.; Williams,S. C.; Boudreau, R.; M. Le Gros, A.; Larabell, C. A. and Alivisatos, A. P. *Nanotechnology*. **2003**, 14, R15. (*d*) Alivisatos, A. P. *Nat. Biotech.* **2004**, 22, 47; (*e*) Alivisatos,A. P.; Gu, W. and Larabell, C. *Annu. Rev. Biomed. Eng.* **2005**, 7, 55.

44) (*a*) Niemeyer, C. M. *Angew. Chem. Int. Ed.* **2001**, 40, 4128. (*b*) Niemeyer, C. M. *Angew. Chem. Int. Ed.* **2003**, 42, 5796.

45) (*a*) Chan, W. C. W.; Maxwell, D. J.; Gao, X.; Bailey, R. E.; Han, M. and Nie, S. *Curr. Op. Biotech.* **2002**, 13, 40. (*b*) Gao, X. and Nie, S. *Trends Biotech.* **2003**, 21, 371. (*c*) Gao,X.; Yang, L.; Petros, J. A.; Marshall, F. F.; Simons, J. W. and Nie, S. *Curr. Op. Biotech.* **2005**, 16, 63.

46) Sutherland, A. J. *Curr. Op. Solid State Mater. Sci*. **2002**, 6, 365.

47) (*a*) Mattoussi, H.; Kuno, M. K.; Goldman, E. R.; Anderson, G. P. and Mauro, J. M. in *Optical Biosensors: Present and Future*, F. S. Ligler and C. D. Rowe Taitt (Eds.), Elsevier: Amsterdam, 2002, p. 537; (*b*) Medintz, I. G.; Uyeda, H. T.; Goldam, E. R. and Mattoussi, H. *Nat. Mater*. **2005**, 4, 435. (*c*) Clapp, A. R.; Medintz, I. L. and Mattoussi, H. *ChemPhysChem*. **2006**, 7, 47. (*d*) Sapsford, K. E.; Berti, L. and I. Medintz, L. *Angew. Chem. Int. Ed.* **2006**, 45, 4562.

48) (*a*) Watson, A.; Wu, X. and Bruchez, M. P. *Biotechniques*. **2003**, 34, 296. (*b*) Wu, X. and Bruchez, M. P. in *Methods in Cell Biology*, Z. Darzynkiewicz, M. Roederer and H. J. Tanke (Eds.), Elsevier: Amsterdam, 2004, vol. 75, p. 171.

49) Green, M. *Angew. Chem. Int. Ed.* **2004**, 43, 4129.

50) Riegler, J. and Nann, T. *Anal. Bioanal. Chem.* **2004**, 379, 913.

51) Willner, I. and Katz, E. *Angew. Chem. Int. Ed.* **2004**, 43, 6042.

52) Lidke, D. S. and Arndt-Jovin, D. J. *Physiology*. **2004**, 19, 322.

53) Jaiswal, J. K. and Simon, S. M. *Trends Cell Biol.* **2004**, 14, 497.

54) Rosi, N. L. and Mirkin, C. A. *Chem. Rev.* **2005**, 105, 1547.

55) Pellegrino, T.; Kudera, S.; Liedl, T.; Muñoz Javier, A.; Manna, L. and Parak, W. J. *Small*. **2005**, 1, 48.

56) Pinaud, F.; Michalet, X.; Bentolila, L. A.; Tsay, J. M.; Doose, S.; Li, J. J.; Iyer,G. and Weiss, S. *Biomater.* **2006**, 27, 1679.

57) Yu, W.; Chang, W. E.; Drezek, R. and Colvin, V. L. *Biochem. Biophys. Res. Commun.* **2006**, 348, 781.

58) Samia, A. C. S.; Dayal, S. and Burda, C. *Photochem. Photobiol.* **2006**, 82, 617.

59) Sandros, M. G.; Gao, D. and Benson, D. E. *J. Am. Chem. Soc.* **2005**, 127, 12198.

60) Palaniappan, K.; Xue, C.; Arumugam, G.; Hackney, S. A. and Liu, J. *Chem. Mater.*, **2006**, 18, 1275.

61) Maruel, V.; Laferrière, M.; Billone, P.; Godin, R. and Scaiano, J. C. *J. Phys. Chem. B*. **2006**, 110, 16353.

62) Clarke, S. J.; Hollmann, C. A.; Zhang, Z.; Suffern, D.; Bradforth, S. E.; Dimitrijevic, N. M.; Minarik, W. G. and Nadeau, J. L. *Nat. Mater.* **2006**, 5, 409.

63) (*a*) Tomasulo, M.; Yildiz, I. and Raymo, F. M. *J. Phys. Chem. B*. **2006**, 110, 3853. (*b*) Yildiz, I.; Tomasulo, M. and Raymo, F. M. *Proc. Natl. Acad. Sci. USA*. **2006**, 103, 11457.

64) Willard, D. M.; Carillo, L. L.; Jung, J. and Van Orden, A. *Nano Lett.* **2001**, 1, 469.

65) Wang, S.; Mamedova, N.; Kotov, N. A.; Chen, W. and Studer, J. *Nano Lett.* **2002**, 2, 817.

66) (*a*) Tran,P. T.; Goldman, E. R.; Anderson, G. P.; Mauro, J. M. and Mattoussi, H. *Phys. Stat. Sol.* **2002**, 229, 427. (*b*) Medintz, I. L.; Clapp, A. R.; Mattoussi, H.; Goldman, E. R.; ,B. and Mauro, J. M. *Nat. Mater*, **2003**, 2, 630. (*c*) Medintz, I. L.; Clapp, A. R.; Melinger, J. S.; Deschamps,J. R. and Mattoussi, H. *Adv. Mater.* **2005**, 17, 2450. (*d*) Goldman, E. R.; Medintz, I. L.; Whitley, J. L.; Hayhurst, A.; Clapp, A. R.; Uyeda, H. T.; Deschamps, J. R.; Lassman, M. E. and Mattoussi, H. *J. Am. Chem. Soc.* **2005**, 127, 6744. (*e*) Medintz, I. L.; Sapsford, K. E.; Clapp, A. R.; Pons, T.; Higashiya, S.; Welch, J. T. and Mattoussi, H. *J. Phys. Chem. B.* **2006**, 110, 10683.

67) (*a*) Patolsky, F.; Gill, R.; Weizmann, Y.; Mokari, T.; Banin, U. and Willner, I. *J. Am. Chem. Soc.* **2003**, 125, 13918. (*b*) Gill, R.; Willner, I.; Shweky, I. and Banin, U. *J. Phys. Chem. B.* **2005**, 109, 23715.

68) Nagasaki, N.; Ishii, T.; Sunaga, Y.; Watanabe, Y.; Otsuka H. and Kataoka, K. *Langmuir.* **2004**, 20, 6396.

69) (*a*) Kim, J. H.; Morikis, D.; Ozkan, M., *Sens. Act. B.* **2004**, 102, 315. (*b*) Kim, J. H.; Chaudhary, S.; Stephens, J. P.; Singh, K. V.; Ozkan, M. *Proc. SPIE*. **2005**, 5705, 175.

70) (*a*) Hildebrandt, N.; L. Charbonnière, J.; Beck, M.; Ziessel, R. F. and Löhmannsröben, H.-G. *Angew. Chem. Int. Ed.* **2005**, 44, 1. (*b*) Charbonnière, L. J.; Hildebrandt, N.; Ziessel, R. F. and Löhmannsröben, H.-G. *J. Am. Chem. Soc*. **2006**, **128**, 12800.

71) Geissbuehler, I.; Hovius, R.; Martinez, K. L.; Adrian, M.; Thampi, K. R. and Vögel, H. *Angew. Chem. Int. Ed.* **2005**, 44, 1388.

72) Chang, E.; Miller, J. S.; Sun, J.; Yu, W. W.; Colvin, V. L.; Drezek, R. and West, J. L. *Biochem. Biophys. Res. Commun.* **2005**, 334, 1317.

73) Dyadyusha, L.; Yin, H.; Jaiswal, S.; Brown, T.; Baumberg, J. J.; Booy, F. P. and Melvin, T. *Chem. Commun.* **2005**, 4, 3201.

74) Hohng, S. and Ha, T. *ChemPhysChem*. **2005**, 6, 956.

75) Oh, E.; Hong, M.-Y.; Lee, D.; Nam, S.-H.; Yoon, H. C. and Kim, H.-S. *J. Am. Chem. Soc.* **2005**, 127, 3270.

76) Bakalova, R.; Zhelev, Z.; Ohba, H. and Baba, Y. *J. Am. Chem. Soc*. **2005**, 127, 11328.

77) Zhang, C.-Y.; Yeh, H.-C.; Kuroki, M. T. and Wang, T.-H. *Nat. Mater.* **2005**, 4, 826.

78) Ma, Q.; Su, X.-G.; Wang, X.-Y.; Wan, Y.; Wang, C.-L.; Yang, B. and Jin, Q.-H. *Talanta*. **2005**, 67, 1029.

79) Nikiforov, T. T. and Beechem, J. M. *Anal. Biochem.* **2006**, 357, 68.

80) Chen, C.-Y.; C.- Cheng, T.; Lai, C.-W.; Wu, P.-W.; Wu, K.-C.; Chou, P.-T.; Chou, Y.-H. and Chiu, H.-T. *Chem. Commun.* **2006**, 263.

81) Zhang, C. and Johnson, L. W. *J. Am. Chem. Soc.* **2006**, 128, 5324.

82) Shi, L.; De Paoli, V.; Rosenzweig, N. and Rosenzweig, Z. *J. Am. Chem. Soc.* **2006**, 128, 10378.

83) Snee, P. T.; R. Somers, C.; Nair, G.; Zimmer, J. P.; Bawendi, M. G. and Nocera, D. G. *J. Am. Chem. Soc.* **2006**, 128, 13320.

84) Wang, C. J.; Shim, M. and Guyot-Sionnest, P. *Science.* **2001**, 291, 2390.

85) Kucur, E.; Riegler, J.; Urban, G. A. and Nann, T. *J. Chem. Phys.* **2003**, 119, 2333.

86) Querner, C.; Reiss, P.; Sadki, S.; Zagorska, M. and Pron, A. *Phys. Chem. Chem. Phys.* **2005**, 7, 3204.

87) Wang, C. J.; Wehrenberg, B. L.; Woo, C. Y. and Guyot-Sionnest, P. *J. Phys. Chem. B.* **2004**, 108, 9027.

88) Callan, J. F.; Mulrooney, R. C.; Kamila, S. and McCaughan, B. J Fluoresc. 2007, online.

89) Gunnlaugsson, T.; Davis, A. P.; Hussey, G. M.; Tierney, J.; Glynn, M. *Org Biomol Chem.* **2004,** 2,1856.

89) Gunnlaugsson, T.; Davis, A. P.; Hussey, G. M.; Tierney, J.; Glynn, M. *Org Biomol Chem.* **2004,** 2,1856.

90) Gill, R.; Freeman, R.; Xu, J.; Willner, I.; Winograd, S.; Shweky, I. and Banin U. *Am. Chem. Soc*. **2006**, 128, 15376.

91) Förster, T. *Ann. Phys.***1948**, 2, 55.

92) Clapp, A. R.; Medintz, I. L.; Mauro, J. M.; Fisher, B. R.; Bawendi, M. G. and Mattoussi, H. *J. Am. Chem. Soc.* **2004**, 126, 301.

93) Clapp, A. R.; Medintz, I. L.; Fisher, B. R.; Anderson, G. P. and Mattoussi, H. *J. Am. Chem. Soc*. **2005**, 127, 1242.

94) Nikiforov, T. T. and Beechem, J. M. *Anal. Biochem.* **2006**, 357, 68.

95) Ji ,J.; Rosenzweig, N.; Griffin, C. and Rosenzweig, Z. *Anal. Chem.* **2000,** 72, 3497.

96) Bernhard, D. D.; Mall, S. and Pantano, P. *Anal. Chem.* **2001**, 73, 2484

97) Lobnik, A.; Oehme, I.; Murkovic, I. and Wolfbeis, O. S. *Anal. Chim. Acta.* **1998**, 367, 159.

98) Nivens, D. A.; Zhang, Y. and Angel, S. M. *Anal. Chim. Acta.* **1998**, 376, 235.

99) Liu, Y. H.; Dam, T. H. and Pantano, P. *Anal. Chim. Acta.* **2000**, 419**,** 215.

100) Cajlakovic, M.; Lobnik, A.; and Werner, T. *Anal. Chim. Acta.* **2002**, 455, 207.

101) Fry, D. R. and Bobbitt, D. R. *Microchem. J.* **2001**, 69, 123.

102) Malins, C.; Glever, H. G.; Keyes, T.E.; Vos, J. G.; Dressick, W. J. and MacCraith, B. D. *Sens. Actuators B.* **2000**, 67, 89.

103) Lobnik, A.; Majcen, N.; Niederreiter, K. and Uray, G. *Sens. Actuators B.* **2001**, 74, 200.

104) Ji, J. and Rosenzweig, Z. *Anal. Chim. Acta.* **1999**, 397**,** 93.

105) Kermis, H. R.; Kostov, Y.; Harms, P. and Rao, G. *Biotechnol. Progr.* **2002**, 18, 1047.

106) Nivens, D. A.; Schiza, M. V. and Angel, S. M. *Talanta.* **2002**, 58, 543.

107) Lin, H. J.; Szmacinski, H. and Lakowicz, J. R. *Anal. Biochem.* **1999**, 269, 162–167.

108) Kosch, U.; Klimant, I. and Wolfbeis, O. S. *Fresenius J. Anal. Chem.* **1999**, 364**,** 48.

109) Ma, L. Y.; Wang, H. Y.; Xie, H. and Xu, L. X. *Spectrochim. Acta Part A.* **2004**, 60, 1865.

110) Snee, P. T.; Somers, R. C.; Nair, G.; Zimmer, J. P.; Bawendi, M. G. and Nocera, D. G. *J. Am. Chem. Soc.* **2006**, 128, 13320.

111) Tomasulo, M.; Yildiz I.; Kaanumalle, S. L. and Raymo, F. M. *Langmuir.* **2006**, 22,184.

112) Tomasulo, M.; Yildiz I. and Raymo, F. M. *J. Phys. Chem.* **2006**, 110, 3853.

113) (*a*) Tomasulo, M.; Yildiz I. and Raymo, F. M. *Aust. J. Chem.* **2006**, 59, 175. (*b*) Tomasulo, M.; Yildiz, I. and Raymo, F. M. *Inorg. Chim. Acta*, **2006**, 359, 5545.

114) (a) Tomasulo, M. and Raymo, F. M. *Org. Lett.* **2005**, *7*, 4633. (b) Tomasulo, M.; Sortino, S.; White, A. J. P. and Raymo, F. M. *J. Org. Chem.* **2006**, *71*, 744.

115) (a) Tomasulo, M.; Yildiz, I. and Raymo, F. M. *Aust. J. Chem.* **2006**, *59*, 175.

116) Yildiz, I. and Raymo, F. M. *J. Mater. Mater.* **2006**, *16*, 1118.

117) The multi-exponential decay of the luminescence intensity is in agreement with literature data on the emissive behavior of similar quantum dots (ref. 62 and 67b).

118) The changes in the absorption and emission spectra of the quantum dots observed with the transformation of **15** into **15-HA** can be reversed with the addition of CF_3CO_2H.

119) The absorption spectra of CdSe–ZnS core–shell quantum dots, lacking the oxazine ligand **15**, recorded before and after the addition of Bu_4NOH are identical. This control experiment demonstrates that the absorption band developing at 553 nm after the addition of Bu_4NOH to the quantum dots coated with **15** is, indeed, a result of the presence of the oxazine ligand on the nanoparticle surface.

120) The emission spectra of CdSe–ZnS core–shell quantum dots, lacking the oxazine ligand **15**, recorded before and after the addition of Bu_4NOH are identical. This control experiment demonstrates that the luminescence decrease after the addition of Bu_4NOH to the quantum dots coated with **15** is, indeed, a result of the presence of the oxazine ligand on the nanoparticle surface.

121) The absorption spectra of CdSe–ZnS core–shell quantum dots, lacking the oxazine ligand **15**, recorded before and after the addition of CF_3CO_2H are also identical.

122) The changes in the emission spectra of the quantum dots observed with the transformation of **15** into **6-IN** can be reversed with the addition of Bu_4NOH.

123) The emission spectra of CdSe–ZnS core–shell quantum dots, lacking the oxazine ligand **15**, recorded before and after the addition of CF_3CO_2H are identical. This control experiment demonstrates that the luminescence increase after the addition of CF_3CO_2H to the quantum dots coated with **6-OX** is, indeed, a result of the presence of the oxazine ligand on the nanoparticle surface.

124) Burda, C.; Green, T. C.; Link, S. and El-Sayed, M. A. *J. Phys. Chem. B*. **1999**, 103, 1783.

125) Crano, J. C. and Guglielmetti, R. (Eds.). *Organic Photochromic and Thermochromic Compounds*, Plenum Press: New York, 1999.

126) McArdle, C. B. (Ed.), *Applied Photochromic Polymer Systems*, Blackie: Glasgow, 1992.

127) (a) Ong, W.; Gómez-Kaifer, M. and Kaifer, A. E. *Org. Lett.* **2002**, 4, 1791. (b) Ong, W. and Kaifer, A. E. *J. Org. Chem.* **2004**, 69, 1383.

128) Kim, H.-J.; Keon, W. S.; Ko, Y. H. and Kim, K. *Proc. Natl. Acad. Sci. USA.* **2002**, 99, 5007.

129) Vajda, S.; Weng, Z.; Rosenfeld, R. and DeLisi, C. *Biochemistry.* **1994**, 33, 13977.

130) Miyamoto, S. and Kollman, P. A. *Proc. Natl. Acad. Sci. U. S. A.* **1993**, 90, 8402.

131) Weber, P. C.; Pantoliano, M. W. and Thompson, L. D. *Biochemistry*. **1992**, 31, 9350.

132) Hendrickson, W. A.; Palher, A.; Smith, J. L.; Satow, Y.; Merritt, E. A. and Phizackerley, R. P. *Proc. Natl. Acad. Sci. U. S. A*. **1989**, 86, 2190.

133) Chan, W. C. W., and Nie, S. *Science*. **1998**, 281, 2016.

134) Dorion, G. H. and Wiebe, A. F. *Photochromism*. Focal Press: New York, 1970.

135) Brown, G. H. (Ed.). *Photochromism*. Wiley: New York, 1971.

136) El'tsov, A. V. (Ed.). *Organic Photochromes.* Consultants Bureau: New York, 1990.

137) Bouas-Laurent, H. and Dürr, H. (Eds.). *Photochromism: Molecules and Systems*, Elsevier: Amsterdam, 1990.

138) Irie, M. (Ed.). *Photo-Reactive Materials for Ultrahigh Density Optical Memory*; Elsevier: Amsterdam, 1994.

139) Irie,M. (Ed.). *Chem. Rev.* **2000**, 100, 1683.

140) (a) Raymo, F. M.; Tomasulo, M. *Chem. Soc. Rev.* **2005**, *34*, 327. (b) Raymo, F. M. and Tomasulo, M. *J. Phys. Chem. A.* **2005**, 109, 7343.

141) Zhu, L.; Zhu, M.-Q.; Hurst,J. K. and Li,A. D. Q. *J. Am. Chem. Soc.* **2005**, 127, 8968.

142) Jares-Erijman, E.; Giordano L.,; Spagnuolo, C.; Lidke, K. and Jovin, T. M. *Mol. Cryst. Liq. Cryst.* **2005**, 430, 257.

143) Medintz,I. L.; Trammell, S. A.; Mattoussi, H. and Mauro, J. M. *J. Am. Chem. Soc.* **2004**, 126, 30.

144) Raymo, F. M. and Tomasulo, M. *Chem. Eur. J*. **2006**, 12, 3186.

145) (a) Bertelson, R. C. in ref. 135, p. 45.

(b) Bertelson, R. C. in ref. 125, vol. 1, p. 11.

146) Kholmanskii, A. S. and Dyumanev, K. M. *Russ. Chem. Rev*. **1987**, 56, 136.

147) Guglielmetti, R. in ref. 136, p. 314 and 855.

148) Tamai, N. and Miyasaka, H. *Chem. Rev*. **2000**, 100, 1875.

149) Minkin, V. I. *Chem. Rev*. **2004**, 104, 2751.

150) (a) Raymo, F. M. and Giordani, S. *J. Am. Chem. Soc*. **2001**, 123, 4651.

(b) Raymo, F. M. and Giordani, S. A.; White, J. P. and Williams, D. J. *J. Org. Chem*. **2003**, 68, 4158.

151) Tomasulo, M.; Giordani, S. and Raymo, F. M. *Adv. Funct. Mater*. **2005**, 15, 787.

152) Giordani, S. and Raymo, F. M. *Org. Lett.* **2003**, 5, 3559.

153) Steigerwald, M. L.; Alivisatos, A. P.; Gibson, J. M.; Harris, T. D.; Kortan, R.; Muller, A. J.; Thayer, A. M.; Duncan, T. M.; Douglass, D. C. and Brus, L. E. *J. Am. Chem. Soc*. **1988**, 110, 3046.

154) Steckel, J. S.; Zimmer, J. P.; Coe-Sullivan, S.; Stott, N. E.; Bulovic, V. and Bawendi, M. G. *Angew. Chem. Int. Ed*. **2004**, 43, 2154.

155) Bavykin, D. V.; Savinov, E. N. and Parmon, V. N. *Langmuir*. **1999**, 15, 4722.

156) Kamogawa, H. in ref. 126 p. 207.

157) Nanasawa, M. in ref. 125 p. 341.

158) Monk, P. M. S. *The Viologens: Physicochemical Properties, Synthesis and Applications of the Salts of 4,4'-Bipyridine* Wiley: New York, 1998.

159) Feng, D.-J.; Li, X.-Q.; Wang, X.-Z.; Jiang, X.-K. and Li, Z.-T. *Tetrahedron.* **2004**, 60, 6137.

160) Alvarado, R. J.; Mukherjee, J.; Pacsial, E. J.; Alexander, D. and Raymo, F. M. *J. Phys. Chem. B*. **2005**, 109, 6164.